AN EXPLORATION FOR TRUTH IN SOIL PARENT MATERIALS IN HYALITE CANYON, MONTANA

by

John Charles Sugden

A thesis submitted in partial fulfillment
of the requirements for the degree

of

Master of Science

in

Land Resources and Environmental Sciences

MONTANA STATE UNIVERSITY
Bozeman, Montana

August 2015

©COPYRIGHT

by

John Charles Sugden

2015

All Rights Reserved

DEDICATION

This thesis is dedicated to my wife, Amanda, our dog Cooper, and my friends and family who have stood by me while I spent countless hours on this work. This work is also dedicated to those working to protect natural resources in Hyalite Canyon and southwest Montana. Without their efforts, undisturbed soil conditions may be much more difficult to find and study.

ACKNOWLEDGEMENTS

I'd like to acknowledge and thank my major advisor, Dr. Anthony Hartshorn, for his dedication, patience, and support. Additionally, I'd like to thank my committee members, Dr. Stephanie Ewing, and Stuart Challender for their input, contributions, and guidance. Their tutelage has strengthened this body of work. I acknowledge Dr. Stephanie Ewing, Dr. John Montagne, and Dr. Cliff Montage for their soil and geology work in Hyalite Canyon. Without their efforts this work would not have been possible.

TABLE OF CONTENTS

1. INTRODUCTION 1

2. A SLICE THROUGH TIME: A HYALITE CANYON LITHOSEQUENCE 5

Contribution of Authors and Co-Authors 5
Manuscript Information Page 6
Abstract 7
Introduction 8
Hyalite Canyon as an MSU Fieldtrip Destination 8
Prior Soil Survey Efforts Across the Gallatin National Forest 13
State Factor Approach 17
Langohr Campground Lithosequence: Climate, Relief & Time Factors 18
Langohr Campground Lithosequence: Biota & Parent Material Factors 20
Fieldtrip Stop Descriptions 24
Methods 26
Results and Discussion 28
Future Directions 35
Conclusions 37
Acknowledgements 38

3. TRACE ELEMENT FINGERPRINTING OF PARENT MATERIAL INPUTS ACROSS A SOIL LITHOSEQUENCE 39

Contribution of Authors and Co-Authors 39
Manuscript Information Page 40
Abstract 41
Introduction 42
Methods 49
Field Design and Sampling 49
Geochemical Analyses 54
Two Mixing Models 58
Mass Balance 62
Combining Mixing Models and Mass Balance 65
Results 69
Mixing Model 69
Total Chemical Weathering 74
Soil Mass Balances 76
Discussion 78
Uncertainty in Mass Balance Calculations 92
Conclusions 94
Acknowledgements 95

TABLE OF CONTENTS - CONTINUED

4. CONCLUSION 96

REFERENCES CITED 97

APPENDICES 107

APPENDIX A: Terrain Attribute Effects on Soil Processes 108
APPENDIX B: Lithosequence Data 108

LIST OF TABLES

Table Page

1. Selected physical and chemical properties of selected soil horizons in the Gallatin National Forest 14

2. Current taxonomic breakdown of two lithosequence soils 15

3. Selected field-estimated physical and chemical properties for the five soil profiles.....23

4. Major and minor (not normalized) elemental composition of lithosequence soils..... 33-34

5. Regional Loess Deposition Estimates.....46

6. Selected physical and chemical properties for the five soil profiles.....55

7. Concentrations, enrichment factors, and differences in enrichment factors.....68

8. Summary of Ti/Zr, Ti/Nb, and Zr/Nb ratios and resulting fractional influences of rock and atmospheric deposition 69

9. Fractional influences of underlying rock and average atmospheric deposition as informed by concentrations 71

10. Depth weighted rock and hybrid chemical depletions fractions 75

11. Rock and hybrid mass losses referenced to rock only, rock and atmospheric deposition, and rock and colluvium 77

LIST OF FIGURES

Figure Page

1. Hyalite Canyon lithosequence project area....9

2. Soil and geologic map of the Hyalite Canyon lithosequence 11

3. Detail from an idealized stratigraphic column for the northern Gallatin Range....12

4. Major elemental composition for rock, soil A horizon, and dust across the lithosequence 32

5. Chondrite-normalized europium to europium anomaly ratios versus chondrite-normalized lanthanum to ytterbium ratios 37

6. General study location and geology in southwest Montana 50

7. Depiction of soil processes occurring on the five lithologies....53

8. Concentrations of Ti, Zr, and Nb for study samples....67

9. Depth plots of concentration ratios of parent materials and soil horizons 70

10. Mixing ratios as fractions calculated using ratios excluded using (DEF<30%) 72

11. Box plot of ranges of fractional rock influences on soil horizons calculated using the DEF<30% threshold. 73

12. Depth weighted chemical depletion fractions of the five soils referenced to Ti, Zr, and Nb in rock and Ti, Zr, and Nb in hybrid 75

13. Calculated total mass fluxes of parent materials: rock only and hybrid rock and average atmospheric deposition....78

LIST OF FIGURES – CONTINUED

Figure Page

14. Mixing ratios as fractions calculated using underlying shale (sh) and limestone (ls) and colluvium.....87

15. Various mass fluxes in soil on shale: rock only and hybrid mass fluxes.....88

16. Various mass fluxes in soil on limestone: rock only and hybrid mass fluxes 90

ABSTRACT

Forested mountain soils are mapped and researched at coarser scales than agricultural areas. Additionally existing mass balance approaches have only recently begun to quantify soil chemical weathering referenced to two parent materials. Forests occupy soils on gneiss, sandstone, shale, limestone, and basaltic andesite in a lithosequence. Differences in the trace chemistry of immobile elements and their ratios were used to determine the influence of underlying bedrock and other parent materials on soils in southwest Montana. Differences between soils and underlying rock and soils and other candidate parent materials were used to determine the relative influence of both parent materials on each soil horizon. A conventional mass balance approach quantified total and elemental chemical weathering for both parent materials. The relative influences, as informed by trace elements and ratios, were used to scale mass fluxes from each parent material into a hybrid mass flux. We characterized one soil pit per lithology, sampled soil horizons, rock type, and collected five samples regionally as deposited loess. Rock samples (as underlying rock and colluvium as appropriate) and atmospheric deposition were considered candidate parent materials to these soils. Samples were analyzed for major and trace elements. The trace elements or ratios used determined the relative influence of underlying rock versus a second parent material. We developed a methods to assess the immobility of specific elements relative to underlying rock. Ratios deemed most immobile were used to determine fractional influences of rock and a second parent material. Most soils had stronger rock influence at depth and stronger influences of atmospheric deposition at the surface, except for soil on sandstone and basaltic andesite. Regardless, accounting for additions of parent materials aside from underlying rock reduced total mass losses in all soils. The biggest mass loss reductions occurred (~50%) in soils on shale and gneiss, whereas mass loss reductions in soil on basaltic were more modest (~15%) when accounting for atmospheric deposition as a second parent material.

1. INTRODUCTION

Knowledge of soil formation patterns can guide and benefit additional study and help land managers target their limited resources and meet their management goals. This thesis examines the role of atmospheric deposition in soil formation in the mountains directly adjacent to the Gallatin Valley in southwest Montana. Many studies have found (see for example Yaalon and Ganor, 1973; Chadwick, 1990; Reheis et al., 1995; Anderson et al., 2002; Ewing et al., 2006; Porder et al., 2007; Muhs et al., 2006, 2008; Muhs, 2013; Pett-Ridge, 2009; Bern et al., 2015) that aeolian inputs have an influence on soil processes and ecosystems. Soils in the Gallatin Valley are largely windblown aoelian loess on benches divided by alluvial fans (Bourne and Whiteside, 1962). The influence of atmospheric deposition outside of valley agricultural areas have not been well studied. It is unlikely that atmospheric deposition stops where the valley floor meets the mountain front, but rather wet and dry deposition of atmospheric particles occur on all land surfaces. Given the complexity of present atmospheric deposition and its impact on ecosystems, additional complexity is encountered because soils can be old. Atmospheric deposition that occurred in present day or thousands of years ago has the ability to influence soil on which it will eventually land. We examined underlying rock, soil, and atmospheric additions to determine their relative influence on and weathering trajectories in existing soil horizons.

Atmospheric or loess deposition and its effects on soil processes are found in four flavors. Soils that are 100% loess, soils with a loess mantle, soils with a loess component, and soils with aoelian contamination (Yaalon and Ganor, 1973; Muhs et al.,

2013). Due to the fact that soil mostly do not have visible loess, we must account for underlying rock and its contribution to soils. We introduce a sequence of five co-located soil pits on five underlying rock types in hopes of seeing how similar depositional environments in wetter climate vary due to underlying rock types: gneiss, sandstone, shale, limestone, and basaltic andesite. We review existing soil survey data in the Gallatin National Forest for soils on these rock types, their formation in geologic time, and estimate relative soil ages.

We zoom into our study site in the Hyalite Canyon in the northern Gallatin Range, describe the five factor approach to soil formation, and discuss the four soil forming factors that vary little within this lithosequence (climate, biota, relief, and time). We introduce our current understanding of the various parent materials: underlying rocks and atmospheric deposition and the varying chemistry of both, review field observations, and share the portion of our dataset used in Chapter 2. We determine the regional composition of loess in the lithosequence using deposition records from the National Atmospheric Deposition Program and combine these with total denudation rates from Idaho (Ferrier et al., 2011) and annual deposition estimates from Colorado (Lawrence et al., 2010). And finally, employ a method that others (Muhs et al., 2008) have used to distinguish the presence of more than one parent using immobile elements, in hopes of quantifying the relative influence of more than one parent material on these soils. Major elemental concentrations of rock samples and soil horizon samples suggest that differential rock weathering and loess deposition both influence the content of soil A horizons. We describe aeolian presence in the lithosequence from the various atmospheric surrogate samples collected in Fall 2013. We compare and contrast parent

materials that would influence soils at the surface and from below. Assuming our soils show evidence of aeolian contamination (sensu Yaalon and Ganor, 1973), we begin our quest to find evidence of aeolian contamination in these soils. We review methods used by Muhs et al. (2008) to differentiate between soil derived from underlying rock and soil derived from exogenous inputs. We step beyond the Muhs approach of identifying different parent materials in soils to attempting to quantify relative influences of parent materials on soil using difference between soil horizons and rock and soil horizons and loess. Chapter 2 closes with future directions of the study including textural control on the fate of exogenous inputs, vegetative effects between the grasslands on shale and forests on the other sites, and mass flux calculations.

Chapter 3 takes an increasingly quantitative approach to further identifying parent materials involved in chemical weathering and their relative influence on important soil mass fluxes. These mass fluxes control critical geologically sourced nutrients availability and play a role in controlling atmospheric carbon dioxide concentrations. We review the history of soil mass balance and note the role of soil processes in the fate and transport of individual elements after chemical weathering in a soil system. We describe atmospheric deposition and recent observed deposition rates and their effects in the Rocky Mountains and pose the question does soil texture control atmospheric deposition and colluvial fate and transport? Previous work (McFadden and Weldon, 1987) suggest that wetter climates weather and incorporate loess into soil profiles quicker than dryer climates. But weathering rates also depend on the deposited and weathered material. Materials that weathering incongruently will take longer to leach from a soil profile. We reintroduce trace elements as tools that have been used to determine soil provenance and develop a

mixing model for soil parent materials. We assume that the range of second parent materials collected represent the range of parent materials that influence soils in the study area and in southwest Montana. We construct a mixing model of two parent materials on soils using trace elements and their ratios to determine their immobility and relative parent material influences.

CHAPTER TWO

2. A SLICE THROUGH TIME: A HYALITE CANYON LITHOSEQUENCE

Contribution of Authors and Co-Authors

Manuscript in Chapter 2

Author: J.C. Sugden

Contributions: Assisted in study design, added two soil pits to an existing sequence, wrote manuscript, crunched data, made figures, collected and processed samples, drafted manuscript revisions, responded to coauthor and reviewer comments.

Co-Author: A.S. Hartshorn

Contributions: Mentored in study design, provided funding and support, revised first and subsequent drafts, revised figures, collected and processed samples, responded to coauthors and reviewer comments.

Co-Author: J.L. Dixon

Contributions: Reviewed data, revised drafts and figures, provided feedback on approach.

Co-Author: C. Montagne

Contributions: Provided soil survey and teaching history of sites, first to teach soils at these sites, reviewed drafts.

Manuscript Information Page

J.C. Sugden, A.S. Hartshorn, J.L. Dixon, C. Montagne
Exploring the Northern Rocky Mountains: Geological Society of America Field Guide
Status of Manuscript:
____ Prepared for submission to a peer-reviewed journal
____ Officially submitted to a peer-review journal
____ Accepted by a peer-reviewed journal
_x__ Published in a peer-reviewed journal

Geological Society of America
Submitted February 2014
Published May 2014
Issue 37

Abstract

On this fieldtrip, participants will get their hands dirty while characterizing soils formed on five different rock types: Archean Gneiss, Flathead Sandstone, Wolsey Shale, Meagher Limestone and Absaroka Volcanics (a basaltic andesite rock). We first recap prior soil survey efforts across the Gallatin National Forest in southwestern Montana and introduce a state factor approach to understanding soils. For over 50 years, MSU faculty have explored parts of this lithosequence, using it as a natural laboratory for thousands of students. We continue this tradition with this field guide, emphasizing how the combination of field and laboratory data can enrich our understanding of soil processes. We will observe and measure striking differences in soils; these differences in physical and chemical properties, from textures and colors to pH and elemental composition, are discussed in the context of quantifying the influence of the underlying rock on soil properties. We use these differences to ask whether heterogeneity in soil properties justifies the inference that soil properties are dominated by the underlying lithology. We conclude that the underlying rock strongly influences soil properties, but in variable ways across this lithosequence. This influence is both direct and indirect: chemical weathering of the rock leads to compositional changes in overlying soil, but rock weathering also leads to coarse fragments in the soil profile, which alters soil hydrology.

Introduction

This field trip will examine the role of parent material in soil formation in Hyalite Canyon. Just ~12 miles south of the Montana State University (MSU) campus in Bozeman, a sequence of five stratigraphic units will enable participants to appreciate the multiple roles lithology can play in soil development. The fieldtrip learning outcomes include:

- how to characterize a soil profile,
- an introduction to geochemical fingerprinting of soils, and
- an understanding of the state factor and lithosequence approaches.

First we review historical MSU educational and research activities in Hyalite Canyon. Then we introduce the state factor approach (Jenny, 1941), and apply it across a lithosequence we will recharacterize as part of this fieldtrip. We conclude with a discussion of future opportunities.

Hyalite Canyon as an MSU Fieldtrip Destination

Our fieldtrip destination has roots in early efforts at MSU to take advantage of the natural laboratory represented by the Gallatin National Forest (GNF) in general, and sites near Langohr Campground in Hyalite Canyon in particular (Figs. 1 and 2). The GNF is a ~2 million-acre forest established in 1899 that stretches from just south of Bozeman to the northwestern corner of Yellowstone National Park and includes portions of seven

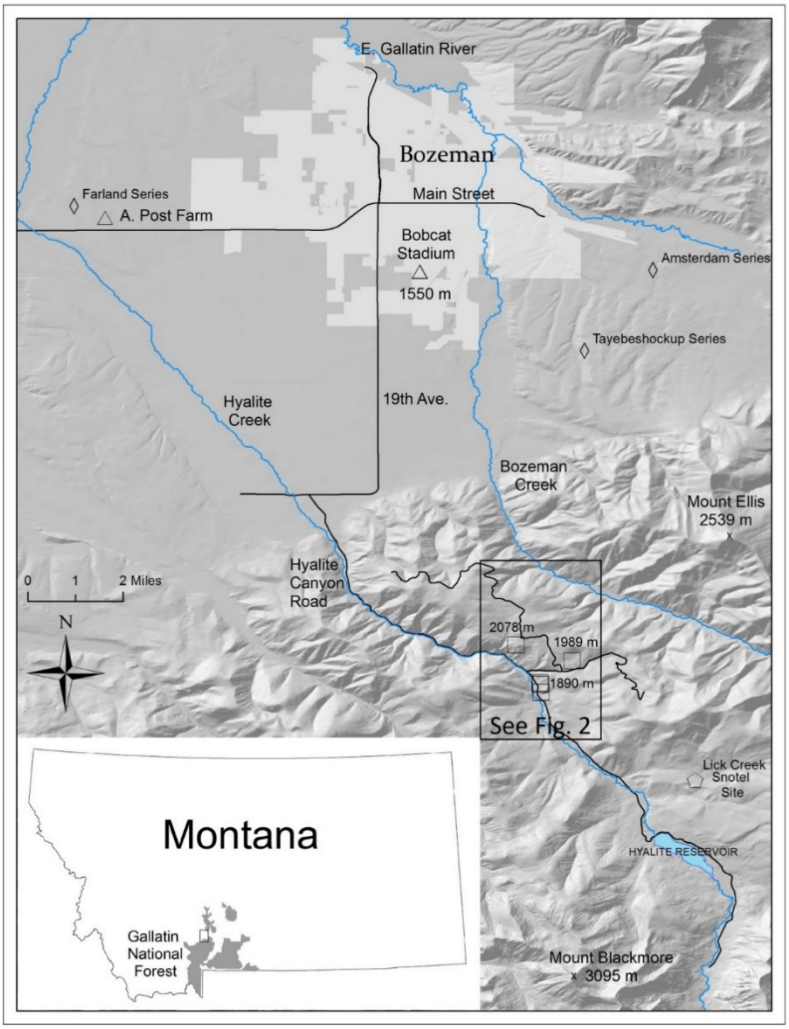

Figure 1. Hyalite Canyon lithosequence project area. Area of Figure 2 is inset. (Data from: (1) U.S. Geologic Survey, 2013, The national map viewer and data platform. http://nationalmap.gov/viewer.html. [data used: National Elevation Datasets 46w111 and 46w112; accessed 15 November 2013]. (2) National Cooperative Soil Survey, National Cooperative Soil Survey Soil Characterization Data: Natural Resources Conservation Service, U.S. Department of Agriculture, http://ncsslabdatamart.sc.egov.usda.gov/. [data used: location information for Amsterdam and Farland Series, Lick Creek and Tayebeshockup soil pits; accessed December 2013]. (3) Montana Bureau of Mines and Geology, 2013, MBMG geologic research/mapping, Montana Tech. of the University of Montana, http://www.mbmg.mtech.edu/gmr/gmr-statemap.asp#quadmaps. [data used: Bozeman and Livingston 1:100,000 quads; accessed: 2 December 2013]. (4) Montana Natural Resource Information System, Montana GIS portal: Montana's primary catalog of GIS data, Montana State Library, State of Montana. http://gisportal.msl.mt.gov/geoportal/catalog/main/home.page. [data used: State of Montana Boundary, National Forests and Ranger Districts in Montana; accessed February 2014].

mountain ranges. In 1998, a Memorandum of Understanding (MOU) between MSU and the US Forest Service (USFS; http://www2.montana.edu/policy/forest_service_use/mou.html) was developed to facilitate student and faculty engagement across the Gallatin and Custer National Forests. This area lies within the Montana metasedimentary sub-province of the Wyoming Province, and provides extensive exposures of Archean rocks uplifted during the Laramide Orogeny (Henry and Mogk, 2003).

More than 50 years ago, John Montagne, a faculty member at MSU hired by the Department of Earth Sciences in 1957, began exploring Hyalite Canyon as a fieldtrip destination. John's teaching assignments included introductory geology, geomorphology, glacial geology, structural geology, and field geology, and he quickly recognized the value of Hyalite Canyon for pedagogic purposes. Together with his Earth Science colleagues, John developed teaching materials including an idealized stratigraphic column stretching from Archean gneiss to the Absaroka Volcanic caprock and younger strata (detail in Fig. 3). Although John passed away in 2008, he conveyed his passion for the site to his son Cliff at an early age. Cliff accepted a teaching position at MSU in what was then called the Department of Plant and Soil Science in 1975; Cliff is currently an emeritus professor in what is now the Department of Land Resources and Environmental Sciences (LRES).

Cliff Montagne refined his father's fieldtrip materials, and identified, characterized, and built the basis of this fieldtrip for his introductory soils and pedology

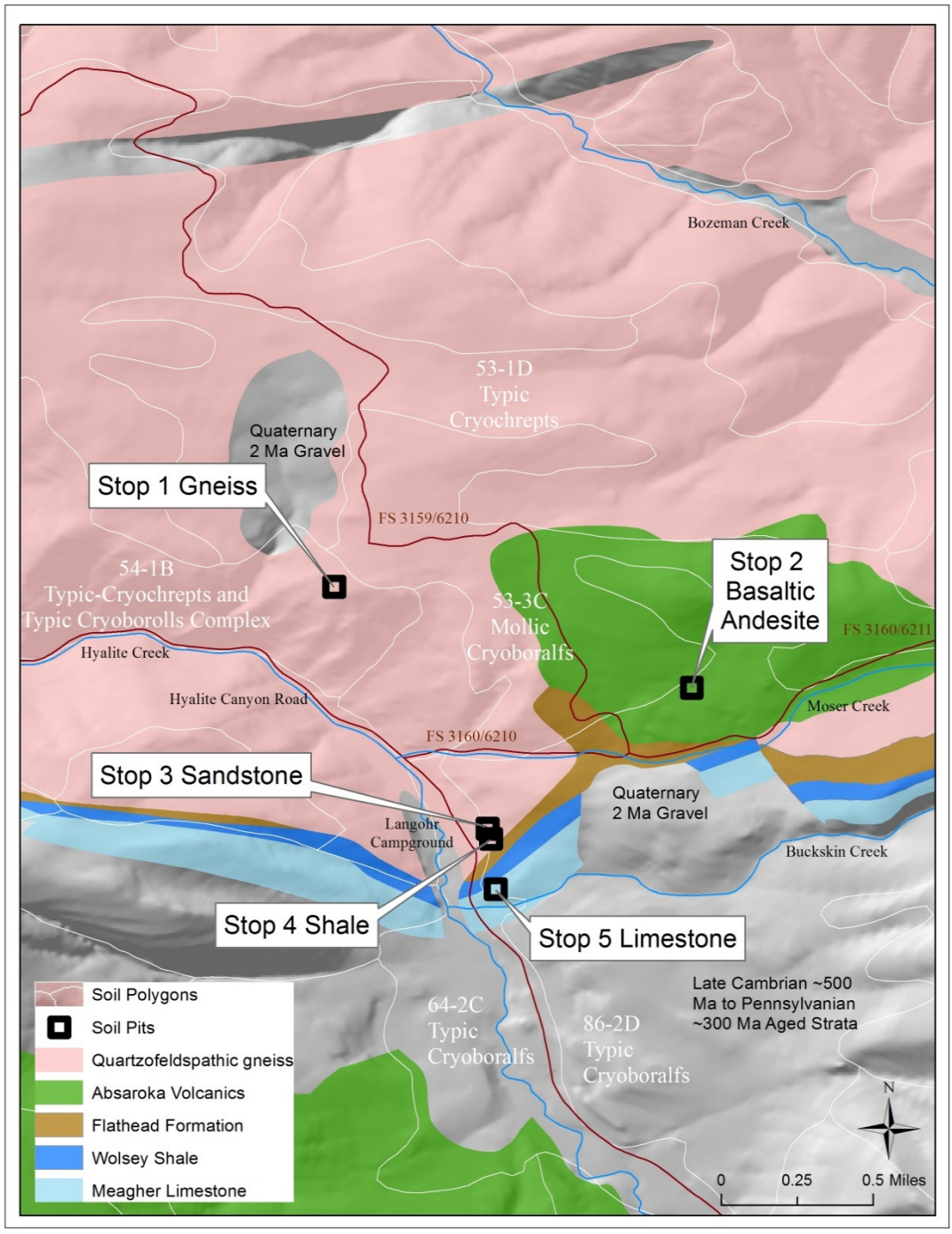

Figure 2. Soil and geologic map of the Hyalite Canyon lithosequence (soil profile locations are represented with bolded squares). Soil map units (polygons) from the 1996 survey are outlined in white (see text); geologic map units (colored regions; 1:100K) are presented at 1:24K to match site details. As a result, boundaries between map units appear to be shifted slightly north and west of their true locations.

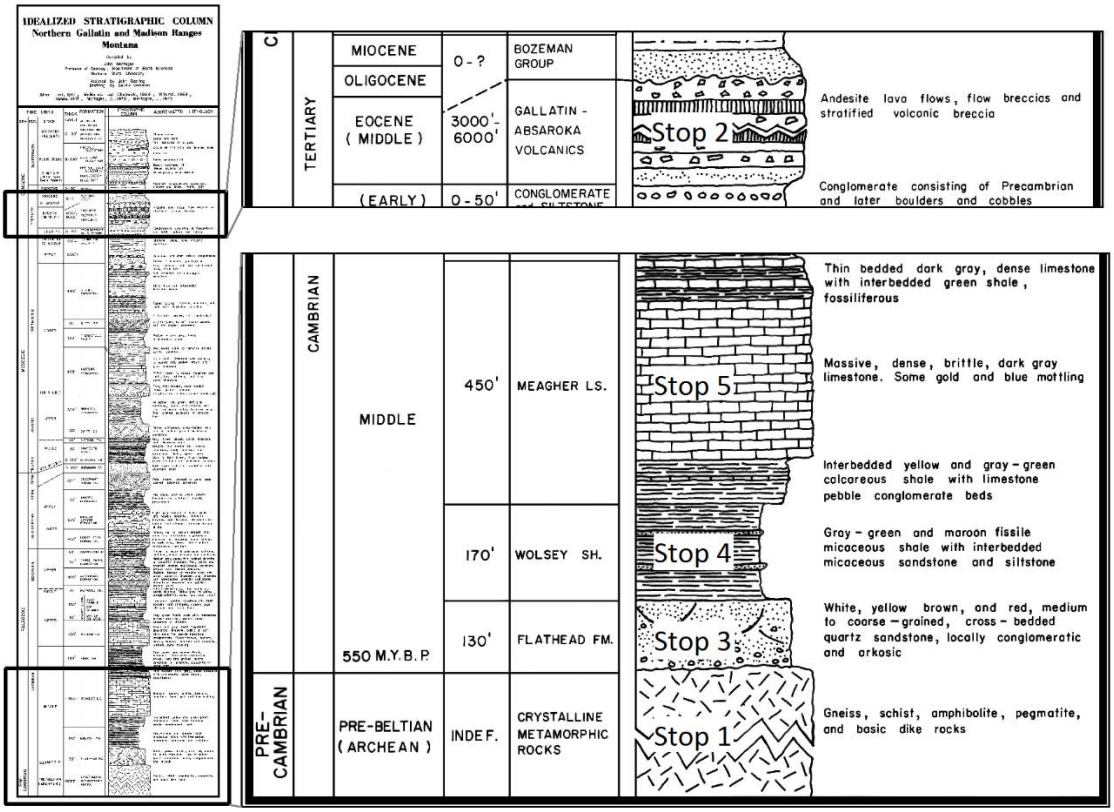

Figure 3. Detail from an idealized stratigraphic column for the northern Gallatin Range (Montagne 1975; full version at http://serc.carleton.edu/research_education/trail_guides/hyalite.html). The five stops on this fieldtrip are indicated; for logistical reasons, we will visit the gneiss soil first, volcanic soil second, sandstone soil third, shale soil fourth, and limestone soil last, out of stratigraphic sequence.

courses. An abridged version of this fieldtrip still forms a core learning experience today, almost 40 years after it was first developed. (Decades of Langohr fieldtrips have carved clearly visible trails in satellite imagery zoomed and centered on 45° 31.993' [N], -111° 0.861' [W].) Together with Jerry Nielsen and Larry Munn, faculty colleagues, Cliff has studied the influence of bedrock lithology, bedrock structure, and geomorphic process on landform, vegetation, and soil properties in this area (e.g., Montagne and Munn, 1980). How fire might interact with lithology to influence post-fire sediment yields remains

unclear, but we will discuss recent GNF-specific findings quantifying forest vulnerability to climate change (Louie, 2013) as well as ongoing research into post-fire responses of volcanic- vs. gneiss-dominated watersheds burned in August 2012 five miles west of this lithosequence. The City of Bozeman also has an interest in mitigating effects of future fires (and any subsequent sediment impairment of water quality) near the Hyalite Reservoir (optional roll-by Stop 6) because this reservoir supplies a large fraction of Bozeman's drinking water. Both the Earth Science and LRES Departments continue to bring students to Hyalite to bolster interest in—and expand our understanding of—soil-landscape relationships.

Prior Soil Survey Efforts Across the Gallatin National Forest

Gallatin National Forest soils have been surveyed (Montagne and Munn, 1980; Davis and Shovic, 1996) and we summarize those findings here. In the mid-1970s, the USFS inventoried soils across the GNF by collecting and characterizing samples from 98 soil profiles for a range of properties including coarse fragments (> 2 mm), Munsell color (hue, value, chroma), texture (proportion sand, silt, clay [particles < 2 μm]; by hydrometer), and structure (grade, size, type: "moderate medium subangular blocky"). Soil survey analyses also included additional physical (e.g., laboratory determination of plant-available water: -33 kPa>ψ >-1500 kPa) and chemical properties (e.g., pH, Bray phosphorus, base cation saturation, organic matter, and electrical conductivity [EC]).

Geological group	Horizon	% Clay	% Plant-available water	pH	% Base cation saturation	% Organic matter
Granitic	A	15	11	5.9	47	2.6
	C	12	6	6.4	66	0.8
Sandstone	A	18	12	5.7	41	2.7
	C	--	--	--	--	--
Shale	A	30	11	6.1	58	4.7
	C	30	6	7.6	100*	1.3
Limestone	A	25	13	7.0	81	6.3
	C	18	11	8.1	100*	0.5
Volcanic	A	17	15	6.0	51	3.6
	C	39	14	6.6	12	0.5

*Reported as >100%.

Table 1. Selected physical and chemical properties of selected soil horizons in the Gallatin National Forest (Montagne and Munn, 1980: Table 49). Samples represent <2 mm material. All values are averages of geological groups; groups are presented in inverted stratigraphic order.

These soil survey results were analyzed and relationships between soil properties and eight geological groups were summarized. Table 1 presents results for the five groups that most closely correspond to those we will visit on this fieldtrip: A horizon clay content ranged from <15% in granitic soils to >30% in shale-derived soils; A horizon pH ranged from 5.7 (sandstone-derived soils) to 7.0 (limestone-derived soil); and A horizon organic matter ranged from 2.6% (granitic rock-derived soils) to 6.3% (limestone-derived soils; Table 1).

The five soils we will visit are mapped as components of three soil map units (Fig. 2; gneiss: 53-1D; sandstone/shale/limestone: 64-2C; and volcanic: 86-2D). Each map unit is composed of subgroup taxonomic classifications as well as unclassified areas mapped as rock. For example, the gneiss soil (Stop 1; Fig. 2) map unit is comprised of a complex of two subgroups, Typic Cryochrepts and Typic Cryoborolls; the sandstone/shale/limestone profiles (Stops 3-5) are mapped as two subgroups, Typic

Cryoboralfs and Argic Cryoborolls, associated with floodplains and terraces; and the volcanic soil (Stop 2) map unit includes two subgroups, Typic Cryoboralfs and Mollic Cryoboralfs. While these classifications are no longer current, we have listed them here to match current online soil maps of this area (http://websoilsurvey.sc.egov.usda.gov/App/HomePage.htm or http://casoilresource.lawr.ucdavis.edu/gmap/). Our five soils (gneiss-sandstone-shale-

Soil	Taxonomic Classification	Taxonomic Level	Formative Element/Explanation
Stop 3: Sandstone	Inc**ept**isol	Order	ept/Weakly developed soil
	Cry**ept**	Suborder	cry/Cold soil temperature regime
	*Haplo*cry**ept**	Great group	haplo/Relatively undistinguished; a *Dystro*cryept, by contrast, would refer to a soil with <50% base cation saturation
	Typic *Haplo*cry**ept**	Subgroup	typic/Relatively undistinguished at the subgroup level
Stop 4: Shale	M**oll**isol	Order	oll/Well-developed soil with a thick, dark surface horizon and generally base-cation rich and fertile
	Cry**oll**	Suborder	cry/Cold soil temperature regime
	*Haplo*cry**oll**	Great group	haplo/Relatively undistinguished; an *Argi*cryoll, by contrast, would imply the presence of translocated (illuvial) clay in a subsurface, argillic horizon
	Aquic *Haplo*cry**oll**	Subgroup	aquic/A wetter soil with reducing conditions

Table 2. Current taxonomic breakdown of two lithosequence soils to illustrate how formative elements propagate into lower order (e.g. subgroup) classifications. Explanations are based on Keys to Soil Taxonomy (Soil Survey Staff, 2010).

limestone-volcanic) would currently be classified to the subgroup level as Typic Dystrocryepts, Typic Haplocryepts, Aquic Haplocryolls, Lithic Haplocryolls, and Typic Haplocryolls, respectively.

For those unfamiliar with hierarchical US soil taxonomic nomenclature, we use two of these current soil classifications to provide examples of how soil properties are used to classify soils (Table 2). We echo recent calls to include soil taxonomic information across a broad spectrum of studies (e.g., Schimel and Chadwick, 2013). Subgroup classifications represent an intermediate level of detail in this taxonomic system, which includes orders, suborders, great groups, subgroups, families, and series. The series level, while the most restrictive taxonomic designation, is unlike the other classification levels because there is no informational value in a soil series name. One cannot tell if the soil mapped as a "Blackmore" under the MSU Strand Union Building, for example, is an Inceptisol or a Mollisol, although online tools (e.g. Soil Survey Division, Official Series Descriptions: https://soilseries.sc.egov.usda.gov/osdname.asp) enable the rapid decoding of any series name.

The Gallatin National Forest survey results (Table 1) were drawn from soils collected over millions of acres, multiple mountain ranges, and at least 10 landforms, whereas this field trip explores soils across a single ~2-mile (~3-kilometer) transect (Fig. 2). Nevertheless, these results defined relationships between lithology and soil properties, in much the same way as has been done for the state of Montana (Veseth and Montagne, 1980). Soils over gneiss or sandstone are generally acidic and coarse-textured, whereas those formed over limestone, shale, or volcanics are generally less acidic and more fine-textured. Slope stability is influenced by these lithology-texture

relationships (Montagne, 1976). For example, gneiss-derived soils weather to quartz-rich matrices with many coarse fragments, macropores, high infiltration, and limited plant-available water. Gneiss can also contribute high amounts of mica to the soil, leading to poor engineering properties and slope failure (Montagne and Munn, 1980). Shale soils are also often prone to slope failure as well as road or other construction problems, and most landslides in the GNF have been associated with shale or shale-derived, clay-rich soils. We may explore a slope failure (optional roll-by Stop 7) that employs hollow-bore soil nails for stabilization purposes (Lundgreen, 2013).

State Factor Approach

A state factor approach (Jenny, 1941) provides a strong foundation to explore soil processes. Five state factors clarify influences on soil development and soil processes: climate (**cl**), organisms (**o**), relief (hillslope or topographic position, **r**), parent material (**p**), and duration of soil-forming processes (commonly shortened to time [**t**]). "Clorpt" factors account for the diversity of soils on many scales. The soils beneath the MSU campus, for example, have a semiarid climate (cl), grassland vegetation (o), occupy a gently north-sloping interfluve (r), are built of alluvium and eolian inputs (p), and have been developing for thousands of years (t).

The fieldtrip and this field guide consider how soil properties differ when only one factor is altered: parent material. Soils formed across parent material gradients are called lithosequences, across which soil properties can be measured and soil processes inferred. Although the importance of parent material to soils has been studied for more than a century (Dokuchaev, 1879 in Heckman and Rasmussen, 2011), there are relatively

few “pure lithosequence studies in the literature” (Heckman and Rasmussen, 2011: p.99). For example, an 8-fold difference in clay, 60-fold difference in acidity, and 6-fold increase in extractable aluminum were reported across a rhyolite-granite-basalt-dolostone lithosequence in Arizona (Heckman and Rasmussen, 2011). As another example, a 3-fold difference in clay, 100-fold difference in acidity, and 30-fold difference in extractable aluminum were reported for a granite-marble-dacite lithosequence in Greece (Yassoglou et al., 1969).

It is challenging, however, to identify locations where only one state factor is varied across space. As one example, climate (cl) is affected by hillslope position (r), which influences soil residence times (t). As a second example, plant communities (o) often reflect underlying parent material (p). Thus, while differences in lithosequence soils perhaps should not be unambiguously attributed to only varying parent materials when plant communities also differ (Jenny, 1941; Jenny, 1958; Druce, 1959), underlying lithologic differences influence plant communities indirectly through effects on soil texture and nutrient availability.

Langohr Campground Lithosequence:
Climate, Relief & Time Factors

Long-term climate data for our lithosequence can be inferred from the Lick Creek SNOTEL site (3 miles [5 km] southeast of Stop 3; 2090 meters [6855 feet]; north northwest aspect; USDA, NRCS, no date; http://www.wcc.nrcs.usda.gov/nwcc/site?sitenum=578&state=mt). Thirty year (1983-2013) mean annual precipitation is 76 cm (30 in) and mean annual air temperature is -

1.1□C. From 2008-2013, volumetric soil moisture at 7.5 cm averaged 18%; at 100 cm, soil moisture averaged 46%. Over the same time period, soil temperatures at 7.5 cm depth averaged 3.9□C and at 100 cm, 4.5□C, suggesting a cryic soil temperature regime.

All five soils on today's fieldtrip have similar aspects (west or northwest), elevations (1900-2100 m; 6200-6880 feet), and slopes (15-20%). These elements of the climate and relief factors are important, because in this area aspect and elevation interact to control plant community composition (Weaver and Perry, 1978). Although these topographic factors are relatively similar, upslope contributing areas could vary, influencing soil processes. While soil ages are not precisely known, advances by Wisconsinan Hyalite Canyon glaciers are unlikely to have reached these soils. The Bull Lake Glaciation may have extended to within 1 mile of the limestone soil (Stop 5; ~150 to 140 thousand years [ka] ago; Pierce, 2003) according to a map by Weber (1965). These five soils were not glaciated during the Pinedale Glaciation either (~21 ka; Pierce, 2003; Weber, 1965). Long-term denudation rates from Idaho (Kirchner et al., 2001) provide a means of estimating soil residence times; these catchment-averaged, ^{10}Be rates ranged from 55 to 327 Mg km^{-2} y^{-1}, with a median flux of 104 Mg km^{-2} y^{-1} (104 g m^{-2} y^{-1}). Assuming a rock density of 2.6 Mg m^{-3} enables the conversion of a denudation rate of 100 Mg km^{-2} y^{-1} to a volumetric flux of 3.8 x 10^{-8} km^3 km^{-2} y^{-1}, or a landscape lowering rate of 0.04 mm y^{-1}. The quotient of the average soil thickness (average depth to base of C horizons [Table 3]: 74 cm) and this estimated overall lowering rate (0.04 mm y^{-1}) yields an estimated soil residence time of ~19 ky.

Langohr Campground Lithosequence:
Biota & Parent Material Factors

This compositionally broad set of rocks has been expressed as part of a stratigraphic sequence (Fig. 3). Like much of southwest Montana, this area is underlain by ~2750 million-year (Ma) Archean gneiss (STOP 1; James and Hedge, 1980). At the north end of Hyalite Canyon, this gneiss forms steep, sandy, scree-filled hillsides. Further south are three Cambrian (550 to 495 Ma) sedimentary rocks characteristic of shallow marine environments (Lebauer, 1964). The oldest is the Flathead sandstone (550 Ma), which uncomformably overlies Archean gneiss (and whose erosional remnants may have formed this sandstone [Middleton, 1980]). The Flathead sandstone (quartzite) is associated with sandy soils (STOP 3) that support forests dominated by lodgepole pine (*Pinus contorta*) and Douglas fir (*Pseudotsuga menziesii*).

Wolsey shale conformably lies on the Flathead sandstone and was formed as the Cambrian oceanic shoreline moved from west to east (Lebauer, 1964). The soil over Wolsey shale (STOP 4) is clay-rich with nonexpanding illite (Lebauer, 1964). This shale soil also contains sandstone colluvium from upslope and supports meadow-like grasslands containing timothy grass (*Phleum pratense*) and common snowberry (*Symphoricarpos albus*). Just a bit further south, Meagher limestone (STOP 5) lies conformably over Wolsey shale creating thin, fine-grained soils supporting mixed grasslands with islands of Douglas fir. Finally, Tertiary-aged Absaroka volcanics (basaltic andesite) lie unconformably on gneiss and sandstone ~1 mile (1.6 km) northeast of Langohr Campground (STOP 2). Absaroka volcanics in the northern Gallatin Range are generally potassium-poor (<~3% K_2O; Table 3) and composed of layered, andesitic

flows interspersed with breccia (Chadwick, 1970). A pre-Wisconsin glacier may have moved these volcanic rocks underlying the Stop 2 soil profile to their current position (Weber, 1965). Their formation is attributed to lithospheric extension and resulting decompressional melting; rock exposures associated with the Tertiary are found throughout local mountain ranges (Feeley et al., 2002). Near Langohr Campground, fine-grained soils on this rock support lodgepole pine forests and aspen (*Populus tremuloides*) groves.

Parent materials can be either residual or transported (e.g., Schaetzl and Anderson, 2005). Residual parent materials underlie a soil and are best visualized as coherent bedrock. Transported parent materials, by contrast, include glacial moraines, alluvium, colluvium, and finer-grained eolian dust (e.g., loess), with the size of materials scaling with the viscosity of the transporting fluid. If that fluid is a glacier, the viscosity of ice enables the transport of large blocks of material. Lower viscosity fluids such as the water in Hyalite Creek can only transport smaller blocks like cobbles. Air is a relatively low viscosity fluid, and so can typically only transport silt-sized particles (2-50 μm). Wind-transported materials originate as either acute events (e.g., the eruptions of Glacier Peak in present-day Washington ~11,000 years ago [Harward and Borchardt, 1972] or Mazama in present-day Oregon ~7,600 years ago [Zdanowicz et al., 1999]) or chronic events (continuous dustfall).

Here we consider the potential for eolian inputs to these lithosequence soils. Although there are no short- or long-term records of atmospheric inputs to the Langohr Campground area specifically, this site lies halfway between two National Atmospheric Deposition Program (NADP) sites: one in Yellowstone National Park about 60 miles

(100 km) southeast (~1900 m elevation; http://nadp.sws.uiuc.edu/nadpdata/ads.asp?site=WY08) and another in Clancy, about 60 miles (100 km) northwest (~1400 m; http://nadp.sws.uiuc.edu/nadpdata/ads.asp?site=MT07). Wet deposition has been monitored at these sites since 1980 and 1984, respectively. From 2008-2012, combined inputs of calcium (Ca), magnesium (Mg), potassium (K), and sodium (Na) averaged 1.5 and 0.8 kg ha^{-1} y^{-1} for the two stations, respectively, with Ca constituting 68% of these inputs. If these average short-term inputs (~1 kg ha^{-1} y^{-1} or ~0.1 g m^{-2} y^{-1}) are representative of long-term inputs (~20 ky; cf. Neff et al., 2008), and we multiply this total by a factor of 6 to account for the fraction of dust comprised of these four elements (Sugden, J., this study), this would translate to a time-integrated atmospheric mass flux to these soils of 120 Mg ha^{-1}, or 12 kg m^{-2}. Global annual suspended dust sediment estimates vary 50-fold (from 60 to 3,000 Mg yr^{-1}; Tegen, 2003), with reported global dust fluxes (deposition to soils) varying >100-fold (from <1 to >100 g m^{-2} yr^{-1}; Lawrence et al., 2013). Estimated dust fluxes into the southern Rocky Mountains range from 10 to 22 g m^{-2} yr^{-1} (100-220 kg ha^{-1} yr^{-1}; Lawrence et al., 2013), about two orders of magnitude greater than our estimated NADP inputs. This discrepancy could reflect greater fluxes to the southern versus northern Rocky Mountains, uncertainties in the fraction of deposition in the form of other elements (e.g., quartz and feldspar components such as silica [Si], aluminum [Al], and oxygen [O]), or that wet deposition is only a fraction of total deposition. Long-term denudation rates from Idaho (~100 g m^{-2} y^{-1}; Kirchner et al., 2001) help contextualize these eolian inputs, since they are 5- to 10-fold greater than the southern Rocky Mountain eolian inputs.

Underlying Rock Lat./Long. *Tentative Tax. Subgroup*	Horizon	Lower depth (cm)	% Coarse fragments	Moist Munsell color	Texture	% Clay	Structure grade, size, type	pH
Gneiss				10 YR	sandy			
45.54535N /	A/B	10	10	2/2	loam	10	2,m,gr	5.2
-111.02085				10 YR	sandy			
Typic	Bw	29	50	3/4	loam	10	1,f,sg	5.7
Dystrocryept				10 YR	loamy			
	C1	40	60	4/4	sand	5	sg	6.1
				10 YR				
	C2	75	80	6/4	sand	5	ma	5.9
Sandstone				10YR	sandy			
45.533843N /	A	5	20	4/4	loam	10	1,m,gr	5.7
-111.013541W				10YR	sandy			
Typic	Bw1	30	35	4/6	loam	10	2,c,sbk	5.5
Haplocryept				7.5YR	sandy			
	Bw2	50	35	4/3	loam	10	2,c,sbk	5.9
	BC	70	40	5YR 4/3	sand	5	sg	6.1
	C	90	50	5YR 4/4	sand	5	sg	6.7
Shale				10 YR				
45.533483N /	A	28	5	3/2	silt loam	20	3,m,sbk	5.8
-111.01337W				10 YR	silty clay			
Aquic	Bt	74	15	5/4	loam	35	1,tn,pl	5.7
Haplocryoll				10 YR				
	C	83	50	5/3	silty clay	50	ma	5.8
Limestone				10 YR	clay			
45.531488N /	A1	25	80	2/2	loam	35	2,f,gr	7.7
-111.013577W				7.5 YR	clay			
Lithic	A2	35	20	3/3	loam	35	3,m,gr	8.0
Haplocryoll				7.5 YR	clay			
	C	55	70	4/4	loam	35	3,f,abk	8.2
Basaltic				10 YR				
Andesite	A	26	0	3/1	clay	50	abk	6.2
45.530967N /				10 YR	clay			
-111.01315W	Bt1	38	3	4/2	loam	35	2,f,abk	6.2
Typic				10 YR	clay			
Haplocryoll	Bt2	49	10	4/4	loam	35	2,m,abk	6.4
				10 YR	clay			
	C	65	45	5/4	loam	35	3,m,sbk	6.3

Table 3. Selected field-estimated physical and chemical properties for the five soil profiles comprising the lithosequence (Sugden, J., this study), presented in inverted stratigraphic order. Methods and nomenclature per Schoeneberger et al. (2012).

We are not the first group to consider the potential impacts of eolian inputs on soil properties in the Rocky Mountains. John Retzer (1962), for example, noticing silt deposited on snow in Colorado's Fraser Experimental Forest, commented "It is not known to what degree this dust influences soil development, or to what extent it is responsible for the silt and clay measured in the soil profiles."

Fieldtrip Stop Descriptions

Mileage	***Directions*** (coordinates in Table 3)
0.0	Depart from Strand Union Building (West Grant St. and South 8th Ave.) on the Montana State University campus, Bozeman. Proceed 5.7 miles south to Hyalite Canyon Road turnoff via 19th Avenue, which doglegs west ~4.5 miles south of Bozeman.
5.7	Turn left (south) on Hyalite Canyon Road. Proceed another 5.7 miles to Moser Creek Road (Forest Service [FS] road 6210/3160).
5.7	Turn left uphill (east) on Moser Creek Road.
0.5	Proceed uphill (east) on Moser Creek Road to the intersection with FS 6210/3159.
1.3	Turn left onto FS 6210/3159, proceed 1.3 miles, and park. ***STOP 1***. ***Gneiss soil profile***. *Location:* ~1000 feet (~300 m) west of parking area over a small hill.
1.3	Reverse direction and proceed back to intersection of FS 6210/3159 and FS 6210/3160.
0.2	Turn left uphill (east) onto FS 6211/3160, proceed 0.2 miles, and park. ***STOP 2. Basaltic andesite soil profile***. *Location*: ~1000 feet (~300 m) north of parking area in a meadow.
0.7	Reverse direction to intersection of Moser Creek Road/ FS 6210/3160 and Hyalite Canyon Road.
0.3	Turn left (south) onto Hyalite Canyon Road and then turn right (west) into Langohr Campground. Park near dumpsters. ***STOPS 3-5. Sandstone, shale, and limestone soil profiles, respectively.*** *Locations*: We will first walk to Stop 3, just uphill (~1000 feet; ~300 m) and northeast of the parking area. Stop 4 is ~500 feet (~150 m) south of Stop 3; Stop 5 is ~1000 feet (~300 m) south of Stop 4.
3.9	Following examination of all five soil profiles, there may be an opportunity for two optional stops. The first (roll-by, ***STOP 6***

	Hyalite Reservoir) is accessed by continuing south of Hyalite Canyon Road from Langohr Campground.
8.6	Reversing direction from Hyalite Reservoir (north), a second (roll-by ***STOP 7***) stop will be on our right (east): a slope failure.
1.3	Return to campus by proceeding north on Hyalite Canyon Road until its intersection with 19th Avenue.
5.7	Turn right and proceed east on 19th Avenue as it doglegs north, to intersection with Lincoln or Kagy to return to Strand Union Building.

Site 1 (the gneiss-derived soil) is the highest soil pit in the lithosequence; it is furthest from Hyalite Canyon Road on the edge of a plateau dividing Hyalite Creek from Bozeman Creek. On the drive or walk in, look south for views of Mount Blackmore and the Mummy. West of the parking area, ascend a short steep hill and wander south to a treed summit. The soil pit we will characterize lies just west and a bit north of this summit on the edge of a treed meadow. This profile is poorly developed with very little clay formation and abundant coarse fragments (>50%) starting at just 10 cm; the relatively dark surface horizon is the most acid horizon we will see across the lithosequence.

Site 2 (the volcanic-derived soil) sits on a boundary between a narrow tight meadow and forest close to the intersection of FS 6210 and FS 6211. Soils here are finely textured, hold water, and boggy conditions may be found on the short walk to the soil pit. Relative to the gneiss-derived soil, this soil is much more finely textured and contains far fewer coarse fragments (<10% through 49 cm).

Site 3 (the sandstone-derived soil) is within a stone's throw of Langohr Campground. Cross the road and walk up hill through the meadow and past Stop 4 (shale), heading north just into the trees. Notice how the slopes steepen slightly after

leaving the meadow. Relative to the volcanic soil, this sandstone-derived soil shows much coarser textures and strikingly red colors at depth.

Site 4 (shale-derived soil) is just south of the sandstone pit, in the middle of a broad meadow. The slumping conditions, textural contrast, distinct horizonation, and coarse fragments are just some of the features distinguishing the shale pit from its sandstone neighbor to the north. We will discuss the pronounced vegetative and soil differences between the sandstone and shale soils.

To reach site 5 (limestone-derived soil) descend ~50 m to an obvious roadbed on the contour below the shale pit and walk south toward Buckskin Creek (Fig. 2). Observe the vegetative changes that shift from a distinct meadow to a forested meadow. This soil pit is ~30 m above the trails just before entering the Buckskin Creek drainage below a small rock outcrop. A limestone outcrop on the other side of Hyalite Creek is the same limestone that lies beneath this soil pit. This intermediately textured soil (clay loam) has an unusual configuration of coarse fragments with depth.

Methods

Soils from the lithosequence were sampled and described following standard methods (Schoeneberger et al., 2012). We will have an opportunity to practice many of these characterization techniques on the fieldtrip, including the definition of horizon boundaries, coarse fragments, soil colors, soil textures, soil structure, root densities, pore densities, pH and EC, and effervescence. For the analyses presented below, two liters (less in thin or very rocky horizons) of soil and rock from each horizon were collected. Soil pH and EC were determined using a portable combination pH/EC meter submerged

in a 1:10 ratio of soil to deionized water. To support this study, we also characterized four samples to serve as proxies for dust inputs to the lithosequence: (i) a relatively unweathered, silt-rich, C-horizon sample of eolian loess from ~1 m depth at the Arthur M. Post Agricultural Experiment Station west of Bozeman ("PF4"; Fig. 1); (ii) a grab sample from a thick volcanic ash packet exposed in Fall 2013 from Helena, ~100 miles north; (iii) a grab sample from the 5th floor roof of the MSU Bobcat Stadium ("BS5"; Fall 2013; Figure 1); and (iv) a grab sample from the 6th floor roof of the same stadium ("BS6"; Fall 2013). Post Farm lies within a transect of five eolian soils characterized as a climosequence, with the most eastern and wettest soil characterized mineralogically (Bourne and Whiteside, 1962). Soil and dust samples were air-dried, and passed through a 2-mm sieve. Textures and clay estimates are from field-texturing.

Of the 38 samples collected to support this study, 28 were soil, six were rock and four were dust; ~50 gram samples were sent to ALS Laboratories (Reno, NV) to determine the concentrations of eight major elements (Si, Al, iron [Fe], Ca, Mg, K, Na, and phosphorus [P], all expressed here on a percent oxide weight basis) by inductively coupled plasma mass spectroscopy. Loss on ignition (LOI) was obtained after 20 minutes at 1000°C. Because rare earth elements (REEs) can be sensitive indicators of material provenance, and so provide a means of chemically fingerprinting soils (Muhs et al., 2008; Nakase et al., 2014), all samples were also analyzed for 5 minor elements (all expressed on a mg kg^{-1} weight basis; europium [Eu], gadolinium [Gd], lanthanum [La], samarium [Sm], and ytterbium [Yb]), all by inductively coupled plasma atomic emission spectroscopy. Analytical uncertainties (as average coefficients of variation [CV] for five

pairs of duplicate samples) were ±7% for major elements except for Ca, Na, and P which were 20, 20, and 13% respectively, or ±10% for the five REEs.

To chemically fingerprint the soils, we calculated two REE ratios. First, however, all soil, rock, and dust REE concentrations were normalized to REE concentrations in chondrite meteorites, which best represent unaltered igneous materials (Taylor and McLennan, 1995). We normalized REE using these corresponding chondrite concentrations: Eu 0.0563, Gd 0.199, La 0.237, Sm 0.148, and Yb 0.161 (McDonough and Sun, 1995). We then calculated the europium anomaly as $Eu^{*} = (Sm_N * Gd_N)^{0.5}$, where Sm_N and Gd_N represent chondrite-normalized Sm and Gd. Our first geochemical ratio is simply Eu_N/Eu^{*}. Our second geochemical ratio is chondrite-normalized lanthanum (La_N) to ytterbium (Yb_N), calculated as La_N/Yb_N. Positive Eu anomalies suggest oceanic crustal origins and mafic rock, whereas negative Eu anomalies are indicative of upper continental origins and felsic rock (Taylor and McLennan, 1995). La_N/Yb_N ratios determine the amount of fractionation between light REE and heavy REE. Higher La_N/Yb_N ratios (>20) can indicate an enrichment of light REE (Muhs et al., 2008).

Results and Discussion

The five soil profiles we will characterize exhibit measurable differences in physical and chemical properties (Table 3). For example, coarse fragments, textures, and colors show large shifts both with depth and across rock types. On this fieldtrip and in this field guide, we will discuss the processes most likely to have produced these patterns.

The soils on gneiss and sandstone have predominantly sandy or sandy loam textures. These coarse textures minimize soil surface area and reduce water holding

capacity, which can ultimately slow soil development relative to the development of finer textured soils. In other settings, however, coarser textures could lead to greater translocation of materials, resulting in greater soil development (e.g., Schaetzl and Anderson, 2005). (Soil textural control of water holding capacity and plant-available water is well-illustrated through an online, interactive tool [Juma, 2012; http://www.pedosphere.ca/resources/texture/triangle_us.cfm].) An important difference between the gneiss and sandstone profiles is the distribution of coarse fragments with depth. Coarse fragments in the gneiss soil profile jump sharply from 10 to 80% by volume (A to C2 horizons), whereas in the sandstone soil profile, coarse fragments increase from 20 to 50% (A to C horizons). These differences may reflect greater bioturbation (vertical mixing by animals or plants) in the sandstone profile relative to the gneiss profile. In fact, we will observe differences in the forests between the gneiss and sandstone profiles: the forest on sandstone appears thicker and to have experienced more windthrow, where trees and their root plates have been blown over, bringing relatively unweathered bedrock and saprolite to the surface. Consistent with greater bioturbation, horizon boundaries are far less clear, and soil colors more uniform—and much redder in hue—in the sandstone soil than in the gneiss soil. Because greater windthrow delivers more weatherable primary minerals (e.g., feldspar) to the surface of the sandstone profile, where chemical weathering can be maximized, this could lead to more rapid and/or intense chemical weathering in this profile.

In the shale and limestone profiles, by contrast, the dominant soil textures are silty clay loams and clay loams, respectively. Generally, the clay-rich soils on shale are less rocky, although we will see evidence of colluvial processes in this profile—the Bt and C

horizons contain coarse fragments consisting of unweathered sandstone. In fact, the sandstone rock sample characterized for this study was actually pulled from a depth of 80 cm in the shale profile (Fig. 4, Table 4). At Stop 4, we will see evidence of solifluction-type slumps within the shale meadow. As a result, roots of larger shrubs and trees may have greater difficulty establishing here. At Stop 5, the soil on limestone is situated below a small limestone outcrop that helps explain the anomalously high rock content (colluvium) throughout the profile, including the surface A horizon (80% coarse fragments). In contrast, the soil on shale has very little rock (5%) in the most mobile A horizon. An important take home message from this fieldtrip will be the critical roles rock fragments play in altering hydrologic pathways and therefore extent and rates of chemical weathering. As Pavich (1986) has noted, "…how climate affects rock weathering is complexly dependent upon soil and rock structure."

Unlike the other two fine-textured lithosequence soils on shale and limestone, the soil on volcanic rock supports stands of Douglas fir, lodgepole pine, and aspen. This soil has relatively high clay content throughout the profile and an abrupt increase in coarse fragments at the transition between B and C horizons. Unlike the existing 1996 soil survey, our profile-specific classifications yielded only two taxonomic orders—Inceptisols (gneiss, sandstone) or Mollisols—and these generally reflected the sharp textural differences (Table 3).

These soils also differ in ways that we cannot observe directly; their elemental composition varies from the surface horizon to bedrock, and between the five profiles (Fig. 4, Table 4). Not surprisingly, Si represents the largest fraction of the rock samples except for the limestone, which was dominated by Ca (47%). Two soils show small, but

clear, reductions in Si from rock (gneiss and sandstone); two soils show large gains in Si (shale and limestone); and the basaltic andesite soil shows a small gain in Si relative to the underlying rock. We interpret these patterns as suggesting differential chemical weathering of the rocks underlying each soil; for example, less weathering of the volcanic rock relative to the sandstone rock could have occurred because of the textural differences of the overlying soils. These patterns could also reflect the incorporation of chemically distinct material as dust or upslope colluvium.

The major elemental composition of the four dust samples also differed from one another (top row Fig. 4; Table 4). These dust samples provide an additional end-member for geochemically fingerprinting A horizons, since these horizons must have formed from a combination of underlying rock and eolian inputs. We quantify the importance of dust to soils with three categories (Yaalon and Ganor, 1973): those composed entirely of eolian inputs (e.g., loess, as appears to be the case at the Post Farm [Fig. 1]); those reflecting comparatively less eolian inputs (e.g., no silt mantle is present); and, finally, those with "eolian contamination." Yaalon and Ganor define eolian-contaminated soils as those where eolian influence can be measured with mineralogical or geochemical fingerprinting techniques, but the eolian material is secondary in importance to the underlying rock material.

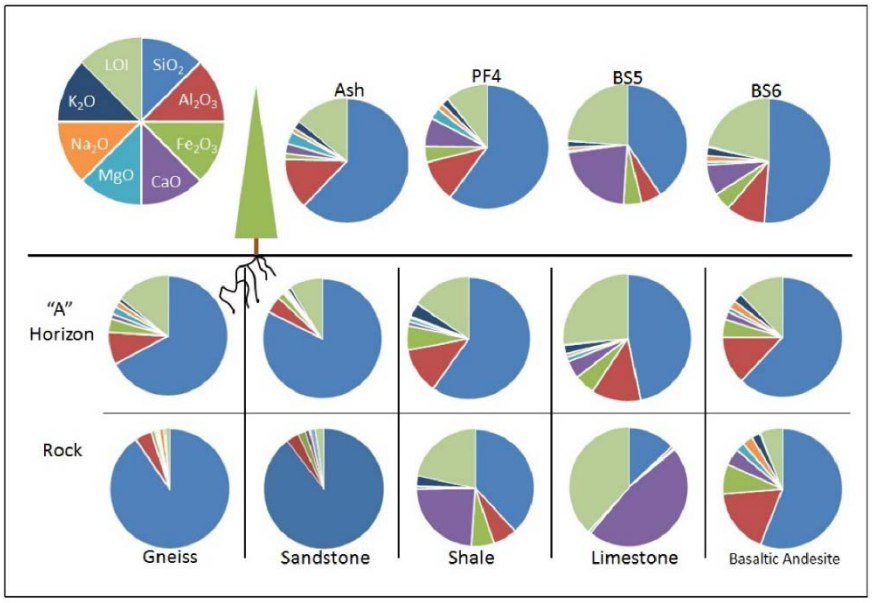

Figure 4. Major elemental composition for rock, soil, and dust across the lithosequence. Raw data are in Table 4. LOI-loss on ignition.

Our REE ratios show that these soils are comprised of varying mixtures of rock and dust (Fig. 5). For example, gneiss soil ratios plot far to the left of the La_N/Yb_N ratios for the underlying gneiss rock (plotted as off-scale in Fig. 5) but overlap with three dust ratios. Similarly, shale soil ratios overlap with dust ratios, but plot to the right of the two underlying shale rock La_N/Yb_N ratios. Limestone soils, by contrast, overlap with both the underlying limestone and dust, particularly the PF4 and BS5 dust samples (Fig. 5, Table 4). (Ratios for these same two dust samples plot most closely to soil ratios from all soil profiles except the volcanic soil profile.) The volcanic soil La_N/Yb_N ratios plot closer to the ratios for the underlying rock than to the dust, but also lie between them. This provides an opportunity to quantify—using Euclidean distances—the fraction rock,

Site/Sample	Horizon	SiO_2	Al_2O_3	Fe_2O_3	CaO	MgO	Na_2O	K_2O	P_2O_5	LOI	Total	Eu	Gd	La	Sm	Yb
Gneiss	A/B	68.1	8.8	3.77	1.44	2.05	1.51	1.18	0.07	14.4	102.0	0.41	1.48	10.9	1.68	0.96
	Bw	77.9	8.2	3.61	1.02	2.91	1.25	1.42	0.03	3.6	100.4	0.27	1.20	8.9	1.28	0.57
	C1	77.9	7.1	4.09	0.63	4.00	0.60	1.65	0.02	3.9	100.3	0.20	0.91	8.3	1.06	0.39
	C2	79.1	7.0	4.00	0.63	3.48	0.75	1.48	0.02	3.6	100.6	0.25	0.99	9.0	1.23	0.59
	Rock	90.3	4.6	1.15	0.54	0.50	1.28	0.54	0.01	1.0	100.0	0.30	0.96	11.6	1.70	0.29
	[C1 dup]	77.9	7.1	4.15	0.59	4.00	0.59	1.64	0.02	3.9	100.3	0.20	0.65	7.4	0.89	0.38
Sandstone	A	82.5	4.6	1.81	0.49	0.41	0.56	0.99	0.07	8.8	100.6	0.49	2.07	15.1	2.15	1.43
	Bw1	87.9	4.7	1.98	0.43	0.41	0.52	1.05	0.07	2.6	100.1	0.55	2.29	19.4	2.67	1.36
	Bw2	89.5	4.2	1.90	0.32	0.38	0.41	1.08	0.05	2.0	100.3	0.56	2.28	18.9	2.83	1.59
	BC	95.8	2.2	1.22	0.16	0.18	0.19	0.63	0.03	0.9	101.6	0.37	1.68	11.9	1.69	1.20
	C	97.6	0.9	1.04	0.03	0.05	0.02	0.27	0.01	0.6	100.7	0.23	1.23	7.2	1.06	0.62
	Rock	90.1	3.4	2.05	1.07	0.19	0.03	1.40	0.06	2.2	100.8	0.78	2.86	12.5	3.42	0.73
	[Bw1 dup]	87.6	5.3	2.28	0.38	0.46	0.59	1.16	0.06	2.5	100.9	0.52	2.59	20.5	3.16	1.68
	[C dup]	96.7	1.0	1.32	0.11	0.05	0.01	0.29	0.02	0.6	100.3	0.27	1.44	7.9	1.25	0.76
Shale	A	59.7	12.2	6.43	1.08	1.02	0.41	3.67	0.23	15.2	100.8	1.44	6.12	40.8	6.32	2.81
	Bt	68.3	12.0	7.16	0.64	0.97	0.33	3.82	0.10	6.7	100.8	1.41	6.00	41.5	6.44	2.88
	C	63.1	14.6	7.45	0.58	1.17	0.22	4.87	0.09	6.7	99.6	1.73	7.07	53.1	8.02	2.99
	Rock 1	37.7	6.5	6.12	23.40	0.62	0.06	2.90	0.08	21.2	99.7	2.10	7.81	26.8	8.58	2.51
	Rock 2	39.1	6.4	5.72	22.90	0.55	0.07	3.11	0.16	20.5	99.5	2.58	10.60	26.3	10.60	3.10
Limestone	A1	46.2	12.4	5.20	4.41	1.20	0.81	2.25	0.33	26.1	99.8	1.20	5.10	40.2	5.75	2.51
	A2	47.6	11.8	4.84	7.71	1.20	0.88	2.06	0.24	21.2	98.3	1.30	5.61	40.0	5.92	2.70
	C	43.4	11.2	4.65	11.15	1.18	0.80	1.94	0.26	23.0	98.3	1.20	5.47	36.6	6.12	2.76
	Rock	13.1	0.7	0.39	47.30	0.69	0.02	0.16	0.03	38.2	100.6	0.13	0.57	4.9	0.62	0.36
Volcanic	A	62.0	13.0	4.79	2.20	1.14	2.08	2.48	0.13	12.2	101.2	1.74	5.54	46.5	6.73	2.71
	Bt1	61.7	14.7	5.28	2.27	1.32	2.16	2.50	0.11	8.8	100.2	1.59	4.71	40.8	5.75	2.52
	Bt2	61.1	15.4	5.55	2.40	1.44	2.17	2.45	0.10	8.8	100.6	1.48	4.23	35.4	5.16	2.35
	C	58.6	15.7	5.77	2.39	1.56	2.11	2.38	0.11	9.2	99.0	1.53	4.14	35.7	5.09	2.31
	Rock	55.1	17.3	7.90	4.47	2.34	2.80	2.28	0.34	5.8	99.7	1.70	4.82	37.6	5.88	1.95
Dust	PF4	60.0	11.0	4.14	7.47	2.88	1.58	1.99	0.21	10.7	100.7	1.24	5.33	38.4	5.53	2.73

BS6	50.2	9.9	4.62	7.78	0.83	1.57	2.16	0.42	20.6	98.8	0.72	2.90	25.6	3.96	1.39
BS5	39.9	5.3	4.75	21.50	0.37	0.90	1.72	0.13	23.4	98.6	0.55	2.36	16.0	2.94	1.09
Ash	62.2	13.2	1.59	2.56	3.13	1.15	2.26	0.03	13.9	100.1	0.07	16.50	18.4	14.30	8.53
[PF4 dup]	59.4	10.5	3.87	7.26	2.71	1.54	1.90	0.19	10.7	98.8	1.20	5.25	38.0	5.51	2.65
[BS6 dup]	51.7	10.0	4.90	7.62	0.85	1.59	2.18	0.42	19.8	99.7	0.77	3.18	27.0	4.40	1.56

Table 4. Major and minor (not normalized) elemental composition of lithosequence soils by morphologic horizon (see Table 3), underlying rock, and four dust samples (Sugden et al., unpublished data). See text for element abbreviations. Major elements are presented as percent oxides; loss-on-ignition (LOI) is also in percent; minor elements (Eu, Gd, La, Sm, Yb) are in mg kg^{-1}. Total column includes eight oxide results and LOI, as well as an additional five elements (data not shown): chromium, titanium, manganese, strontium, and barium. Five duplicate samples are bracketed. Sites are listed in inverted stratigraphic order except for dust samples.

which we estimate at 0.6 for the volcanic A horizon soil. Finally, the sandstone soil La_N/Yb_N ratios plot to the left of *both* dust and rock La_N/Yb_N ratios, with minimal overlap, suggesting the potential for weathering-related shifts in these REE ratios.

Our combination of field observations; the elemental composition of the soil, rock, and dust; and our REE ratios together show pronounced differences in soils across this 2-mile lithosequence. These differences suggest the underlying rock drives soil differentiation, although further research is required to determine whether lithology-driven textural differences lead to selective retention of eolian materials. If so, this would imply that heterogeneity in both parent materials and their chemical weathering lead to complex soil development pathways over the very fine spatial scales of this lithosequence.

Future Directions

This field trip and field guide illustrate the influence of parent material on soil properties. It is, as with any field study, a Rumsfeldian effort: we go to the field with the tools (field and laboratory data, a state factor approach) and sites we have, not with the tools and sites we want or wish we had at a later time (e.g., Suarez, 2004). We look forward to building on this fieldtrip in several ways and include these future directions to promote further discussion.

First, we are eager to explore ways of separating the biota and lithology factors. Despite the possibility of variable dust influence on soils, texture and vegetation community differences could affect whether and how soils incorporate long-term dust

inputs. For example, a relatively high concentration of clays associated with weathering of shales could slow incorporation of dust inputs into the soils overlying shale; conversely, we could expect greater incorporation of dust into the more quartz-rich soils with high infiltration capacities associated with the gneiss and sandstone profiles. Textural control on the fate of eolian inputs—whether these are integrated into the soil or simply washed downslope—could derive from the underlying rock, weathered dust, or their combination. Differences between the forest-dominated sandstone and grassland-dominated shale provide an additional complication to quantifying dust inputs, since the much greater leaf area associated with the forest could serve as a more effective dust trap, funneling eolian inputs into these soils.

Second, we look forward to determining particle size distributions and particle size-specific (e.g., silt and clay) mineralogy for these lithosequence soils as these physical and mineralogical fingerprinting approaches complement our geochemical fingerprinting method (e.g., Muhs et al., 2008). A useful target across this lithosequence could be Mazama glass. Third, once we have completed our measurements of soil bulk densities, we can calculate mass fluxes, both on an individual element basis and total mass basis. Finally, quantifying total denudation rates would enable the definition of both chemical weathering as well as physical erosion rates (Riebe et al., 2003). We recognize the lithologic limitations to this technique as only the gneiss and sandstone are likely to have the requisite quartz, but we could also use fallout nuclides to measure erosion via mixing rates (Dixon et al., 2009; Kaste et al., 2007). Either approach would

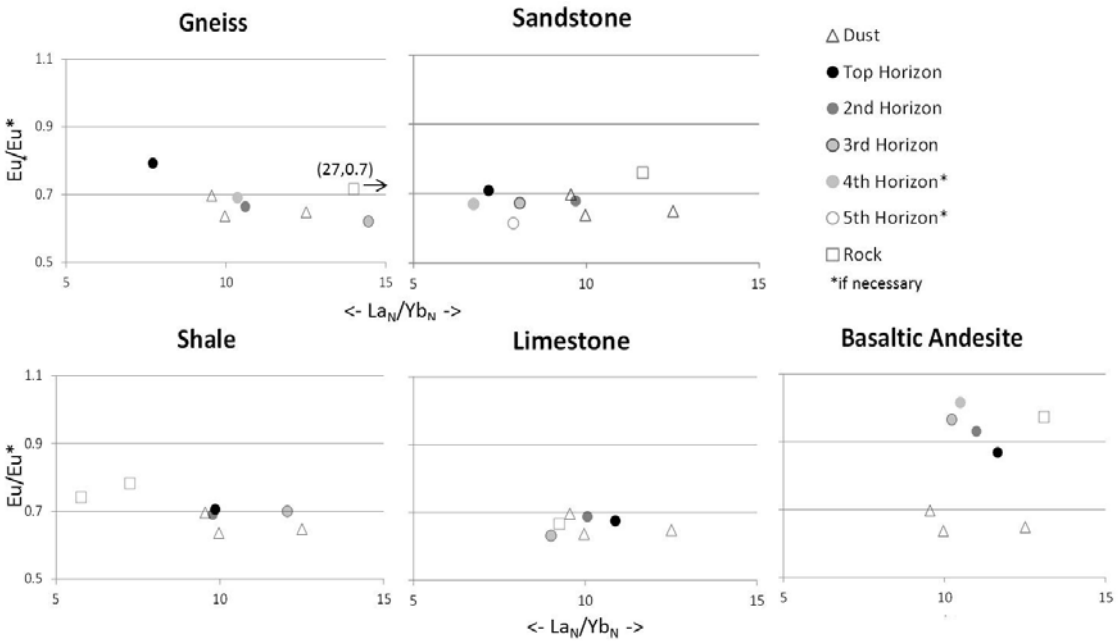

Figure 5. Chondrite-normalized europium to europium anomaly ratios (y axis; see text for details) versus chondrite-normalized lanthanum to ytterbium ratios (x axis) for the five soil profiles. Note two samples are omitted for clarity: the gneiss rock had corresponding values of 27 and 0.7 (indicated) and the Helena ash sample had corresponding x, y values of 1.5 and 0.01, respectively (not indicated).

build on prior regional efforts (^{10}Be: Licciardi and Pierce 2008; ^{137}Cs: Arnalds et al., 1989).

Conclusions

This fieldtrip to a lithosequence in the Gallatin National Forest continues a tradition begun decades ago with the efforts of John Montagne to use Hyalite Canyon for hands-on, in-field learning. For this fieldtrip, we apply a state factor approach to soils formed from a spectacular stratigraphic sequence of five rock types: gneiss, sandstone, shale, limestone, and basaltic andesite. Field and laboratory data showed the influence of rock on soil properties, revealing clear differences. Although this heterogeneity could

imply eolian materials are not an important influence on soil properties, lithology-driven vegetation and texture differences could lead to uneven retention (and consequent weathering) of any eolian materials. Where eolian inputs are sufficient in both duration and magnitude, a readily observable (and geochemically distinct) silt mantle can form, but we do not observe this across this lithosequence. The differences we observe in underlying parent materials appear to control the coarse fragment content of soil profiles, altering soil hydrology, and ultimately contributing to striking soil differences across this lithosequence.

Acknowledgements

We thank the following colleagues for their constructive reviews of earlier versions of this manuscript: Cory Cleveland, Stephanie Ewing, Paul McDaniel, Larry Munn, Jerry Nielsen, Jay Norton, Todd Preston, and T. Weaver. We thank Tom Howes and Ron Wiens for their help collecting dust samples. These fieldtrips would not have been possible without the cooperation and support of the Bozeman Ranger District, U.S. Forest Service. This work was funded in part by the MSU Vice President for Research, the MSU College of Agriculture, and a Faculty Excellence Grant (Hartshorn). We are also appreciative of over 40 years of students' and colleagues' questions, critiques, and discussions of portions of this fieldtrip and the ideas they have sparked.

CHAPTER THREE

3. TRACE ELEMENT FINGERPRINTING OF PARENT MATERIAL INPUTS ACROSS A SOIL LITHOSEQUENCE

Contribution of Authors and Co-Authors

Manuscript in Chapter 3

Author: J.C. Sugden

Contributions: Led study design, analyzed data, collected and processed samples, wrote manuscripts, designed figures

Co-Author: S.A. Ewing

Contributions: Helped to inspire study design, helped to revise manuscript

Co-Author: A.S. Hartshorn

Contributions: Mentored study design, provided funding and support, revised manuscript, edited figures

Manuscript Information Page

J.C. Sugden, S.A. Ewing, A.S. Hartshorn
Geoderma
Status of Manuscript:
_x__ Prepared for submission to a peer-reviewed journal
____ Officially submitted to a peer-review journal
____ Accepted by a peer-reviewed journal
____ Published in a peer-reviewed journal

Elsevier

Abstract

Soil landscapes are built from the addition, breakdown, retention, and loss of parent material. We quantified how chemical weathering of one parent material, underlying rock, appears to alter the incorporation, retention, and weathering of non-rock or exogenous parent material inputs across a southwest Montana lithosequence. Potential exogenous inputs include atmospheric deposition and colluvial materials. Along this 3-km lithosequence, soils are underlain by five distinct geologic formations: gneiss, sandstone, shale, limestone, and basaltic andesite. Our work suggests that fractional parent material influences depend on which elements or ratios were used requiring the development of a framework to address the strength of a particular ratio and its ability to represent chemical weathering in a soil horizon. We developed a difference between factors of enrichment (DEF) to assess the strength of each ratio on each horizon. We evaluated concentrations and ratios of trace elements in an effort to quantify the fraction of surficial soil horizons sourced from underlying rock versus exogenous materials, and then used those fractions to estimate mass losses indexed to immobile elements. For example, using our atmospheric deposition proxy as a second parent material, fine-textured soils overlying limestone and basaltic andesite appear more than 0.7 rock-influenced with horizon specific rock influences varying from 0.71 to 0.92, whereas soil on shale appeared half rock-influenced with horizon specific rock influences ranging from 0.48 to 0.59. Coarse-textured soils over gneiss and sandstone appeared half to 0.6 rock-influenced with horizon specific rock influences ranging from 0.35 to 0.92. Indexed only to underlying rock, the greatest mass losses (-2855 kg m^{-2}) were observed for

limestone soils, roughly ten times greater than mass losses from gneiss soils. Incorporating exogenous parent material generally reduced total mass losses, with the greatest mass loss observed for limestone soils (-2146 kg m^{-2}) and smallest mass loss for gneiss soils (-113 kg m^{-2}). Our work suggests (i) differential weathering of the underlying bedrock has created different depositional settings for exogenous inputs such as atmospheric deposition and colluvium and (ii) mass losses calculated entirely with respect to underlying bedrock can overestimate losses by between 13 to as much as 245%, most strikingly in soils on sandstone and shale. Ultimately, our lithosequence approach shows there are important interactions between bedrock geochemistry, chemical weathering of this substrate, and retention of exogenous inputs.

Introduction

The Earth's terrestrial surface reflects the long-term sculpting of landscapes through physical erosion and chemical weathering, and these sculpted surfaces provide food, fiber, and other environmental services. Soils are built from the breakdown of parent material, but estimates of the rates at which soils are built (and eroded and/or weathered) are often complicated by the impossibility of pinpointing a soil's full set of parent materials over the lifetime of a soil, particularly where a soil's residence stretches into millennia. Aside from daily inputs of organic matter, many soils also receive ongoing inputs geochemically unrelated to underlying rock. For example, valley-bottom soils might receive retransported colloidal material, including material that has been atmospherically deposited higher in the watershed (e.g., dust that may be restricted to silt-sized particles, i.e. loess), material that has been deposited and retransported by streams

or rivers (e.g., alluvial or fluvial deposits), or material that has moved colluvially down a hillslope or catena). Because of these complexities in shifting parent material inputs over time, soil mass balance calculations are often dependent on assumptions regarding the composition and temporal flux of these inputs to a soil. Recent advances in mass balance approaches using immobile elements have improved our understanding of the importance of exogenous inputs to soils (e.g., Brimhall and Dietrich, 1987; Chadwick et al., 1999; Ewing et al., 2006; Ferrier et al., 2011; Lawrence et al., 2013), but clarifying chemical weathering effects on these exogenous inputs can be challenging without additional geochemical characterization (e.g. Kurtz et al., 2001; Muhs et al., 2008).

Soil development modifies materials at the surface via physical erosion and chemical weathering. Physical erosion moves all surface materials downslope, while chemical weathering is more selective with immobile elements retained in soils while soluble or mobile elements are lost to ground or surface waters. This retention, and subsequent residual enrichment, of immobile elements is what allows their use to index extent (e.g., chemical depletion fractions) and rates of chemical weathering (e.g., Dixon and Riebe, 2014). For example, soil chemical weathering can be quantified by comparing concentrations of immobile elements in unweathered parent material such as underlying rock and the concentrations of the same elements in weathered soil. In general, because chemical weathering attacks primary minerals containing alkali and alkali earth elements and these elements are then removed from the soil profile either through leaching or plant uptake, chemical weathering is typically associated with a residual enrichment—an apparent concentration increase—of immobile elements and/or

high field strength elements (HFSE) due to a low ionic potential and a small radius combined with a high charge and therefore a high electrical field (Salters, 1998: 209-210). Greater durations of chemical weathering and/or conditions that facilitate more intense chemical weathering can often lead to high residual enrichment of immobile elements, such as transition metals like titanium (Ti), zirconium (Zr), niobium (Nb), and rare earth elements (REE): yttrium (Y), gadolinium (Gd), terbium (Tb), dysprosium (Dy), holmium (Ho), erbium (Er), thulium (Tm), ytterbium (Yb), and Lutetium (Lu) (Taylor and McLennan, 1995, 13). As REEs and other specific trace elements are generally immobile, comparisons of elemental concentrations and concentration ratios in soils and candidate parent materials have been used to determine soil provenance (Taylor and McLennan, 1985; Kurtz et al., 2000; Muhs et al., 2008; Pierce et al., 2011; Heckman and Rasmussen, 2011; Ferrier et al., 2011). Many sources suggest that HFSE and REE serve as ideal candidates for soil parent material and mass balance studies, yet only few (Kurtz et al., 2000) assess elemental immobility before running mass balance.

Because of mixing and weathering processes in soil, atmospheric inputs may be difficult to detect in the field and require the use of trace geochemistry of particular elements that best capture weathering profiles in soils on specific lithologies. Specific examples include identifying particles of similar morphology on diverse lithologies, quartz on quartz free basalt, Ti and Zr concentrations that vary between rock and soil, soil quartz with different oxygen isotope ratios than underlying rock, downwind decreases in particle sizes at greater distance from source areas, illite (mica) enrichment in soil compared to underlying rock (Chadwick et al., 1999; Kurtz et al., 2000; Hesse and

McTainsh, 2003; Muhs, 2013). Specifically, Muhs et al. (2008) used particle size variations, mineralogy, and trace and rare earth element ratios to distinguish between felsic Mojave Desert-sourced loess and mafic rock inputs to California Channel Island soils, while Heckman and Rasmussen (2011) used Ti and Zr ratios to account for volcanic cinder additions to soil on dolostone, a sedimentary carbonate rock with abundant dolomite [$CaMg(CO_3)_2$] in Arizona. In some cases, however, these approaches cannot distinguish between geochemically similar aeolian and rock inputs (Yaalon and Ganor, 1973; Ewing et al., 2006; Muhs and Benedict, 2006).

Arguably no bedrock derived soil consists entirely of one parent material due to pervasive aeolian inputs. Wind-transported materials originate as either acute events (such as volcanic eruptions [Harward and Borchardt, 1972; Zdanowicz et al., 1999; Clynne et al., 2005] or glacial episodes [e.g., Pierce et al., 2011]) or chronic events (such as rainfall leading to wet deposition). No records of atmospheric inputs specific to our field sites exist, but records from elsewhere contextualize relative dust inputs to southwest Montana and suggest that western North America is dusty. Recent estimated dust fluxes into the southern Rocky Mountains range from 10 to 22 grams per meter squared per year ($g\ m^{-2}\ y^{-1}$) (Lawrence et al., 2013). Other reported regional dust fluxes (Table 5) range from 4 to 36 $g\ m^{-2}\ y^{-1}$.

Atmospheric deposition is ubiquitous in arid and semiarid climates where it can control geomorphic processes. Regional atmospheric deposition strongly influences geochemistry of the driest soils, whereas it infiltrates and leaches through more humid soils (Ewing et al., 2006). Soil hydrology controls the net loss of materials during soil

Location	Lat., Long.	Deposition Rate (g m^{-2} y^{-1})	Duration (years)	Source
Mesa Verde, CO	37.2, -108.5	36	2	Arrhenius and Bonnatti, 1965
San Juan Range, CO	37.9, -107.7	13	5	Lawrence, unpublished
Coast Mountains, BC	50.4, -122.9	11	1	Owens and Slaymaker, 1997
Front Range, CO	40, -105.5	5	1	Ley et al., 2004
Wind River Range, WY	43, -109.5	4	2	Dahms and Rawlins, 1996
Southern Rocky Mountains, CO	37, -108	10-22	4	Lawrence et al., 2010
Mojave Desert, CA and NV	36, -116	4-16	5	Reheis and Kihl, 1995
Bighorns, MT and WY	44.5, -108	5-12	1	Reheis, 1987a

Table 5. Regional atmospheric deposition estimates (adapted from Lawrence and Neff, 2009).

formation (McFadden and Weldon, 1987; Reheis et al., 1995; Stonestrom et al., 1998; Chadwick et al., 1999). In extremely dry settings, even the most soluble components of atmospheric deposition may be retained (Ewing et al., 2006), whereas wetter settings hasten the loss of soluble components and enhance the incorporation of aeolian and colluvial materials. Soil immobile elemental concentrations and ratios act as a retained record of past rock, colluvium, and loess inputs that can illuminate soil mass balance in more humid locations, whereas soluble portions of loess, colluvium, and bedrock are long gone.

In this work, we use a combination of trace element concentrations and ratios to evaluate the extent to which two parent materials influence soils on five lithologies. As soil conditions vary widely across lithologies and certain settings are best explained by specific trace elements, we used ratios of two elements to determine relative parent

material influence (Muhs and Benedict, 2006; Muhs et al., 2008; Pierce et al., 2011). Use of HFSE concentrations, for the purpose of determining parent material influence, requires the assumption that underlying rock and second parent materials have weathered at similar rates over the same timescales. This is because soil horizon concentrations are subjected to both parent material influence and the extent of chemical weathering. It is also likely that soils receive varying rates of atmospheric deposition. It is for those reasons that we look to ratios of trace elements to limit the distorting effects the extent of weathering has on the concentrations of each immobile element. While chemical weathering will tend to enrich immobile element concentrations, ratios of immobile elements should remain the same as one parent material weathers into soil (Kurtz et al., 2000; Porder et al., 2007). By comparing differences between trace element ratios of rock and other candidate parent materials to soil, we capture a snapshot of the relative influences of each parent on existing soil horizons. In settings receiving atmospheric deposition and colluvial inputs, the underlying rock could become progressively less important – or uncoupled – from dominant soil-forming processes. Trace element ratios enabled us to see past a soil's trajectory at birth when underlying rock is the only parent material to the point when enough deposition and weathering has occurred that underlying rock may only play a secondary or even tertiary role in soil processes. The widespread uniformity of trace elements, is precisely what makes their ratios good fingerprinting tools. Trace elements such as Ti, Zn, Nb, and REE are often found at low concentrations across a broad range of lithologies, making ratios of these potentially immobile elements (e.g. Ti/Zr) useful for quantifying inputs to soils from an end-member

mixing model (EMMM) approach. In the case where a soil is assumed to have formed from two inputs such as underlying rock and an exogenous aeolian or colluvial input, this approach requires characterization of the Ti/Zr for each of these inputs, as well as the Ti/Zr of the specific soil horizon of interest. An end-member fraction of the underlying rock contribution to a specific soil horizon can then be calculated. With a two end-members, the fraction of the non-rock parent material can be obtained by difference from one. An understanding of parent material inputs garnered from ratios of immobile elements provides an increased understanding of weathering of major soil elements. Major elements include (n=8: silica [SiO_2], aluminum [Al_2O_3], iron [Fe_2O_3], calcium [CaO], magnesium [MgO], sodium [Na_2O], potassium [K_2O], and phosphorus [P_2O_5]).

Sugden et al. (2014) reported major elemental concentrations (n=8: SiO_2, Al_2O_3, Fe_2O_3, CaO, MgO, Na_2O, K_2O, and P_2O_5) and minor elemental concentrations (n=5: europium [Eu], gadolinium [Gd], lanthanum [La], samarium [Sm], and ytterbium [Yb]) for lithosequence soil profiles. In summary, REE were chondrite-normalized (e.g., Eu_N, McDonough and Sun, 1995) and used to estimate the fraction of aeolian input to A horizons across the lithosequence via a graphical analysis of Eu anomalies (Eu_N*) and La_N/Yb_N ratios (sensu Muhs et al., 2008) for rock, loess, and soil samples. Sugden et al. (2014) suggested that while the approach was potentially useful for surface soils overlying basaltic andesite (estimated fraction aeolian input = 0.4, fraction underlying rock input = 0.6), however it was not useful across the remaining four lithologies. This shortcoming has served as a motivation for the present study.

Lithologic differences can create soil matrices that retain exogenous inputs (loess and/or colluvium) differently. For example, differences in soil textures and coarse fragments could control the duration between the deposition and retention aeolian materials and movement of colluvium in and through soil profiles. Additionally, atmospheric deposition may then be subjected to different durations of weathering on each lithology resulting in increasingly different mass losses due to varied underlying rock and aeolian and colluvial materials. This study aims to quantify rock influences on soil texture and soil textural influences on aeolian deposition and colluvium. How does bedrock weathering influence the fate and transport of inputs of atmospheric deposition and colluvium? Here we take advantage of a representative lithosequence in southwest Montana (fig. 1a) and explore the use of immobile elements to further quantify aeolian, colluvium, and bedrock inputs to soils.

Methods

Field Design and Sampling

Just ~25 kilometers (km) south of the Montana State University (MSU) campus in Bozeman, five stratigraphic units, each representing a distinct parent material, were used to develop a soil lithosequence (fig. 6b; Vuke et al., 2002) in order to explore how variations in this one state factor (sensu Jenny, 1941) are manifest in soil properties. As described previously and summarized here, the other four state factors (climate, biota, relief, and time) are comparable across this lithosequence (Sugden et al., 2014) with one exception. All soils receive mean annual precipitation (MAP) of 76 centimeters (cm) and

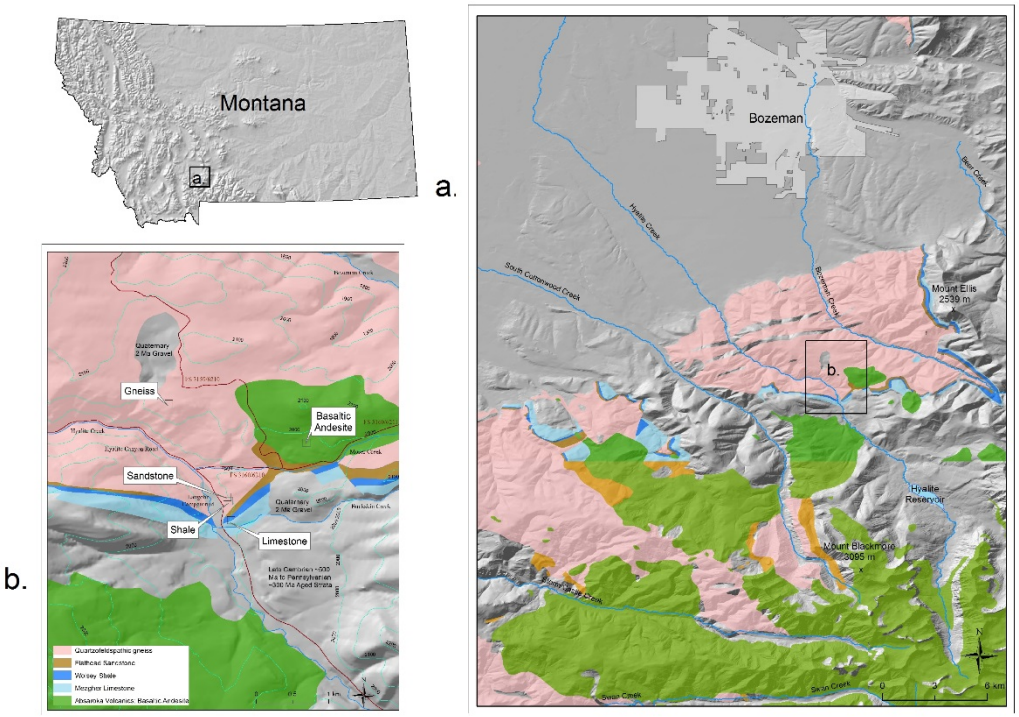

Figure 6. General study location in **(a)** southeast corner of the Gallatin Valley of southwest Montana showing the **(b)** five soil profile locations and general lithologic trends. Original mapping (Vuke et al. 2002) was performed at a 1:100,000 scale covering 1800 km^2, which introduces artifactual offsets in lithologic boundaries at the much finer 1:24,000 scale (~3 km^2) of inset (**b**). One consequence of this downscaling is sandstone and shale soil profiles plot over the gneiss unit.

have mean annual air temperatures (MAAT) of -1.1^{0}C since all soils lie between 1900 to 2100 meters in elevation within a roughly ~3-km transect; four of the five soils support forests dominated by lodgepole pine (*Pinus contorta*), while the shale soil is dominated by sedge meadow vegetation (the state factor exception across the lithosequence); all five soils have westerly aspects on 15-20 percent slopes; the similarities in slopes and

geomorphological settings suggest similar soil residence times of ~19,000 years (Sugden et al., 2014).

A range of soil conditions were observed in the five lithosequence soils. The lithosequence (Figure 6) brackets soils on silica rich (gneiss and sandstone) and mafic (basaltic andesite) end-members, two types of clastic sedimentary rocks (sandstone and shale), and a chemical or organic sedimentary rock (limestone) (Schaetzl and Anderson, 2005: 179-183). These five types of parent material are unlikely to chemically weather at the same rates, and the different mineralogical compositions of each parent material likely yield a range of soil textures. Transported parent materials, by contrast, include fine-grained atmospheric deposition by wind (e.g., aeolian loess) or colluvial inputs by gravity, which could range from solutes to colloids to coarser gravels, cobbles, and boulders. The five neighboring lithologies create five pairwise settings to receive, weather, and/or retain exogenous inputs.

Each of the five soil profiles occupy similar slopes and aspects and we assume soil production and physical erosion are in steady state equilibrium and therefore not getting thicker or thinner. On hillslopes where erosion and soil production from underlying rock are equal, soils have a constant thickness (Heimsath et al., 2005; Dixon et al., 2009). Second, we assume that for the landscape contour that our sampled soils are representative of, mass in from upslope colluviation (run-on) = mass out (run-off).

We average three samples to serve as one model proxy for atmospheric deposition to these soils: (i) a relatively unweathered, silt-rich, Ck-horizon sample of loess from ~1 m depth beneath a calcic horizon at the Arthur M. Post Agricultural Experiment Station

west of Bozeman ("PF4"); and (ii) two grab samples from Floor 5 ("BS5") and Floor 6 ("BS6") (collected in fall 2013) of Montana State University's Bobcat Stadium. We assume the examples of atmospheric deposition are the same as the materials the atmosphere likely deposits in study area soils. We chose to omit two samples of atmospheric deposition: one Bobcat Stadium sample (collected in fall 2014 to explore temporal variability for one sample location) because it was a lumped sampled from both sites sampled in 2013 due to limited sample size. We did not include the volcanic ash sample because of its geochemically anomalous profile. For example, ash Ti, Zr, and Nb concentrations were 420, 214, and 103 mg kg^{-1} (Appendix B), respectively, yielding Ti/Zr, Ti/Nb, and Zr/Nb ratios of 2, 4, and 2, respectively. For reference, across the 19 soil horizons characterized for this lithosequence, corresponding Ti/Zr, Ti/Nb, and Zr/Nb ratios ranged from 3-17, 216-487, and 13-159, respectively. It is of utmost importance to consider the implications of various methods of combining the chemistry of atmospheric deposition samples. The atmospheric deposition chemistry against which soil horizons are compared will undoubtedly drive critical findings. We chose to do a simple arithmetic mean of resulting concentrations of elements from BS5, BS6, and PF4. The roof of Bobcat Stadium is an advantageous sample location for atmospheric deposition characterization: sample locations were 20-25 meters (m) above the ground surface, which should minimize the contribution of very local (e.g. parking lot) inputs; the stadium occupies a topographically high and downwind setting within the Gallatin Valley (~270 m higher and 47 km southeast of the town of Three Forks, where the Missouri River originates at the confluence of the Jefferson, Madison, and Gallatin Rivers), and the

installation of a new roof in 2012 provided temporal constraints on the timing of depositional events, with relatively little opportunity for in situ, post-deposition, weathering and alteration. Therefore sampling done in 2013 represents only one year of atmospheric deposition.

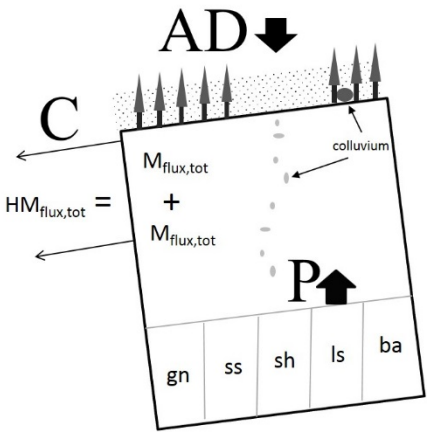

Figure 7. Depiction of soil processes occurring on the five lithologies (gneiss [gn], sandstone (ss), shale [sh], limestone [ls], basaltic andesite [ba]), which interface with atmospheric deposition (AD), soil production (P) due to underlying rock, colluvium (C), and AD. Observed colluvium is sandstone colluvium in soil on shale and basaltic andesite colluvium in soil on limestone. Adapted from Ferrier et al., (2011) and Dixon and Riebe, (2014).

In addition to comparing trace element chemistry of underlying rock, a model atmospheric deposition input, and soil, we explored the potential for specific colluvial inputs between specific lithologies (Figures 6b, 7). For the purposes of this colluvial analysis, we assumed that unweathered rock elemental concentrations or concentration ratios best characterized initial colluvial inputs from an uphill lithologically distinct portion of the project area to a downhill soil profile. As basaltic andesite is the highest elevation stratigraphic unit (serving as the "cap-rock" for the Hyalite Creek Watershed),

it could colluvially influence any down gradient soil horizons, whether they overlie gneiss, sandstone, shale, and limestone. Pitted basaltic cobbles and boulders were found on the surface nearby the limestone soil (J. Sugden, personal observation). Because limestone weathers congruently (Schaetzl and Anderson, 2005: 179; Egli et al., 2008), we did not consider the potential for limestone rock to have any colluvial influence on other soils. Because gneiss is the deepest stratigraphic unit the lithosequence, (serving as a regional "basement rock"), and generally lies down-gradient of the other four lithologies, we did not evaluate gneiss as a potential source of colluvium to other soils. Because sandstone, shale, and limestone are tightly juxtaposed lithologic units (Figure 7; sandstone cobbles were also observed in the shale soil profile), these rock types were evaluated as reciprocal colluvial inputs to these three soils profiles.

Geochemical Analyses

We characterized three sample types: five rock, five proxies for atmospheric deposition, and 19 morphologic horizon (Table 6) specific soil samples comprising a single soil profile overlying the corresponding rock (four gneiss, five sandstone, three shale, three limestone, and four basaltic andesite). Maximum depths for soil horizons were 0.75, 0.90, 0.83, 0.55, and 0.65 m, respectively. We also characterized the Ap (0-0.39 m), Bt (0.39-0.55 m), and Bk horizons (0.55-0.81 m) overlying the Ck horizon (0.81). Soil and atmospheric deposition samples were air-dried and passed through a 2-mm sieve. Roughly ~50 grams of rock, loess, or soil were analyzed. Fine earth (<2mm) particle size distributions (% sand [0.05-2mm]), % silt [2-50 μm]) were obtained after mixing 50 gram soil samples with one L of sodium hexametaphosphate (0.08 *M*) using a

hydrometer to measure the density of the solution after 40 seconds and roughly seven hours depending on the temperature of the solution, respectively; % clay was obtained by difference from 100% (Poonam, 2008). Because the samples contained relatively low

Underlying Rock Lat./Long.	Horizon	Lower Depth (cm)	% Coarse	Texture	% Clay	Bulk(ρ_b) Density (Mg m^{-3})	CV (ρ_b)	SD (ρ_b)	LOI
Gneiss (gn)	A	10	10	SCL	21	0.93	0.02	0.02	2
45.54535N /	Bw	29	50	SCL	22	1.66	0.12	0.07	0.4
-111.02085W	C1	40	60	LS	8	2.14	0.06	0.03	0.2
	C2	75	80	SL	17	1.5*			0.2
Sandstone	A	5	20	SCL	21	1.36	0.12	0.09	1
(ss)	Bw1	30	35	SCL	22	1.47	0.05	0.03	0.2
45.53384N /	Bw2	50	35	SCL/SL	20	1.43*			0.1
-111.01354W	BC	70	40	LS	6	1.58*			0.1
	C	90	50	LS	7	1.65*			0
Shale (sh)	A	28	5	C	41	1.55	0.21	0.13	1.5
45.53336N /	Bt	74	15	CL/C	40	1.63	0.1	0.06	0.4
-111.01337W	C	83	50	C	46	1.81	0.09	0.05	0.4
Limestone	A1	25	80	C	45	1.08	0.03	0.03	2.6
(ls)	A2	35	20	SiC	45	1.94	0.8	0.4	1.7
45.53149N /									
-111.01358W	C	55	70	CL	30	1.25*			1.7
Basaltic				CL/SiC			0.13	0.11	
Andesite	A	26	0	L	33	0.93			1.4
(ba)	Bt1	38	3	CL	38	1.66	0.13	0.08	0.7
45.53097N /	Bt2	49	10	CL	30	2.14	0.22	0.17	0.7
-111.0132W	C	65	45	C	47	1.5*	0.07	0.03	0.6

Table 6. Selected physical and chemical properties for the five soil profiles, presented in inverted stratigraphic order. Methods and nomenclature per Schoeneberger et al. (2012). Textural classes and %clay were determined using the hydrometer method. Because soil aggregates were not available for six asterisked (*) horizons, bulk density for these horizons were estimated from hydrometer-determined textures and a soil bulk density calculator (Saxton et al., 1986).

organic matter, they were not treated with hydrogen peroxide to remove organic matter prior to hydrometry. Loss on ignition (LOI) was determined after five gram samples dried in a 1000-watt microwave oven for six minutes were combusted for six hours at

400^0C, average CVs were 11%. Bulk density was obtained by measuring the displacement of weighed soil aggregates; CVs averaged 5%.

Here we expand on this work. Concentrations of major elements (Si, Al, Fe, Ca, Mg, Na, K, and P) were obtained via lithium metaborate fusion and ICP-MS at ALS Laboratories (Reno, NV; method ME-ICP06), along with concentrations of an additional five elements (Ba, Cr, Mn, Sr, and Ti), which together were a small fraction of the total weights of analyzed rock, aeolian proxies, or soils (averages $\leq 0.7\%$). Though Sugden et al. (2014) reported results for five "minor" elements, including Yb, a heavy rare earth element (HREE), concentrations for an additional 26 elements were obtained via lithium metaborate fusion and ICP-AES at ALS (method ME-MS81), including Zr, Nb, and the remaining seven HREE (Tb, Dy, Ho, Er, Tm, Lu, and Y), which are reported here.

The use of elemental concentrations, as opposed to concentrations ratios, to determine the influence of underlying rock and exogenous inputs on soil horizons comes with unique limitations. Immobile elements should not enter solution during chemical weathering reactions. As chemical weathering removes soluble materials, immobile elements become residually enriched. Therefore, concentrations of individual immobile elements are subjected to both initial content of the parent material and the amount of weathering that has occurred. If using only concentrations to compare soils and parent materials, then degree of weathering confounds numerical comparisons to derive relative parent material influences. Therefore, fractional influences determined using concentrations require assumptions to account for changes in these concentrations due to enrichment via weathering. Fortunately, ratios of trace elements enable a more robust

comparison than elemental concentrations alone (Ferrier et al, 2011; Bern et al., 2015). As weathering occurs, all trace elements, if they are immobile, should enrich at similar rates. Therefore, immobile elements ratios minimize artifacts introduced by chemical weathering providing a more robust means by which to establish the EMMM for soils composed of mass from more than one parent material source. The enrichment of immobile elements including Ti, Zr, and Nb were considered referenced to underlying rock. Elemental enrichment factors were compared to identify similarly enriched pairs of elements to use as ratios. This approach suggested that lithologic variations in immobility of specific elements exist, perhaps because of associated differences in organic matter content, soil pH, coarse fragments and others. We performed a sensitivity analysis at three thresholds of differences between enrichment factors (DEF) to evaluate the robustness of each ratio in each soil horizon. If enrichments between these elements differ in a soil horizon, then fractional rock and second parent material influences will also be different. Differences in enrichment factors provide a means to compare influences derived from ratios and elements.

Because of these lithologic and textural differences, we evaluate Hyalite soils and their candidate parent materials using developed methods (Muhs et al., 2008; Heckman and Rasmussen, 2011; Ferrier et al., 2011) and propose a new method to numerically derive the relative influence of two parent materials. Differences between concentration ratios of rock and second parent materials were then used to develop an EMMM of rock and exogenous inputs and result in fractional influences of selected parent materials. To determine relative influences, differences between soil horizon elemental ratios and

candidate parent material (rock and atmospheric deposition or colluvium) elemental ratios provided guidance as to which candidate is more similar to other soil horizons. A smaller difference suggests a parent material is more similar to a soil horizon.

Two Mixing Models

Mass balance and chemical weathering calculations are customarily referenced only to underlying rock in cases where soils are assumed to have formed entirely from that underlying rock or where the influence of exogenous inputs has been estimated as inconsequential. The two- end-member mixing models capitalized on differences between ratios of trace elements of model atmospheric deposition proxy or a single colluvial input, in addition to underlying rock, to define the fractional rock influence for each lithosequence soil horizon. Specifically, inputs to the mixing models relied on the arithmetic average immobile element concentration (or average element concentration ratio) of three atmospheric deposition proxies (BS5, BS6, and PF4) or one of three colluvial samples (sandstone, shale, or basaltic andesite). To account for depositional and parent material variability, we compared outputs from two end-member mixing models to determine the differences between soil horizons and candidate parent materials. Mass balance estimates are traditionally referenced to underlying rock and soils are assumed to lack the inputs from a second parent material, but here differences between ratios of trace elements were used to determine the fractional influence of underlying rock on each lithosequence soil horizon.

We evaluated the immobility of Ti, Zr, and Nb in lithosequence soils using enrichment factors (EF_i) relative to underlying rock. The enrichment ratio (EF_i)

normalizes concentrations of individual elements (C_i) for either soil horizons ($C_{i,w}$) or unweathered parent materials ($C_{i,p}$) such as underlying rock.

$$EF_i = C_{i,w}/C_{i,p} \quad \text{Eq. 1}$$

In general, these enrichment factors should be greatest at the surface and decline with depth and with decreasing distance to an underlying parent material. At Post Farm, where soil morphological properties and the geomorphological setting suggest a single parent material, for example, EF for Ti, Zr, or Nb reached a minimum of 0.96 and a maximum of 1.20. Across the lithosequence, by contrast, EF ranged more widely. The limestone A1 horizon, for example, showed an EF_{Ti} of 20, EF_{Zr} of 18, and an EF_{Nb} of 16; the basaltic andesite A horizon by contrast showed corresponding EF of 0.9, 1.5, and 1.3, respectively, but these EF calculations are sensitive to the assumption of a single parent material. As EFs at Post Farm are quite similar, Ti/Zr for this single-parent material soil profile ranged from 10.0 to 11.8 (Appendix B) with the lowermost "parent material" Ck horizon used in composite proxy for average atmospheric deposition at 10.4 (Table 4). These are quite modest shifts in Ti/Zr compared with those reported by Bern et al., (2015). Zr/Nb at Post Farm ranged from 21 to 23.6 (Appendix B) with the Ck horizon at 23. Compared to a Hawaiian chronosequence, the range in Zr/Nb observed at Post Farm is quite modest (Kurtz et al., 2000). Alternatively the driest sites (0.2 m and 0.5 m of annual precipitation) of a Hawaiian climosequence showed comparable differences in Zr/Nb to Post Farm, while wetter sites showed a much greater range in Zr/Nb (Kurtz et al., 2000).

Concentrations of immobile elements in soil horizons that are subject to multiple parent materials have been subjected to different degrees of chemical weathering. We assume immobile elements (Ti, Zr, and Nb) that enrich by more similar factors suggest similar chemical weathering patterns and that ratios of more similarly enriched elements are more representative of the extent of chemical weathering than elements that are less similarly enriched.

$$DEF = (EF_1\text{-}EF_2)/[\min (EF_1, EF_2)]*100 \quad \text{Eq. 2}$$

DEF is the percent difference between enrichment ratios. Differences in enrichment ratios were compared across progressively stricter thresholds. If multiple ratios meet set thresholds, then fractional rock influences were presented as arithmetic averages of those influences. DEF thresholds used include $<\infty$, $<100\%$, and $<30\%$. With three ratios and 19 soil horizons, this makes a total of 57 potential ratios that could inform relative parent material influences, compare degrees of alteration, and contextualize chemical weathering.

We next assume that proximity between trace immobile elemental ratios denote a quantifiable similarity between candidate parent materials and soil horizons. To determine this relative proximity, differences between ratios of trace elements for candidate parent materials (rock and colluvium or loess) and soil horizons were calculated by first determining differences between elements (equation 3) and elemental ratios (equation 4).

$$D_{trx} = (C_{trx,w}) - (C_{trx,p}) \quad \text{Eq. 3}$$

$$DR_{trx,trxy} = (C_{trx,w}/C_{try,w}) - (C_{trx,p}/C_{tryp}) \quad \text{Eq. 4}$$

$DR_{trx,trxy}$ is the difference between ratios of trace elements between each soil horizon ($C_{trx,w}/C_{try,w}$) and candidate parent materials ($C_{trx,p}/C_{try,p}$) for elements x and y. Differences in ratios of Ti/Zr, Zr/Nb, and Ti/Nb were considered that might best represent weathering conditions based on DEF thresholds. This process was also done using individual element concentrations (equation 3) to compare estimated fractions rock determined from elemental concentrations for comparison to concentration ratios. Elemental concentrations considered include mean HREE (Tb, Dy, Ho, Er, Tm, Yb, Lu, and Y), Ti, Zr, and Nb. We assume that influences on the fine fractions (<2 mm) of all soil horizons can be represented as the sum of the fractional influence of underlying rock (F_{rock}) and a second parent material (F_{p2}).

$$1 = F_{rock} + F_{p2} \quad \text{Eq. 5}$$

Therefore, if we can determine the fractional influence of one parent material (F_{rock}), the fractional influence of the second parent material (F_{p2}) can be determined. To find the fractional rock influence using the first mixing model, we divide the absolute values of the differences between trace elements concentrations of soil and rock (equation 6, $|D_{trx,rock}|$) by the sum of the absolute values of the difference between trace element concentrations of soil and rock ($|D_{trx,rock}|$) and soil and the second parent material ($|D_{trx,p2}|$).

$$F_{rock} = 1 - [|D_{trx,rock}|/(|D_{trx,rock}| + |D_{trx,p2}|)] \quad \text{Eq. 6}$$

$$F_{rock} = 1 - [|DR_{trx,try,rock}|/(|DR_{trx,try,rock}| + |DR_{trx,try,p2}|)] \quad \text{Eq. 7}$$

$DR_{trx,try,rock}$ is the difference in ratios of trace elements x and y between a soil horizon and underlying rock. Fractions rock were calculated using these differences in concentrations

or ratios of concentrations between soil horizons and candidate parent materials. ($|DR_{trx,try,p2}|$) is the difference in ratios of trace elements x and y between the second selected parent material and the soil horizon of interest; and F_{rock} is the influence of underlying rock.

A second mixing model, the classic (EMMM) was used to verify that parent materials used in equations 6 and 7 can serve as end members of soil horizons and buttress findings of which ratios best represent chemical weathering in soils on each lithology. We begin by assuming that ratios of immobile elements in soil (R_w) are equal to the sum of the fractional influence of the second parent material times the same ratio in the second parent material and the fractional influence of the rock and the same ratio in the underlying rock. We then substitute $1-F_{p2}$ for fraction rock giving us

$$R_w = F_{p2}*R_{p2} + (1-F_{p2})*R_r \quad \text{Eq. 8}$$

R_{p2} is the ratio of elements in the second parent material and R_r is the ratio of elements in underlying rock. We rearrange equation 8 to the fractional influence of a second parent material (Chadwick et al., 1999; Lawrence et al, 2011).

$$F_{p2} = (R_w-R_r)/(R_{p2}-R_r) \quad \text{Eq. 9}$$

Values for F_{p2} fall between 0 and 1 if soil horizon values are between the values of the two end- members.

Mass Balance

Once fractional influences of rock were calculated, chemical depletion fractions (CDF) were calculated to determine the fraction of mass lost due to chemical weathering, referenced to each parent material and to a calculated hybrid parent material using

concentrations of the immobile element Ti, Zr, and Nb. CDFs referenced to any one parent material were calculated as:

$$CDF = 1 - (C_{i,p}/C_{i,w}) \quad \text{Eq. 10}$$

where $C_{i,p}$ is the Ti, Zr, or Nb concentration in the parent material and $C_{i,w}$ is the Ti, Zr, or Nb concentration in the soil horizon (Riebe et al., 2003). CDF values, irrespective of parent, were depth weighted to 0.29 and 0.49 m and represent total chemical weathering with respect to the identified parent material. CDF values closer to 1 indicate greater chemical weathering whereas values closer to 0 indicate little or no chemical weathering relative to parent material. To create a hybrid $C_{i,p}$, Ti, Zr, or Nb concentrations of rock and a second parent material were scaled using the trace element mixing model for each horizon. Hybrid CDFs (HCDF), referenced to more than one parent material, are calculated as in equation 10, the only difference being that $C_{i,p}$ is composed of two Ti, Zr, or Nb concentrations scaled according to the results of the mixing model. If parent materials were well chosen and negative CDF values result, then we propose a chemical alteration fraction (CAF) as depletion does not occur with negative CDF values.

$$HC_{i,p} = (C_{i,rock} * F_{rock}) + (C_{i,p2} * F_{p2}) \quad \text{Eq. 11}$$

$HC_{i,p}$ is the scaled hybrid Ti, Zr, or Nb concentration of underlying rock and a second parent material. Negative CDF values either indicate that assumed parent materials are incorrect or that net additions of parent materials have occurred.

To calculate total mass fluxes, we calculated the transfer coefficient tau (τ) for eight major elements: SiO_2, Al_2O_3, Fe_2O_3, CaO, MgO, Na_2O, K_2O, and P_2O_5 as oxides (denoted with subscript j) using Equation 12.

$$\tau_j = [(C_{j,w} * C_{i,p})/(C_{j,p} * C_{i,w})] - 1 \quad \text{Eq. 12}$$

τ_j is the mass loss or gain of a mobile element j; $C_{j,w}$ is the concentration of a mobile element (e.g., Na) in soil; $C_{i,p}$ is the concentration of an immobile element such as Zr in parent material; $C_{j,p}$ is the concentration of a mobile element in parent material; and $C_{i,w}$ is the concentration of an immobile element in soil. Tau values generally range from -1 to 1, but in some cases are even higher. A tau value of -1 indicates a 100% loss of that element in a soil relative to a parent material. Values greater than 1 imply that the soil contains more of that element than existing in the parent material to which all losses and gains are being indexed.

Strain ($\varepsilon_{i,w}$) is a measure of the volume of material lost or gained throughout soil development using densities of parent material and soil. Soil densities were calculated in the lab, samples permitting, using wax or saran to determine volume by displacement. When soil samples were unsuitable to measure bulk density, bulk density values were estimated from soil textures (Saxton et al., 1986) measured by hydrometer. Estimated loess densities were set at 1.3 Mg m^{-3} as the dry bulk density of typical loess is between 1.1 and 1.5 Mg m^{-3} (Pye, 1987).

$$\varepsilon_{i,w} = [(\rho_p * C_{i,p})/(\rho_w * C_{i,w})] - 1 \quad \text{Eq. 13}$$

Where $\varepsilon_{i,w}$ (Eq. 13) is strain on the soil horizon; ρ_p is the density of the parent material; $C_{i,p}$ is the concentration of Zr of the parent material; ρ_w is the bulk density of the soil; and $C_{i,w}$ is the concentration of Zr of the soil. Strain values were calculated using rock and loess as parent materials.

Mass fluxes estimate net mass changes that occur to a parent material over time due to chemical weathering. Mass fluxes do not account for effects of physical erosion.

$$M_{j,flux} = \rho_p * C_{j,p} * \tau_j * [z_w (1-\Pi)] * [1/ (\varepsilon_{i,w} +1)] \quad \text{Eq. 14}$$

Where $M_{j,flux}$ (Eq. 14) is the mass flux; ρ_p is the density of the parent material; $C_{j,p}$ is the concentration of major element j of the parent material; τ_j is the mass transfer coefficient of element j; z_w is the soil horizon thickness; Π is the fraction rock; and $\varepsilon_{i,w}$ is strain. Total elemental mass fluxes were calculated by summing individual mass fluxes Si, Al, Fe, Ca, Mg, K, Na, and P as oxides using both candidate parent materials: rock and a second parent material. Elemental mass fluxes were summed for each parent material to determine total mass fluxes.

$$M_{flux,tot} \sum_{w=1}^{k} \sum_{i=1}^{n} \{M_{j,flux} = \rho_p * C_{j,p} * \tau_j * [z_w (1-\Pi)] * [1/ (\varepsilon_{i,w} +1)]\} \quad \text{Eq. 15}$$

$M_{flux,total}$ (Eq. 14) is the sum of mass fluxes for all 8 elements (n) across all soil horizons (k) (Heckman and Rasmussen, 2011). Combined 8 major elements and loss on ignition (LOI) compose an average of 99.4% of sample mass. Mass fluxes were calculated indexed rock and each candidate parent material.

Combining Mixing Models and Mass Balance

Differences in ratios of selected trace elements were used to create the mixing model, which determined the fractional influences of each candidate parent material. Values closer to zero have a higher fractional influence than values further from zero. Mixing model outputs were used to scale individual parent material mass fluxes into hybrid mass fluxes of two combined parent materials. Mass fluxes were calculated for

each soil horizon referenced to underlying rock and selected second parent materials. These scaled mass fluxes were combined into a hybrid mass flux, $HM_{flux,tot}$.

$$HM_{flux,tot} = (M_{rock,flux,tot} * F_{rock}) + (M_{p2,flux,tot} * F_{p2}) \quad \text{Eq. 16}$$

Where $M_{rock,flux,tot}$ represents mass flux for bedrock and F_{rock} represents the fractional influence of rock on the specific soil horizon. This is repeated for the second selected parent material. To standardize mass fluxes (Eq. 16) across the varying thicknesses of soil profiles in the lithosequence, mass fluxes were calculated only to either a depth of 0.29 m, the bottom of gneiss Bw horizon and 0.49 m, the bottom of the basaltic andesite Bt2 horizon. Our hybrid approach was to calculate mass fluxes separately for rock and second parent materials, and subsequently combine these fluxes in proportion to trace element differences between parent materials and soils.

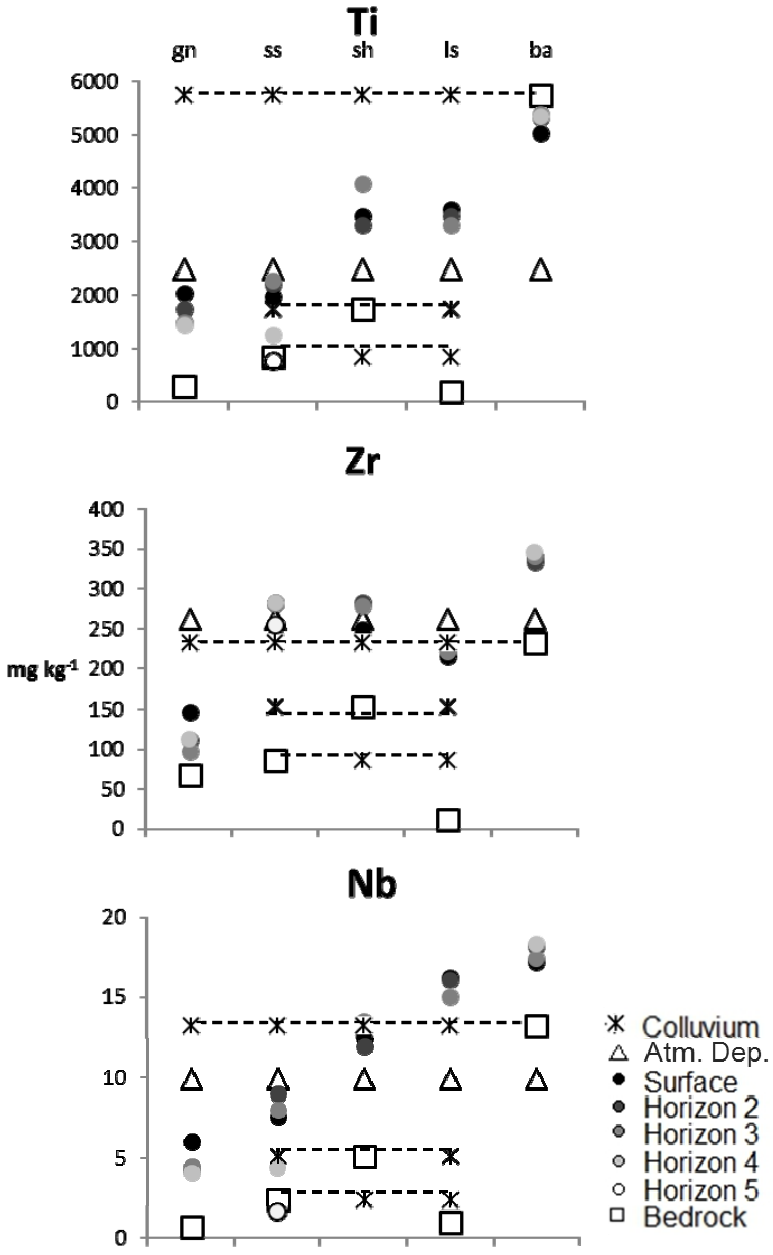

Figure 8. Concentrations of Ti, Zr, and Nb in soil horizons, underlying rock, and candidate parent materials. Colluvial as limestone and gneiss were not considered because limestone weathers congruently and gneiss is downgradient of all other lithologies. Dashed lines indicate that underlying rock chemistry was used to represent upgradient colluvial influence.

Lithology	Horizon	Ti mg kg^{-1}	Zr mg kg^{-1}	Nb mg kg^{-1}	Ti EF	Zr EF	Nb EF	Ti/Zr DEF (%)	Ti/Nb DEF (%)	Zr/Nb DEF (%)
Gneiss	A	2038	147	6	7	2.2	9	215	**26**	297
Gneiss	Bw	1738	111	4	6	1.6	6	255	**3**	268
Gneiss	C1	1498	97	5	5	1.4	6	251	**29**	351
Gneiss	C2	1438	112	4	5	1.6	6	191	**19**	247
Gneiss	Rock	300	68	0.7						
Sandstone	A	1978	283	8	2.4	3.3	3.2	*40*	*34*	**4**
Sandstone	Bw1	2218	282	9	2.6	3.3	3.8	**24**	*42*	**14**
Sandstone	Bw2	2278	337	8	2.7	3.9	3.3	*44*	**23**	**18**
Sandstone	BC	1259	282	4	1.5	3.3	1.8	119	**22**	*79*
Sandstone	C	779	254	1.6	0.9	3.0	0.7	218	*39*	343
Sandstone	Rock	839	86	2.4						
Shale	A	3476	249	12	2.0	1.6	2.4	**23**	**22**	*49*
Shale	Bt	3296	283	12	1.9	1.8	2.3	**2.5**	**23**	**26**
Shale	C	4076	279	14	2.3	1.8	2.6	**29**	**13**	*45*
Shale	Rock	1738	153	5						
Limestone	A1	3596	216	16	20	18	16	**11**	**23**	**11**
Limestone	A2	3476	229	16	19	19	16	**1.3**	**20**	**19**
Limestone	C	3296	221	15	18	18	15	**0.5**	**22**	**23**
Limestone	Rock	180	12	1						
Basaltic Andesite	A	5035	339	17	0.9	1.5	1.3	*67*	*49*	**12**
Basaltic Andesite	Bt1	5334	333	18	0.9	1.4	1.4	*55*	*49*	**4**
Basaltic Andesite	Bt2	5394	340	17	0.9	1.5	1.3	*56*	*41*	**11**
Basaltic Andesite	C	5334	345	18	0.9	1.5	1.4	*60*	*50*	**7**
Basaltic Andesite	Rock	5754	232	13			*DEF<100%*	*13/19*	*19/19*	*14/19*
							DEF<30%	**7/19**	**12/19**	**11/19**
AD	Avg	2477	262	10						
AD	PF4	3416	329	14						
AD	BS6	2697	160	8						
AD	BS5	1319	298	7						

Table 7. Concentrations, enrichment factors (EF), and differences in enrichment factors (DEF) relative to underlying rock, soil, and atmospheric deposition (AD) for Ti, Zr, and Nb and ratios of these elements excluded by DEF thresholds in lithosequence soils. DEF in *italics* meet <100% threshold, while DEF in **bold** meet <30% threshold. DEF not in bold or italics do not meet either threshold. Fractions at bottom right denote number of horizons that meet respective threshold for that particular ratio.

Results

Mixing Model

A 30% threshold of differences in enrichment factors (DEF) suggest that ratios

Lithology	Horizon	Ratios			Fractional Influences						No Exclusion	Exclusion	
		Ti/Zr	Ti/Nb	Zr/Nb	Ti/Zr		Ti/Nb		Zr/Nb		All 3 ratios	DEF <100%	DEF <30%
					AD	Rock	AD	Rock	AD	Rock	Frock	Frock	Frock
Gneiss	A	14	340	25	0.68	0.32	0.50	0.50	0.97	0.03	0.28	0.50	0.50
Gneiss	C2	13	360	28	0.71	0.29	0.39	0.61	0.98	0.02	0.31	0.61	0.61
Gneiss	Rock	4	428	97	Median	0.34		0.56		0.02	0.30	0.56	0.56
					IQR	0.04		0.20		0.02	0.05	0.20	0.20
Sandstone	**A**	7	260	37	0.53	0.47	0.91	0.09	0.12	0.88	0.48	0.48	0.88
Sandstone	C	3	487	159	0.51	0.49	0.37	0.63	0.48	0.52	0.55	0.37	NA
Sandstone	Rock	10	350	36	Median	0.47		0.34		0.57	0.48	0.46	0.49
					IQR	0.01		0.26		0.19	0.04	0.11	0.14
Shale	A	14	280	20	0.37	0.63	0.67	0.33	0.60	0.40	0.45	0.45	0.48
Shale	C	15	302	21	0.39	0.61	0.43	0.57	0.61	0.39	0.52	0.52	0.59
Shale	Rock	11	341	30	Median	0.63		0.33		0.39	0.49	0.49	0.49
					IQR	0.14		0.14		0.04	0.04	0.04	0.05
Limestone	A1	17	222	13	0.19	0.81	0.59	0.41	0.09	0.91	0.71	0.71	0.71
Limestone	C	15	220	15	0.01	0.99	0.56	0.44	0.19	0.81	0.75	0.75	0.75
Limestone	Rock	15	180	12	Median	0.97		0.44		0.85	0.75	0.75	0.75
					IQR	0.09		0.04		0.05	0.03	0.03	0.03
Basaltic Andesite	A	15	293	20	0.65	0.35	0.77	0.23	0.24	0.76	0.45	0.45	0.76
Basaltic Andesite	C	15	291	19	0.61	0.39	0.78	0.22	0.14	0.86	0.49	0.49	0.86
Basaltic Andesite	Rock	25	436	18	Median	0.41		0.23		0.82	0.50	0.50	0.82
Loess	AD	9	251	27	IQR	0.04		0.03		0.10	0.03	0.03	0.10

Table 8. Summary of Ti/Zr, Ti/Nb, and Zr/Nb ratios and resulting fractional influences of rock and atmospheric deposition (AD) as determined using equation 5 for soil horizons and medians and interquartile ranges (IQR) of fractional rock influence for entire soil profiles. Fractional rock influences are presented at the three DEF thresholds (DEF<∞, 100%, and 30%). See Appendix B for all soil horizons.

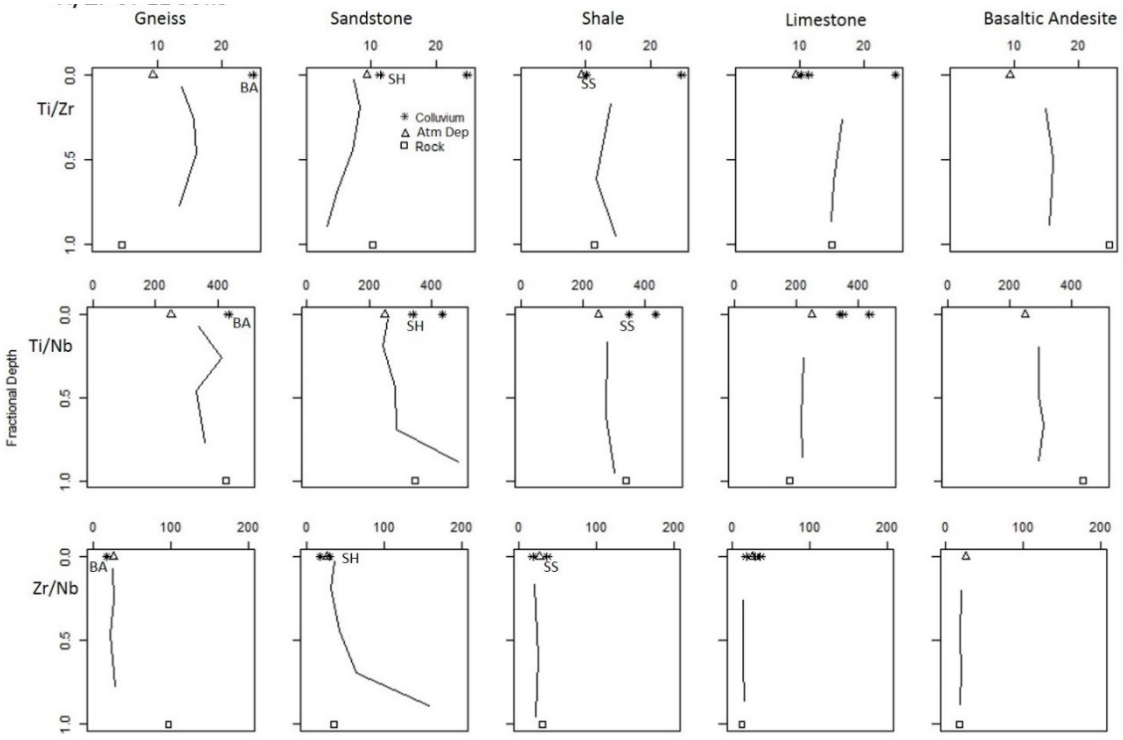

Figure 9. Depth plots of concentration ratios of parent materials and soil horizons in the lithosequence.

of Ti and Nb enriched most similarly across the most soil horizons (12 of 19) in the lithosequence. Using Ti/Nb ratios (Table 8), our end-member mixing model (EMMM) showed the fractions rock for surface horizons across the lithosequence were not constant, ranging from 0.50 (gneiss) to 0.09 (sandstone), suggesting exogenous inputs have contributed unevenly to these co-located soils despite their geographic proximity and state factor similarities. At the 30% DEF threshold that included all ratios, fractional rock influences (Table 8, Figure 10) on surface horizons ranged from 0.48 (shale) to 0.88 (sandstone). At the <100% DEF threshold, fractional rock influences on surface horizons

ranged from 0.45 (shale) to 0.88 (limestone). At the <∞ DEF threshold, fractional rock influences on surface horizons ranged from 0.28 (gneiss) to 0.71 (limestone).

Soils had unique DEF thresholds (Table 7) at which ratios were excluded because they likely did not represent the influences of chemical weathering on underlying rock. Generally, ratios for limestone and shale soils were not excluded at any threshold, except for Zr/Nb for the A and C horizons on shale with DEFs of 45 and 50%, respectively and

		HREE		Ti		Nb		Zr	
Lithology	Horizon	Fp2	Frock	Fp2	Frock	Fp2	Frock	Fp2	Frock
Gneiss	A	0.42	0.58	0.97	0.03	0.36	0.64	0.02	0.98
Gneiss	Bw	0.18	0.82	0.85	0.15	0.11	0.89	0.00	1.00
Gneiss	C1	0.08	0.92	0.92	0.08	0.27	0.73	0.01	0.99
Gneiss	C2	0.17	0.83	0.88	0.12	0.18	0.82	0.01	0.99
Sandstone	A	0.48	0.52	0.96	0.04	0.48	0.52	0.09	0.91
Sandstone	Bw1	0.56	0.44	0.94	0.06	0.45	0.55	0.10	0.90
Sandstone	Bw2	0.77	0.23	0.98	0.02	0.51	0.49	0.03	0.97
Sandstone	BC	0.21	0.79	0.86	0.14	0.19	0.81	0.10	0.90
Sandstone	C	0.22	0.78	0.82	0.18	0.13	0.87	0.20	0.80
Shale	A	0.10	0.90	0.93	0.07	0.46	0.54	0.14	0.86
Shale	Bt	0.06	0.94	0.84	0.16	0.26	0.74	0.03	0.97
Shale	C	0.06	0.94	0.88	0.12	0.35	0.65	0.11	0.89
Limestone	A1	0.71	0.29	0.92	0.08	0.25	0.75	0.04	0.96
Limestone	A2	0.69	0.31	0.81	0.19	0.10	0.90	0.02	0.98
Limestone	C	0.69	0.31	0.93	0.07	0.28	0.72	0.05	0.95
Basaltic Andesite	A	0.37	0.63	0.83	0.17	0.23	0.77	0.03	0.97
Basaltic Andesite	Bt1	0.30	0.70	0.82	0.18	0.08	0.92	0.01	0.99
Basaltic Andesite	Bt2	0.18	0.82	0.81	0.19	0.21	0.79	0.02	0.98
Basaltic Andesite	C	0.14	0.86	0.82	0.18	0.13	0.87	0.02	0.98

Table 9. Fractional influences of underlying rock and average atmospheric deposition as informed by concentrations (mean HREE, Ti, Nb, and Zr) of soil horizons, underlying rock, and candidate parent materials as determined by equation 4.

did not meet the <30% threshold. Basaltic andesite soil horizons had no ratios excluded at DEF<100%, but at DEF<30% ratios that include Ti were excluded with DEFs between 40 and 70%. Gneiss soil at both thresholds excluded both Ti/Zr and Zr/Nb with DEFs remained the same at both thresholds. Sandstone soil DEF<100% were the least

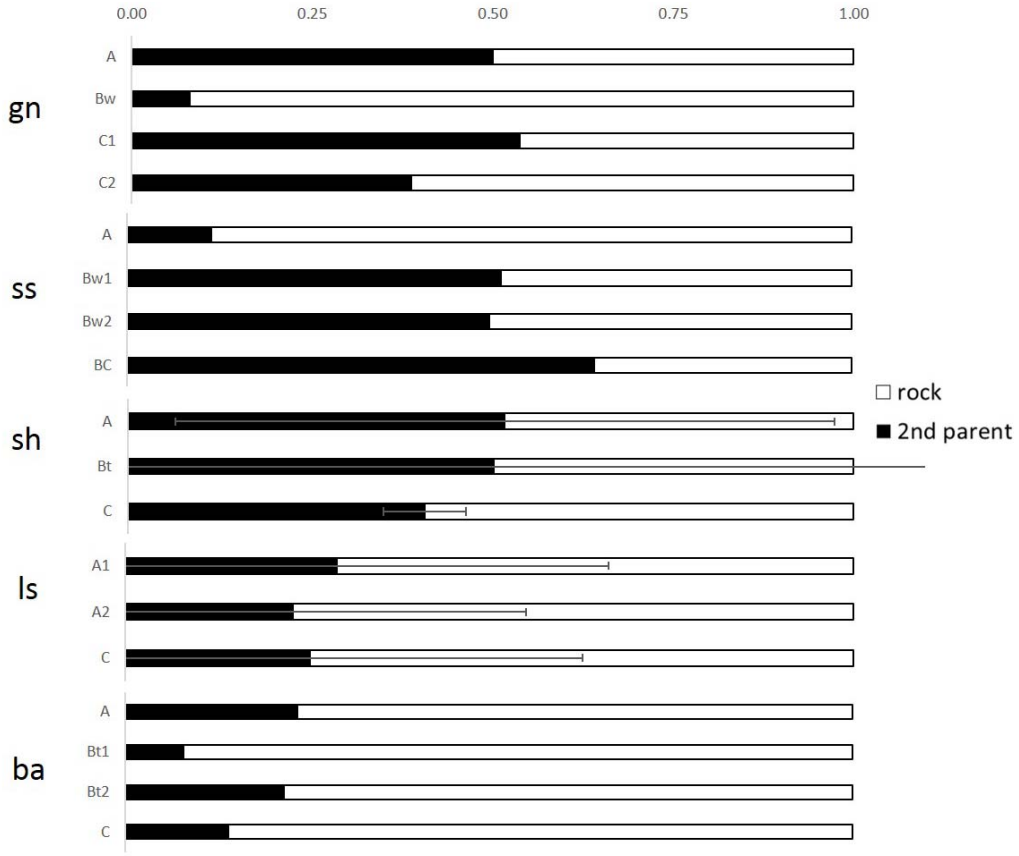

Figure 10. Mixing ratios as fractions calculated using ratios excluded using (DEF<30%) between soil horizons on gneiss (gn), sandstone (ss), shale (sh), limestone (ls), and basaltic andesite (ba) and atmospheric deposition and underlying rock. Error bars represent coefficients of variation (CV) for horizons that had multiple ratios meeting the DEF<30% threshold. CV for the Bt horizon on shale was 0.68 because rock influence from ratios meeting this threshold ranged in fractional influence from 0.29 to 0.88.

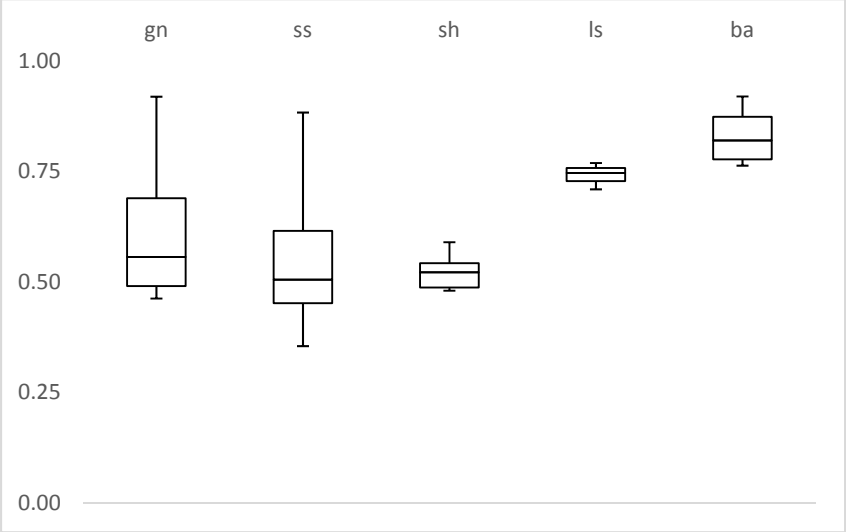

Figure 11. Box plot of ranges of fractional rock influences on soil horizons calculated using the DEF<30% threshold.

between 191 and 351% for all horizons. Therefore, fractional rock influence on gneiss consistent with the BC and C horizons excluded for Ti/Zr and the C horizon excluded for Zr/Nb. At DEF<30%, only certain horizons met the criterion for each ratio, with Ti/Zr for the Bw1 horizon, Ti/Nb for the Bw2 and BC horizons, and Zr/Nb for the A, Bw1, and Bw2 horizons. No ratios met the DEF<30% criterion for the sandstone C horizon.

Each DEF threshold (Table 7) resulted in a range of fractional rock influences (Table 8, Figure 10) on each soil horizon. Uncensored ratios in gneiss soil resulted in fractional rock influences from 0.28 to 0.43. At both DEF<100% and 30% in gneiss soil, fractions rock increased to between 0.46 and 0.92. Uncensored ratios and DEF<100% for the top three soil horizons on sandstone had fraction rocks from 0.34 to 0.51. At DEF<30%, fractional rock influences increased to between 0.48 and 0.88.

Influences calculated using elemental concentrations (Table 9) only suggest that Ti and Zr concentrations best predicted fractions rock calculated by Ti/Nb or DEF<30%. For soil on shale, fractional rock influences at DEF<∞ and 100% ranged from 0.45 to 0.52 and at DEF<30% slightly increased to 0.48 to 0.59. Nb predicted fractional rock influence on shale better than other elements when considering atmospheric deposition as a second parent material. At all three thresholds, DEFs on limestone were all the same and rock influences ranged from 0.71 to 0.77. Fractional influences calculated using elemental concentrations (Table 9) suggested that HREE concentrations predicted the most similar influences of atmospheric deposition and underlying limestone as Ti/Nb and Zr/Nb ratios. For basaltic andesite soil, fractional rock influences at DEF<∞ and 100% ranged from 0.45 to 0.53, and at DEF<30% increased fractional rock influences from 0.76 to 0.92. Interestingly, fractional influences as determined by Nb concentrations (table 5) were similar to those determined by Zr/Nb concentration ratios.

Total Chemical Weathering

Chemical depletion fractions (CDF, Figure 12, Table 10) or total chemical weathering estimates were each referenced to Ti, Zr, and Nb concentrations of two parent materials: underlying rock and a hybrid parent material. CDF referenced to bedrock using Zr ranged from 0.3 for soil on basaltic andesite to 0.95 for soil on limestone, while soil on gneiss and shale had CDFs ~0.4 and soil on sandstone had a CDF ~0.7. CDFs for rock only were largely homogenous between the three elements except for soil on gneiss referenced to Zr which were roughly half of CDF referenced to Ti and Nb and CDFs on

		Ti		Zr		Nb	
Lithology	Parents	0.29 m	0.48 m	0.29 m	0.48 m	0.29 m	0.48 m
Gneiss	Rock	0.84	0.84	0.44	0.40	0.85	0.84
	Hybrid	0.6	0.39	0.12	-0.16	0.47	0.21
Sandstone	Rock	0.61	0.62	0.70	0.71	0.72	0.72
	Hybrid	0.28	0.28	0.42	0.45	0.35	0.31
Shale	Rock	0.50	0.49	0.39	0.42	0.59	0.58
	Hybrid	0.39	0.38	0.16	0.20	0.39	0.38
Limestone	Rock	0.95	0.95	0.94	0.95	0.94	0.94
	Hybrid	0.77	0.77	0.62	0.64	0.78	0.79
Basaltic Andesite	Rock	-0.14	-0.11	0.31	0.31	0.24	0.24
	Hybrid	0.01	0.01	0.29	0.30	0.28	0.28

Table 10. Depth weighted rock and hybrid chemical depletions fractions for Ti, Zr, and Nb.

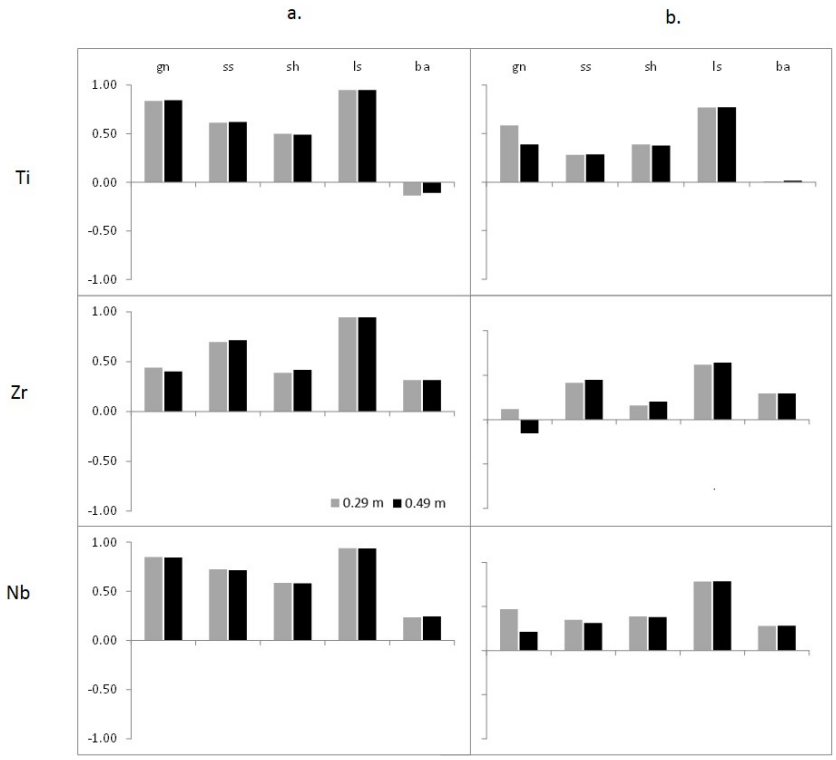

Figure 12. Depth weighted chemical depletion fractions (CDF) of the five soils referenced to Ti, Zr, and Nb in rock (a) and Ti, Zr, and Nb in a hybrid rock (b).

basaltic andesite referenced to Ti which were negative as opposed to Zr and Ti. CDF referenced to hybrid rock and atmospheric deposition samples were less than CDFs referenced to rock only, except for basaltic andesite calculated with Ti and Nb. Hybrid CDFs referenced to Zr ranged from -0.16 for soil on gneiss to 0.79 for soil on limestone. Hybrid CDFs on sandstone and gneiss were by and large much less than CDFs referenced to rock only on these lithologies. Hybrid CDFs on gneiss referenced to Ti and Nb were greater than CDFs referenced to Zr. Hybrid CDFs calculated using Zr on limestone were less than hybrid CDFs on limestone calculated with Ti and Nb. Hybrid CDFs on sandstone were not as disparate.

Soil Mass Balances

Running mass balances (equations 12, 13, and 14) for rock only and hybrid parent materials suggested that second parent materials have varied effects on chemical weathering in each soil. Soils on gneiss, shale, and basaltic andesite have comparatively less weathered referenced to rock only than soils on limestone and sandstone. Among the three ratios, incorporating average atmospheric deposition reduced mass fluxes on all lithologies with the biggest reductions in coarse soils on gneiss and shale. The biggest mass loss reductions (~60%, Table 11) occurred in the soil on shale and were reduced to -126 kg m^{-2} at depth, while a ~50% mass loss reduction occurred when incorporating atmospheric deposition in soil on gneiss. Mass fluxes referenced to rock only in soils on sandstone, limestone, and basaltic andesite overestimated chemical weathering by~1.8 times on sandstone, ~1.3x on limestone, and ~1.2x on basaltic andesite.

Lithology	Depth (m)	gn	ss	sh	ls	ba	
Total	0-0.29	-209	-642	-177	-1257	-164	
kg/m^2	0.29-0.49	-60	-529	-138	-1599	-116	RO
	0-0.49	-269	-1171	-315	-2855	-281	
Total	0-0.29	-122	-348	-67	-931	-129	
kg/m^2	0.29-0.49	9	-282	-59	-1215	-116	AD
	0-0.49	-113	-630	-126	-2146	-245	
Total	0-0.29			-155	-1023		
kg/m^2	0.29-0.49			-136	-1287		C_ba
	0-0.49			-292	-2310		
Total	0-0.29				-964		
kg/m^2	0.29-0.49				-1240		C_sh
	0-0.49				-2204		
Total	0-0.29				-1017		
kg/m^2	0.29-0.49				-1314		C_ss
	0-0.49				-2331		

Table 11. Rock and hybrid mass gains and losses referenced to underlying rock only (RO), underlying rock and atmospheric deposition (AD), and underlying rock and colluvium (C_ba) as noted for soil on gneiss (gn), sandstone (ss), shale (sh), limestone (ls), and basaltic andesite (ba) for varying depths of soils. Mass losses calculated with two parent materials used ratios that exceeded the DEF<30% threshold.

Soil mass losses calculated with two parent materials (rock and atmospheric deposition) to a depth of 0.49 m ranged across two orders of magnitude, from -113 kg m^{-2} for gneiss to -2146 kg m^{-2} for limestone (Table 11, Figure 13) when referenced to atmospheric deposition. Profile mass losses to a depth of 0.49 m were -617 kg m^{-2} for sandstone, -126 kg m^{-2} for shale, and -245 kg m^{-2} for basaltic andesite. Referenced to only underlying rock, mass losses are overestimated by between 13% on basaltic andesite

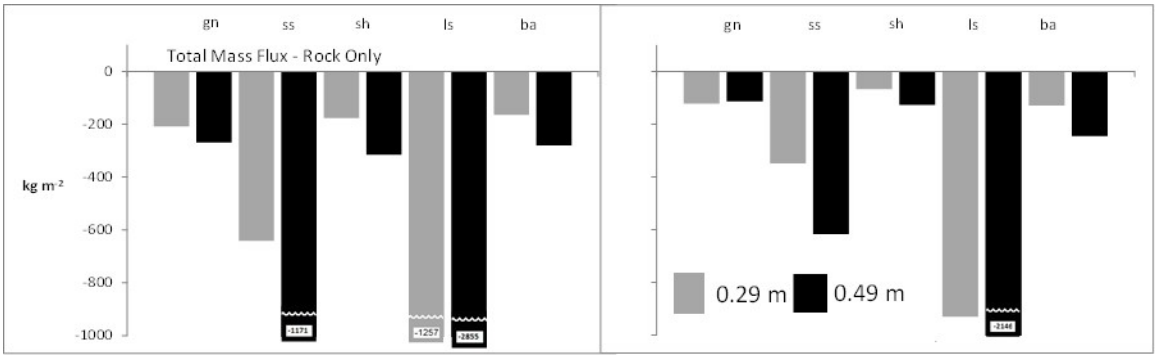

Figure 13. Calculated total mass fluxes of parent materials: rock only (1) and hybrid rock and average atmospheric deposition (2) for the top 0.29 m and 0.49 m depth for soils on gneiss (gn), sandstone (ss), shale (sh), limestone (ls), and basaltic andesite (ba). Hybrid mass fluxes were weighted using trace element mixing ratios that met the DEF<30% threshold for rock and atmospheric deposition.

and 245% on shale when using atmospheric deposition as the second parent material. Alternatively, mass losses on gneiss are over estimated by a factor of nearly 2.5 when referenced to rock only. Limestone mass losses referenced only to underlying rock were overestimated by over 30%. SiO_2, Al_2O_3, and CaO accounted for the majority of total rock chemical weathering and contextualized soils on these five lithologies. SiO_2 accounted for over 90% of rock weathering in soil on gneiss and sandstone. CaO accounted for over 80% of rock weathering in soil on shale and limestone. Together SiO_2, Al_2O_3, and CaO accounted for roughly 75% of rock chemical weathering in soil on basaltic andesite at a ratio of 4:2:1, respectively.

Discussion

Exogenous inputs to soils such as atmospheric deposition provide an alternative end-member, as opposed to bedrock, for geochemically fingerprinting soil. The importance of atmospheric deposition to soils has been quantified conceptually (Yaalon

and Ganor, 1973): soils can be categorized into those that are comprised entirely of aeolian inputs (e.g., loess); those reflecting intermediate and lower percentages of aeolian inputs (e.g., a silt mantle may or may not be present); and those serving as examples of "aeolian contamination" where aeolian influence can only be measured via sophisticated mineralogical or geochemical fingerprinting techniques, but the aeolian material is secondary in importance to the pedogenic role played by underlying rock. Beyond this conceptual model (also graphically depicted in Muhs, 2013), quantifying exogenous inputs requires numerous assumptions, particularly regarding transformations of these exogenous inputs following deposition and retention, including possible translocations of relatively immobile geochemical elements used to index these inputs. Exogenous inputs such as atmospheric deposition and/or colluvium potentially complicate a mass balance approach because immobile element concentrations (and their ratios) vary between parent materials. Fortunately, however, these variations can be used to infer contributions from each parent material if certain simplifying assumptions are made. The underlying rock and the manner and pace at which weathering and erosion are expressed partly govern the type of soil textures into which exogenous mass may be introduced, retained, and weathered.

Initial efforts to fingerprint these lithosequence soils relied on a dual ratio approach comparing europium anomalies (Eu_N/Eu^*) to ratios of lanthanum and ytterbium (La_N:Yb_N; Sugden et al., 2014). Though Muhs et al. (2008) used this method originally to separate parent materials derived from mafic and felsic rocks, these authors did not use this approach to quantify mathematically the influence of each type of parent material.

Rather, this dual-ratio approach was used instead to simply determine the likelihood of aeolian material contributions to the soil horizons they examined. Our results (described in Sugden et al., 2014) using Eu_N anomalies and La_N/Yb_N to define parent material contributions to the basaltic andesite A horizon suggested this horizon was 41% rock influenced using Euclidean distance and equation 7 to determine fractional rock influences. This dual-ratio method unfortunately did not provide adequate end-members, however, for distinguishing between underlying rock and potential exogenous inputs across the remaining four profiles of the lithosequence (Sugden et al., 2014).

A comparison of the individual trace element and ratio differences between soil horizons and candidate parent materials (Tables 7 and 8) suggested which other parent materials (atmospheric deposition or colluvium) might most influence each soil horizon. The Eu_N* and La_N/Yb_N analysis suggested that soil elemental abundance should lie between the elemental abundance of its selected parent materials (Sugden et al., 2014). A similar approach was used to assess the strength of the scaling ratios developed from differences in trace element ratios. Ti/Zr in parent materials and soils were used to develop a mixing model across an Arizona lithosequence (Heckman and Rasmussen, 2011). Whereas in Arizona, Ti/Zr ratios were 13 for dolostone and 113 for volcanic cinders, Ti/Zr ratios did not vary as much in our Montana lithosequence. Nonetheless, Ti/Zr proved useful in quantifying the relative influences of atmospheric deposition and colluvium as basaltic andesite in shale and limestone soils. These influences were generally under 20% for colluvium as basaltic andesite in soils on shale and limestone, but enough to slightly reduce chemical weathering as compared to rock weathering alone.

Concentrations lent credence to the feasibility that ratios of a candidate parent material has actually contributed materials to a particular soil horizon, whereas differences in enrichment factors (DEF) were used to evaluate how representative ratios were of chemical weathering relative to underlying rock. Ti (EF=4.8-6.8x) and Nb (EF=5.7-8.6x) are similarly enriched (DEF<30%) in soil on gneiss. Zr was comparatively less enriched (EF=1.4-2.2x and DEF>190%) relative to Ti and Nb and therefore Ti/Zr and Zr/Nb did not meet either the 100% or the 30% DEF thresholds. Enrichment factors implied that Ti/Nb ratios were more robust in soil on gneiss than ratios of Ti/Zr and Zr/Nb because of similar degrees of enrichment. Low Nb (0.7 mg kg^{-1}) concentrations in gneiss rock increased rock Ti/Nb ratios (Table 4, 428). Soil horizon Ti/Nb (333-414) ratios suggested that additions of exogenous material with increased Nb had been incorporated into soil horizons on gneiss. Ti/Nb ratios (251) of mean atmospheric deposition likely diluted gneiss soil horizon ratios and were used to evaluate the fractional influences of various parent materials on this soil.

DEFs on sandstone soils were the least consistent in the lithosequence and at the DEF<30% threshold, each ratio best represented chemical weathering in one, two, or three horizons. Additionally, deeper horizons in this soil did not meet thresholds as part of the study perhaps due to Nb mobility or other factors. Soil on sandstone was similarly enriched compared to underlying rock as indicated by Ti (Table 7, EF=0.9-2.7) and Nb (EF=0.7-3.8x), whereas Zr (EF=3-3.9) enrichment was consistently higher especially in BC and C horizons. Ti/Nb ratios in most soil horizons on sandstone were diluted as compared to underlying rock suggesting exogenous influences; alternatively low Nb

concentrations (1.6 mg kg^{-1}) in the sandstone C horizon increased Ti/Nb ratios (487) and suggest a stronger weathering regime and greater Ti enrichment here than in upper soil horizons. All the upper horizons (246-286) on sandstone had Ti/Nb ratios similar to average atmospheric deposition (247). At DEF<100% for Ti/Zr, the A, Bw1 and Bw2 horizons remain uncensored, while only the Bw1 horizons remain uncensored at DEF<30%. The Ti/Zr of the Bw1 horizon was 7.8, while the Ti/Zr of rock and atmospheric deposition at 9.4 and 9.8, respectively, and did not dilute the Bw1 horizon from parent rock. Looking to concentrations, rock and atmospheric deposition were good end-members for Ti in the Bw1 horizon, whereas Zr would have to be enriched from both rock and atmospheric deposition to have increased soil Zr concentrations to 282 mg/kg. The top three surface horizons met the DEF<30% threshold for Zr/Nb and soil horizons Nb concentrations for rock and atmospheric deposition were good end-members.

Soil horizons on shale were residually enriched in Ti, Zr, and Nb with enrichment factors (Table 7) ranging from as low as 1.6 at the surface for Zr to 2.6 at depth for Nb. Zr and Nb in soil horizons on shale were enriched above the DEF<30% threshold and the A and C horizons, therefore these Zr/Nb ratios were not used in mass flux calculations. Enrichment factors for elements in Ti/Zr and Ti/Nb ratios were within DEF<30% of one another, therefore these ratios were used to assess the relative influences of parent materials in soil on shale. While DEF of Ti/Zr and Ti/Nb suggested elements in these ratios were similarly enriched, Ti/Zr on shale suggested that material with a higher Ti/Zr ratio influenced the A and C horizons, while the Bt horizon was most similar to underlying shale. Alternatively, the Ti/Nb ratio suggested that material with a lower

Ti/Nb ratio had influenced shallow horizons on shale. The Ti/Nb ratio of atmospheric deposition (247) may have reduced soil horizon Ti/Nb ratios. But Ti and Nb concentrations of atmospheric deposition were lower than Ti and Nb concentrations in all soil horizons on shale. Therefore, another second parent material likely inflated Ti/Nb in shale soils.

Soils on limestone were the most enriched as compared to underlying rock. Limestone rock had the lowest concentrations (Table 7) of Ti (180 mg kg^{-1}), Zr (12 mg kg^{-1}), and Nb (1 mg kg^{-1}) of any soil, rock, or atmospheric deposition sample. Alternatively, limestone soil horizons contained more similar levels of Ti to soil on shale, but more Ti than soils on gneiss and sandstone. As soil horizon ratios of Ti, Zr, and Nb concentrations had similarly high DEF (15-20x) relative to underlying rock, all three immobile elements were representative of soil formation in horizons on limestone. As limestone rock was so depleted in immobile elements relative to soil horizons, other rock types, and atmospheric deposition samples, colluvium (sandstone, shale, or basaltic andesite), all these parent materials potentially influenced these soil horizons. Although sandstone and shale rock as colluvium had less Ti, Zr, and Nb than limestone soil horizons, weathering could have enriched concentrations of these elements to levels observed in limestone soil horizons. Average atmospheric deposition may have enriched Ti and Nb concentrations in these soil horizons. Atmospheric Zr sources (279 mg kg^{-1}) appear not to have enriched soil horizon concentrations (216-221 mg kg^{-1}). Ratios of these elements in underlying rock, potential colluvial sources, atmospheric deposition, and soil horizons on limestone revealed less disparity between limestone soil horizons

and candidate parent materials. Ti/Zr (Table 8) ratios suggested atmospheric deposition cannot have influenced limestone soils because soil horizon Ti/Zr ratios (14.9-16.6) were greater than or equal to limestone rock Ti/Zr ratios (15) and atmospheric deposition (9.4) cannot have enriched these soils horizons. Alternatively, some question Zr immobility (Kurtz et al., 2000) which could have potentially decreased Ti/Zr ratios. Therefore, we consider Ti/Zr of atmospheric deposition as a potential input. Ti/Nb ratios suggested equal inputs of atmospheric deposition and rock, while Zr/Nb of atmospheric deposition suggested a much stronger influence from underlying rock (Zr/Nb: 12) on soil horizons (Zr/Nb: 13.3-14.7) than atmospheric deposition (Zr/Nb: 25.4).

Soil horizons on basaltic andesite had the highest concentrations of Ti, Zr, and Nb of any soil horizon or atmospheric deposition sample in the lithosequence and basaltic andesite rock contained more of all three of these elements than any basaltic andesite soil horizon. A comparison of enrichment factors relative to underlying rock suggests that Zr and Nb have enriched more similarly than Ti on basaltic andesite. Some doubt the immobility of Ti in quartz rich soils in the central Amazon (Cornu et al., 1999). Additional inquiries have revealed that Zr has greater mobility than Nb at wetter sites in a Hawaiian climosequence (Kurtz et al., 2000). Enrichment factors in our lithosequence for Zr and Nb were comparable between 1.3 and 1.5x and only vary between 4 and 12% of one another. This suggested that Zr/Nb may better represent chemical weathering conditions than the use of Ti in a ratio. A look at Zr/Nb ratios in soil on basaltic andesite (18.3-19.7) suggested some influence from exogenous materials. As basaltic andesite

served as the caprock in Hyalite, colluvial influences from other lithologies cannot have influenced soil on basaltic andesite.

We tested our trace element mixing model in Montana to determine what forces control soil formation and mass fluxes. Soil mass fluxes suggest that soil textures alone do not control mass fluxes in both coarse and fine soils. Both soils on gneiss and sandstone have sandy clay loams at the surface and sandy loam and loamy sand at depth. But the coarse soils show drastically different mass fluxes with gneiss soil showing less mass losses at both depths. Sandstone soils show large mass losses at both depths (Table 11, Figure 14). Estimated soil bulk densities had little effect on mass fluxes because these estimates were for horizons beneath 0.49 m. All three fine soils are mostly clay and clay loam textured, but soils on limestone have comparatively ten times greater mass losses than soil on shale and basaltic andesite. Plant communities alone do not account for varying mass fluxes in these five soils. Grass and shrub land communities on shale differ from the other four sites which are forested largely by lodgepole pine (*P. contorta*). But mass losses in soil on shale are more similar to losses on gneiss than to losses on basaltic andesite and sandstone which are both greater.

Increased mass fluxes in soils on limestone and sandstone may be accounted for by having the greatest amount of coarse fragments throughout those respective profiles. Additionally high mass losses may be due to the fact that calcite, a dominant mineral in limestone, weathering rates are higher at lower temperatures due to retrograde solubility (Egli et al., 2008). As mean annual air temperatures in the lithosequence are around freezing, retrograde solubility may account for the highest rock and hybrid mass fluxes in

the study area. Soils on limestone have the highest pHs (Table 3) in the lithosequence which may have increased susceptibility to weathering and increased mass losses.

Soil on gneiss and sandstone had similar textures, but mass fluxes were nearly six times greater on sandstone than on gneiss. Soils on gneiss supported twice as much organic material (Table 2) as soils on sandstone. Negative CDFs suggested this primarily occurs in soils on gneiss and indicated that developmental upbuilding permits and enhances aeolian assimilative pedogenesis (Almond and Tonkin, 1999). Mass losses to 0.49 m were over four times greater on sandstone when referenced to underlying rock only and nearly six times greater on sandstone than gneiss when referenced to two parent materials. Additionally, mass losses occurred from 0.29 to 0.49 m in soil on sandstone, whereas in soil on gneiss at this depth the only mass gains in the lithosequence occur. This suggested an increased ability of soil on gneiss to retain second parent materials. Scant organic matter in soil on sandstone limits that soils' ability to hold onto second parent materials throughout its horizons. Therefore soil textures alone suggest little about the behavior of the two coarse soils in this lithosequence. Aside from lithologic controls, decreased mass fluxes on gneiss as opposed to sandstone may be driven by elevation combined with landscape position. The gneiss soil sits ~200 m higher than the gneiss soil on an isolated knoll. The gneiss soil likely receives more frozen precipitation than the sandstone soil, but this precipitation maybe scoured by wind and/or subjected to greater sublimation. Additionally, this isolated knoll landscape position at a higher elevation in Hyalite Canyon may have subjected this soil to increased atmospheric deposition which may have increased moisture retention and organic matter formation. These alternative

explanations may work in conjunction with or independent of underlying rock weathering. Regardless, these similarly textured soils overlie rock with similar chemistry that have contrasting chemical weathering patterns and mass fluxes.

Colluvial sandstone cobbles were observed in the shale soil and rounded, pitted basaltic andesite boulders were observed on the surface of the limestone soil; and potential colluvial influences were assessed for logic based on geomorphic position and ratios. Colluvium dissimilar from underlying rock was observed in soils on shale and limestone (Figure 7). Only ratios meeting the DEF<30% (Tables 7 and 8) threshold were used to assess colluvial influences. When rock and basaltic andesite were the two considered parent materials for the shale soil, Ti/Zr ratios were more similar to underlying shale than basaltic andesite. Fractional influences of basaltic andesite colluvium on shale soil ranged from 0.02 to 0.24 (Table 11, Figure 14). Mass fluxes

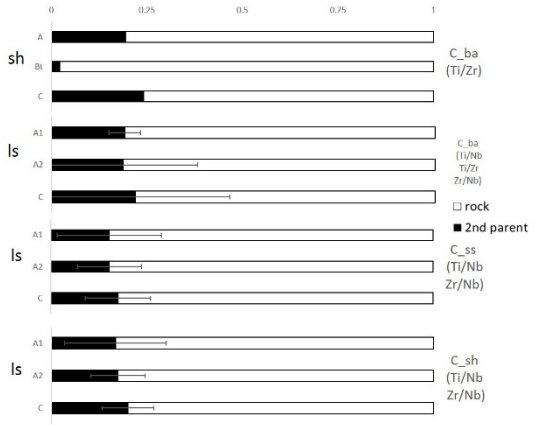

Figure 14. Mixing ratios as fractions calculated using ratios of trace elements between soil horizons on shale (sh) and limestone (ls) and colluvium as selected by fit from rock focused enrichment rations, concentrations and concentration ratios.

changed minimally whether or not basaltic andesite as colluvium was referenced as a second parent material, much less than when this soil was referenced to atmospheric deposition as colluvium. Colluvium as basaltic andesite, shale, and sandstone all could have potentially influenced soils on limestone because of high discrepancies between soil on limestone and underlying rock concentrations and ratios. Ti/Zr ratios in soil on limestone (14.9-16.6, Table 8) could be influenced by basaltic andesite (24.8), but not by sandstone (9.8) and shale (11.4). Ti/Nb and Zr/Nb suggest soil on limestone could be influenced by basaltic andesite, sandstone, or shale as colluvium. In all cases Ti/Nb and Zr/Nb ratios in underlying limestone were less than in soil on limestone, while concentration ratios in basaltic andesite, sandstone, and shale rock as colluvium were

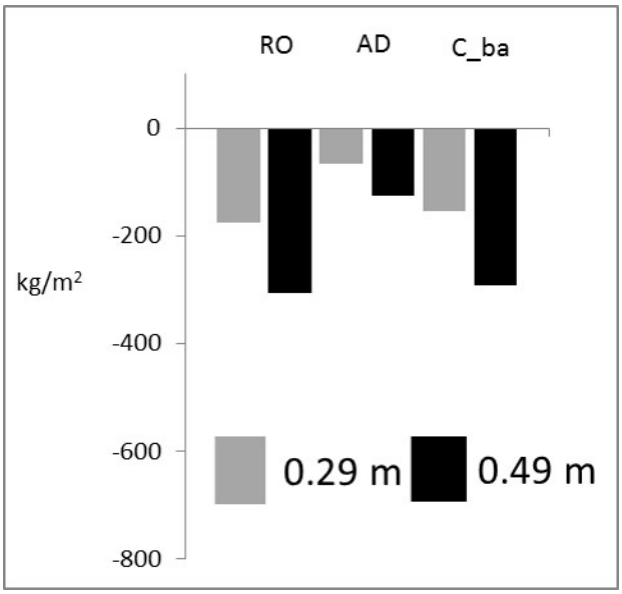

Figure 15. Various mass fluxes in soil on shale: rock only (RO) and hybrid mass fluxes (using rock and atmospheric deposition [AD] and rock and basaltic andesite as colluvium [C_ba]) as informed by the trace element mixing model.

higher than in soil on limestone soils. Concentrations of Ti, Zr, and Nb can be enriched from limestone rock to concentrations in soil on limestone or alternatively, diluted from any of the three colluvial options. If colluvial basaltic andesite was the second parent material in soil on limestone, colluvial influence ranged from 0.19 to 0.22, while underlying rock influence ranged from 0.78 to 0.81. With colluvial sandstone as the second parent material, colluvial influences ranged from 0.15 to 0.17, while underlying limestone influence ranged from 0.83 to 0.85. With colluvial shale as the second parent material, colluvial influence in soil on limestone ranged from 0.17 to 0.2, while underlying limestone influence ranged from 0.80 to 0.83. With fractional influences across all three colluvial second parent materials ranging from 0.15 to 0.2, the impacts of these three materials on limestone total mass fluxes was similar. The Ti/Zr ratio of basaltic andesite rock (25) was higher than that of shale soils (12-15) due to elevated Ti concentrations (5754 ppm) as compared to shale soil concentrations (3297-4076 mg kg^{-1}). Zr concentrations in basaltic andesite rock (232 mg kg^{-1}) could have enriched materials that weather from shale rock (Zr: 153 mg kg^{-1}). The combination of basaltic andesite and underlying shale rock could have residually enriched current shale Zr concentrations (249-283 mg kg^{-1}). Sandstone colluvial influence, as informed by this approach, on shale soils appear minimal as all three ratios would dilute shale soils horizons of Ti/Zr and enrich Ti/Nb and Zr/Nb, but the opposite was observed in shale soils. Therefore, we rule out sandstone colluvium as a second parent material in shale soil. The three colluvial candidate parent materials also reduced mass fluxes by slightly less than atmospheric deposition (Figures 15 and 16), but not by much.

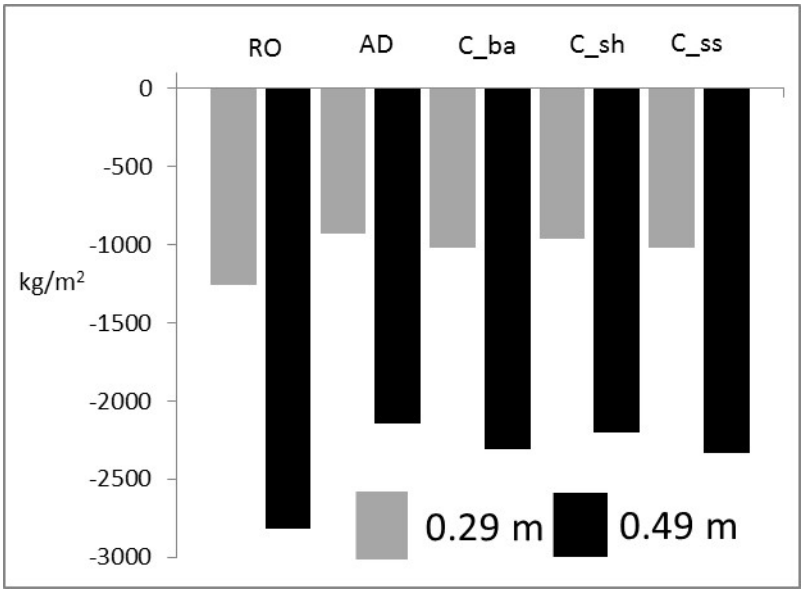

Figure 16. Various mass fluxes in soil on limestone: rock only (RO) and hybrid mass fluxes (using rock and atmospheric deposition [AD], rock and basaltic andesite as colluvium [C_ba], rock and shale as colluvium [C_sh], and rock and sandstone as colluvium [C_ss]) as informed by the trace element mixing model.

We also attempted to quantify potential colluvial influences to soils that did not have observed colluvial influences from other lithologies. Due to its geomorphic position on an isolated knoll, basaltic andesite colluvium was the only potential source of colluvium to soil on gneiss. The Ti/Nb ratio in basaltic andesite (436, Table 8), as colluvium, cannot have diluted the values of these ratios in soil on gneiss so that cannot be the second parent material in this soil, therefore we did not account for a colluvial influence in this soil. In soil on sandstone, each ratio met the DEF<30% threshold for specific horizons and not the entire soil profile. Ti/Zr for the Bw1 horizon (the only horizon that met the DEF<30% threshold for Ti/Zr in the sandstone soil) was less than Ti/Zr values than colluvial shale and basaltic andesite and underlying sandstone. Therefore, Ti/Zr cannot be used to fingerprint colluvial influence in this soil. For the

Bw2 and BC horizons, the Ti/Nb ratios of underlying sandstone and colluvial shale and basaltic andesite were greater than those ratios in soil horizons. Because of these differences, Ti/Nb cannot define the influence of underlying sandstone and colluvial shale and basaltic andesite on these horizons. Zr/Nb met the 30%<DEF threshold for the top three horizons (A, Bw1, and Bw2) on sandstone. Contrasting Zr/Nb ratios of these horizons with underlying rock and colluvial sources suggested that both colluvial shale and basaltic andesite could have influenced only the Bw1 horizon as end-members. With Zr/Nb having the potential to serve as a candidate second parent material for only one horizon, we calculated their potential influence on this horizons, but did not calculate mass fluxes as in the case of soil on shale and limestone as ratios suggested that colluvial influences may have played a role in the development of all soil horizons on those lithologies. Zr/Nb ratios of colluvial shale and basaltic andesite and underlying sandstone suggested that each colluvial influence opposed the other. Using shale colluvium as a second parent material with a Zr/Nb ratio suggested that underlying sandstone had a 0.23 influence on the Bw1 horizon on sandstone. Contrastingly, using basaltic andesite colluvium as a second parent material with the same ratios suggested that underlying sandstone has a 0.75 influence on the Bw1 horizon on sandstone.

A sensitivity analysis tested the effects of a range of loess densities on total mass fluxes. Loess densities were input at three values: 1.1, 1.3, and 1.5 Mg m^{-3} as the dry bulk density of typical loess is between 1.1 and 1.5 Mg m^{-3} (Pye, 1987) to see the impacts on total mass fluxes referenced to loess. This analysis suggested that loess densities in this range did not have a drastic effect on mass fluxes referenced to loess. CVs for the

loess density sensitivity analysis were all under 15%, except for total mass losses referenced to loess on sandstone at 0.29 m depths (47 %).

Uncertainty in Mass Balance Calculations

Sources of uncertainty in these estimates included the amount of atmospheric deposition and how to combine mass fluxes. Soils in close proximity may receive varying atmospheric deposition rates. For example, estimated dust fluxes in a 326 ha watershed in the Loquillo Mountains of Puerto Rico ranged from 14-28 g m^{-2} y^{-1} (Pett-Ridge, 2009). Parent material chemistry may not be homogenous (Riebe et al., 2003; Ewing et al., 2006) limiting the scope and incorrectly assigning a second parent material can both propagate error in mass balance estimates. We overcame this obstacle by averaging the atmospheric deposition samples into one model proxy. We assumed that atmospheric deposition samples we collected in the Gallatin Valley represented the material deposited in southwest Montana. We assumed that enrichment ratios referenced to underlying rock adequately represent enrichment of similarly immobile elements. Nonetheless, we addressed lack of parent material homogeneity with our mixing model. An alternative approach to combine mass fluxes would be to use a single hybrid $C_{i,p}$ in equations 12, 13, 14, and 15 in proportion to trace elemental ratio differences and not use equation 16. Calculating mass fluxes from a single $C_{i,p}$ entailed adjustment of parent material bulk densities. As we were uncertain about extending the influence of trace elements to physical properties like density, we selected the first approach. Alternatively, as CDF is composed of only Zr concentrations, CDF was calculated for rock, loess, and hybrid. Additionally, assigning soil parenthood to a loess sample using the trace element

mixing model with chemistry from the average of three atmospheric deposition samples comes with assumptions. Elemental CVs for the two pairs of duplicate atmospheric deposition samples (BS6 and PF4) were <10% for 11 (Ti, Zr, Nb, and HREE) elements. The average CV for 11 elements between one pair of BS6 duplicates was <10%, except for Dy (11%), Ho (10%), and Tb (17%). Average CVs for four pairs of duplicate hydrometer samples were <10% for all soil horizons, except for PF4 (22%) mainly due to a 5% sand discrepancy from 9% to 4%. Common shortcomings of mass balances studies include the use elements thought immobile, but might be transported during clay and colloid formation (Bern et al., 2015) and an inability to detect differences between nonvolcanic rock, soil, and other exogenous inputs. Assumptions of elemental immobility may not hold depending on the setting, and multiple metrics must be considered (Kurtz et al., 2000; Muhs et al., 2008; Muhs, 2013; Pierce et al., 2011). Our approach assessed immobility of several elements and elemental ratios used in the past to quantify mass balance.

Future studies should collect more rock and atmospheric deposition data to ensure a full range of parent materials and their associated trace and major element chemistry to capture a more complete picture of additional influences on southwest Montana soils. Replicate soil pits will capture the range of physical and geochemical variability that occurs on each lithology. Additional focus should be directed at the lower horizons in the sandstone soil as ratios that include Nb (Zr/Nb, Ti/Nb, Figure 9, Table 8) suggested potential Nb mobility. Mass losses should be used to account for varied rates of naturally occurring carbon dioxide fixation resulting from chemical weathering on each lithology.

Additional efforts should attempt to quantify the varied patterns of atmospheric deposition that occur on each vegetation type in hopes of determining the varied influences of lodgepole pine forest versus grass and shrublands. Additional immobile element ratios warrant attention as they may alter fractional rock influences or bolster current findings. Similarities in heavy rare earth and other trace element concentrations were noted between the fine lithosequence soils and unweathered aeolian loess at Post Farm. Even though concentrations are subject to parent material influence and chemical weathering, the proximity of these concentrations and their cause warrants additional study. Finally, motivation for this study came from a need to improve mass flux calculations using more than one parent material. Through the course of developing our two parent material model, we calculated the potential influence of colluvium as a second parent material. In reality, it is likely than underlying bedrock, atmospheric deposition, and colluvium influence soil horizons in the lithosequence. Therefore, a mixing model incorporating three parent materials may improve mass flux estimates even further. Additionally, expanding the definition of colluvium to soil horizons instead of just underlying bedrock may additionally improve flux estimates as fine soils from other lithologies likely influence these soil profiles.

Conclusions

In this study, we applied a state factor approach to soils formed from an intriguing stratigraphic sequence of five lithologies. We compared field characterization data and trace element concentrations to quantify the influence of candidate parent materials: underlying rock, atmospheric deposition, and colluvium. These influences were used to

quantify chemical weathering referenced to two parent materials. Mass losses referenced to two parent materials were greatest on limestone likely due to congruent underlying rock weathering. Alternatively, fluxes were lowest on gneiss likely due to retention of atmospheric inputs and high organic matter. Mass losses in soil on sandstone were nearly six times greater on gneiss despite similar underlying rock chemistry. Despite improving mass balance estimates by accounting for two parent materials, the search for truth in parent materials in soils impacted by colluvium, atmospheric inputs, and underlying rock remains incomplete. New approaches using trace elements show promise in the development of a three parent materials models for soils development

Acknowledgements

We additionally thank Ron Wiens, Tom Howes, and Jarrod Leonard for their assistance in collecting atmospheric deposition samples and Michael True, Jake Hoffman, Lauren Bryant, Russell Callahan, and others for their assistance in soil pit characterization, sample collection, and laboratory analysis. This research would not have been possible without the cooperation and support of the Bozeman Ranger District, U.S. Forest Service.

4. CONCLUSION

Determining the relative influences of more than one parent material on soil horizons that receive exogenous inputs was a simpler task than trying to calculate total mass fluxes. The over estimation of mass loss when referenced to rock only may prove substantial, but the most important values have yet to be fleshed from this work. Rather now, it would seem the scaled fluxes rather than the combined influences of both parent materials on mass flux may prove more important.

No one factor seems more important to control of soil horizon observations and loess influence than which rock underlies a soil. Soils on sandstone flush and move exogenous inputs quicker than soils on other lithologies. Soils on limestone, once established, seem nearly entire built of loess. But if these lithologies were different, then soils that from on top of them would certainly differ. Clay textures derive from shale combined with meadow vegetation ensure that underlying rock has more control over chemical weathering on shale than exogenous inputs. Soil on gneiss, even though similarly textured, form more organic matter and subsequently catch and retain exogenous inputs more efficiently than soil on sandstone.

Comparing the outputs of Appendix A, terrain attributes, to soil mass fluxes suggest that topographic position has little control on mass flux.

REFERENCES CITED

Almond, P.C., Tonkin, P.J., 1999. Pedogenesis by upbuilding in an extreme leaching and weathering environment, and slow loess accretion, south Westland, New Zealand. Geoderma. 92, 1-36, doi: 10.1016/S0016-7061 99 00016-6.

Arnalds, O., Cutshall, N.H., Nielsen, G.A., 1989. Cesium-137 in Montana soils. Health Physics. 57, 6, 955-958.

Arrhenius, G., Bonatti, E., 1965. The Mesa Verde loess: Soc. Amer. Arch. Mem., Contributions of the Wetherill Mesa Archeological Project. 19, 92-100.

Bern, C.R., Thompson, A., Chadwick, O.A., 2015. Quantification of colloidal and aqueous element transfer in soils: The dual-phase mass balance model. Geochimica et Cosmochimica Acta, 151, 1-18, doi: 10.1016/j.gca.2014.12.008.

Bourne, W.C., Whiteside, E.P., 1962. A study of the morphology and pedogenesis of a medial chernozem developed in loess. Soil Science Society of America Journal, 26, 484-490.

Brimhall, G.H., Dietrich, W.E., 1987. Constitutive mass balance relations between chemical composition, volume, density, porosity, and strain in metasomatic hydrochemical systems: Results on weathering and pedogenesis. Geochimico et Cosmochimica Acta. 51, 567-587, doi: 10.1016/0016-7037(87)90070-6.

Chadwick, O.A., Darry, L.A., Vitousek, P.M., Huebert, B.J., Hedin, L.O., 1999. Changing sources of nutrients during four million years of ecosystem development. Nature. 397, 491-497, doi: 10.1038/17276.

Chadwick, R.A., 1970. Belts of eruptive centers in the Absaroka-Gallatin volcanic province, Wyoming-Montana. Geological Society of America Bulletin. 81, 267-274.

Clynne, M.A., Ramsey, D.W., Wolfe, E.W., 2005. Pre-1980 eruptive history of Mount Saint Helens, WA, USA. U.S. Department of Interior, U.S. Geologic Survey, U.S. Forest Servive. USGS Fact Sheet 2005-3045. http://pubs.usgs.gov/fs/2005/3045/fs2005-3045.pdf [accessed 3 April 2015].

Cornu, S., Lucas, Y., Lebon, E., Ambrosi, J.P., Luizao, F., Rouiller, J., Bonnay, M., Neal, C., 1999. Evidence of titanium mobility in profiles, Manaus, Central Amazonia. Geoderma. 91, 281-295, doi: 10.1016/S0016-7061(99)00007-5.

Damhs, D.E, Rawlins, C.L., 1996. A two-year record of eolian sedimentation in the Wind River Range, Wyoming, U.S.A. Arctic and Alpine Research. 28, 2, 210-216, doi: 10.2307/1551762.

Davis, C. E., Shovic, H. F., 1996. Soil Survey of Gallatin Forest, Montana: Gallatin National Forest, Bozeman, Montana. USDA Forest Service. p. 9, 53-59, 78-79, 104-105.

Dixon, J.L., Heimsath, A.M., Kaste, J., Amundsen, R., 2009. Climate driven processes of hillslope weathering. Geology. 37, 11, 975–978, doi: 10.1130/G30045A.1.

Dixon, J.L, Riebe, C.S., 2014. Tracing and pacing soil across slopes. Elements. 10, 5, 363-368, doi: 10.2113/gselements.10.5.363.

Dokuchaev, V.V., 1879. Short historical description and critical analysis of the more important soil classifications. Trav. Soc. Nat. St. Petersburg. 10, 64–67.

Druce, A.P., 1959. An empirical method of describing stands of vegetation. Tuatara. 8, 1-11. http://nzetc.victoria.ac.nz/tm/scholarly/tei-Bio08Tuat01-t1-body-d1.html.

Egli, M., Merkli, C., Sartori, G., Mirabella, A., Plotze, M., 2008. Weathering, mineralogical evolution and soil organic matter along a Holocene soil toposequence developed on carbonate-rich materials. Geomorphology. 97, 675–696, doi: 10.1016/j.geomorph.2007.09.011.

Ewing, S.A., Sutter, B., Owen, J., Nishiizumi, K., Sharp, W., Cliff, S.S., Perry, K., Dietrich, W., McKay, C.P., Amundson, R., 2006. A threshold in soil formation at Earth's arid-hyperarid transition. Geochimica et Cosmochimica Acta, 70, 5293-5322, doi:10.16/j.gca.2006.08.020.

Feeley, T.C., Cosca, M.A., Lindsay, C.R., 2002. Petrogenesis and implications of calc-alkaline cryptic hybrid magmas from the Washburn volcano Absaroka volcanic province, USA. Journal of Petrology. 43, 4, 663-704, doi: 10.1093/petrology/43.4.663.

Ferrier, K.L., Kirchner, J.W., Finkel, R.C., 2011. Estimating millennial-scale rates of dust incorporation into eroding hillside regolith using and immobile weathering tracers, J. Geophys. Res. 116, F03022, doi: 10.1029/2011JF001991.

Harward, M.E., Borchardt, G.A., 1972. Mineralogy and trace element composition of ash and pumice soils in the Pacific Northwest of the United States, in Harward, M.E. ed., Mineralogy and trace-element composition of ash and pumice soils in the Pacific Northwest of the United States: Special Report No. 276: Oregon Agricultural Experiment Station, p. B.5.1-B.5.12.

Heckman, K., Rasmussen, C., 2011. Lithologic controls on regolith weathering and mass flux in forested ecosystems of the southwestern USA. Geoderma. 164, 99-111, doi: 10.1016/j.geoderma.2011.05.003.

Heimsath, A.M., Furbish, D.J., Dietrich, W.E., 2005. The illusion of diffusion: Field evidence for depth-dependent sediment transport. Geology. 33, 12, 949–952, doi: 10.1130/G21868.1.

Hesse, P.P., McTainsh, G.H., 2003. Australian dust deposits: Modern processes and the quaternary record. Quaternary Science Reviews. 22, 2007–2035, doi: 10.1016/S0277-3791(03)00164-1.

Jenny, H., 1941. Factors of Soil Formation: A System of Quantitative Pedology. Mineola, New York, Dover Publications, Inc. (reprinted 1994).

Jenny, H., 1958. Role of the plant factor in the pedogenic functions: Ecology v. 39, p. 5-16.

James, H.L., Hedge, C.E., 1980. Age of the basement rocks of southwest Montana. Geologic Society of America Bulletin. 91, 11-15.

Juma, N., 2012. Pedosphere.ca: Empowering soil science students, educators & professionals. http://www.pedosphere.ca/ (accessed February 2014).

Neff, J.C., Ballantyne, A.P., Farmer, G.L., Mahowald, N.M., Conroy, J.L., Landry, C.C., Overpeck, J.T., Painter, T.H., Lawrence, C.R., Reynolds, R.L., 2008. Increasing eolian dust deposition in the western United States linked to human activity. Nature Geoscience, 1, 189 – 195, doi: 10.1038/ngeo133.

Kaste, J.M., Heimsath, A.M., and Bostick, B.C., 2007. Tracing short-term soil mixing with fallout radionuclides. Geology. 35, 243-246, doi: 10.1130/G23355A.1.

Kirchner, J.W., Finkel, R.C., Riebe, C.S., Granger, D.E., Clayton, J.L., King, J.G., Megahan, W.F., 2001. Mountain erosion over 10 yr, 10 k.y., and 10 m.y. time scales. Geology. 29, 7, 591–594, 10.1130/0091-7613(2001)029<0591:MEOYKY>2.0CO;2.

Kurtz, A.C., Derry, L.A., Chadwick, O.A., Alfano, M.J., 2000. Refractory element mobility in volcanic soils. Geology. 28, 8, 683–686, doi: 10.1130/0091-7613(2000)28<683:REMIVS>2.0.CO;2.

Kurtz, A.C, Derry, L.A., Chadwick, O.A., 2001. Accretion of Asian dust to Hawaiian soils: Isotopic, elemental, and mineral mass balances. Geochimica et Cosmochimica Acta. 65, 12, 1971–1983, doi: 10.1016/s0016-7037(01)00575-0.

Lawrence, C.R., Neff, J.C., 2009. The contemporary physical and chemical flux of Aeolian dust: A synthesis of direct measurements of dust deposition. Chemical Geology. 267, 46-63, doi:10.1016/j.chemgeo.2009.02.005.

Lawrence, C. R., Painter, T. H., Landry, C. C., Neff, J. C., 2010. Contemporary geochemical composition and flux of aeolian dust to the San Juan Mountains, Colorado, United States. J. Geophys. Res. 115, G03007, 1-15, doi:10.1029/2009JG001077.

Lawrence, C.R., Neff, J.C., Farmer, G.L., 2011. The accretion of aeolian dust in soils of the San Juan Mountains, Colorado, USA. J. Geophys. Res. 116, F02013, 1-20, doi: 10.1029/2010JF001899.

Lawrence, C.R., Reynolds, R.L., Ketterer, M.E., Neff, J.C., 2013. Aeolian controls of soil geochemistry and weathering fluxes in high-elevation ecosystems of the Rocky Mountains, Colorado. Geochimica et Cosmochimica Acta. 107, 27–46, doi:10.1016/j.gca.2012.12.023.

Lebauer, L.R., 1964. Petrology of the middle Cambrian Wolsey shale of southwest Montana. Journal of Sedimentary Petrology. 34, 3, 503-511.

Ley, R., Williams, M., Schmidt, S., 2004. Microbial population dynamics in an extreme environment: Controlling factors in talus soils at 3750 m in the Colorado Rocky Mountains. Biogeochemistry. 68, 3, 297-311, doi: 10.1023/B:BIOG.0000031032.58611.d0.

Liccardi, J.M., and Pierce, K.L., 2008. Cosmogenic exposure-age chronologies of Pinedale and Bull Lake glaciations in greater Yellowstone and the Teton Range, USA. Quaternary Science Reviews. 27, 814-831, doi: 10.1016/j.quascirev.2007.12.005.

Louie, J.Y., 2013. Pilot National Forest Reports: Gallatin National Forest, *in* Assessing the vulnerability of watersheds to climate change. Results of national forest watershed vulnerability pilot assessments: General Technical Report PNW-GTR-884, 33- 49. http://www.fs.fed.us/ccrc/wva/PilotNFWatershedVulnerabilityReport.pdf (accessed February 2014).

Lundgreen, C.A., 2013. Stabilization of an infinite slope failure utilizing hollow bar soil nails with long-term monitoring plan: Breckenridge, Colorado. Association of Conservation Engineers Conference. http://conservationengineers.org/conferences/2013.html (accessed February 2014).

McDonough, W.F., Sun, S., 1995. The composition of the Earth. Chemical Geology. 120, 223–253, doi:10.1016/0009-2541(94)00140-4.

McFadden, L.D, Weldon, R.J., 1987. Rates and processes of soil development on Quaternary terraces in Cajon Pass, California. Geological Society of America Bulletin. 98, 280-293.

Middleton, L.T., 1980. Sedimentology of middle Cambrian Flathead sandstone, Wyoming [Ph.D. thesis]. Laramie, Wyoming. Department of Geology. University of Wyoming.

Montagne, C., 1976. Slope stability evaluation for land capability reconnaissance in the northern Rocky Mountains [Ph.D. thesis]. Bozeman, Montana. Montana State University.

Montagne, C., Munn, L., 1980. Statistical summaries of soil characterization and site data: Summary report. Gallatin National Forest Contract No. R1-11-80-30.

Montagne, J., Goering, J., Vaniman, C., 1975. Compilers. Idealized stratigraphic column—northern Gallatin and Madison Ranges, Montana. Montana State University. www.montana.edu/wwes/programs/Images/localstrat.pdf (accessed March 2014).

Muhs, D.R., Benedict, J.B., 2006. Eolian Additions to Late Quaternary Alpine Soils, Indian Peaks Wilderness Area, Colorado Front Range. Arctic, Antarctic, and Alpine Research. 38, 1, 120–130, doi: 10.1657/1523-0430(2006)038[0120:EATLQA]2.0.CO;2.

Muhs, D.R., Budahn, J.R, Johnson, J.L., Reheis, M., Beann, J., Skip, G., Fischer, E., Joes, S.A., 2008. Geochemical evidence for airborne dust additions to soils in Channel Islands National Park, California. GSA Bulletin. 120(1/2), 106-126, doi: 10.1130/B26218.1

Muhs, D.R., 2013. The geologic records of dust in the Quaternary. Aeolian Research. 9, 3-48, doi: 10.1016/j.aeolia.2012.08.001.

Nakase, D.K., Hartshorn, A.S., Spielmann, K.A., Hall, S.J., 2014. Eolian deposition and soil fertility in a prehistoric agricultural complex in central Arizona, USA. Geoarchaeology. 29, 79-97, doi: 10.1002/gea.21463.

National Atmospheric Deposition Program. Annual data for site: MT07 (Clancy). http://nadp.sws.uiuc.edu/nadpdata/annualReq.asp?site=MT07 (accessed 20 November 2013).

National Atmospheric Deposition Program. Annual data for site: WY08 (Yellowstone National Park-Tower Falls). http://nadp.sws.uiuc.edu/nadpdata/ads.asp?site=WY08, (accessed 20 November 2013).

Owens, P.N., Slaymaker, O., 1997. Contemporary and post-glacial rates of aeolian deposition in the Coast Mountains of British Columbia, Canada. Geografiska Annaler. Series A, Physical Geography. 79, 4, 267-276, doi: 10.1111/j.0435-3676.1997.00022.x.

Pavich, M.J., 1986. Processes and rates of saprolite production and erosion on a foliated granitic rock of the Virginia Piedmont, *in* Colman, S.M., and Dethier, D.P. eds., Rates of chemical weathering of rocks and minerals. Orlando, Florida. Academic Press, p. 551-590.

Pett-Ridge, J.C., 2009. Contributions of dust to phosphorus cycling in tropical forests of the Luquillo Mountains, Puerto Rico. Biogeochemistry. 94, 1, 63-80, doi: 0.1007/s10533-009-9308-x.

Pierce, K.L., 2003. Pleistocene glaciations of the Rocky Mountains. Developments in Quaternary Science. 1, 63-76, doi: 10.1016/S1571-0866(03)01004-2..

Pierce, K.L, Muhs, D.R., Fosberg, M.A., Mahan, S.A., Rosenbaum, J.G., Licciardi, J.M., Pavich, M.J., 2011. A loess–paleosol record of climate and glacial history over the past two glacial–interglacial cycles (~150 ka), southern Jackson Hole, Wyoming. Quaternary Research. 76, 119–141, doi: 10.1016/j.yqres.2011.03.006.

Porder, S., Hilley, G.E., Chadwick, O.A., 2007. Chemical weathering, mass loss, and dust inputs across a climate by time matrix in the Hawaiian Islands. Earth and Planetary Science Letters. 258, 414–427, doi:10.1016/j.epsl.2007.03.047.

Poonam, J., 2008. Particle size analysis for soil texture, Kellogg Biological Station, Michigan State University, http://lter.kbs.msu.edu/protocols/108.

Pye, K., 1987. Aeolian dust and dust deposits, Academic Press: London, England.

Reheis, M.C., 1987a. Gypsic soils on the Kane alluvial fans, Big Horn County, Wyoming. U.S., Soil Chronoseqeunces in the western United States, Geological Survey Bulletin 1590-c, http://pubs.usgs.gov/bul/1590c/report.pdf.

Reheis, M.C., Goodmacher, J.C., Harden, J.W., McFadden, L.D., Rockwell, T.K., Shroba, R.R., Sowers, J.M., Taylor, E.M., 1995. Quaternary soil and dust deposition in southern Nevada and California. Geological Society of America Bulletin. 107, 9, 1003-1022.

Reheis, M.C, Kihl, R., 1995. Dust deposition in southern Nevada and California: Relations to climate, source, and source lithology. Journal of Geophysical Research. 100, D5, 8893-8919.

Retzer, J.L., 1962. Soil Survey of Fraser Alpine Area, Colorado. Colorado Agricultural Experiment Station, U.S. Forest Service, U.S. Department of Agriculture. Series 1956, 20, 1-47, www.fs.fed.us/rm/pubs_other/rmrs_1962_retzer_j0001.pdf (accessed March 2014).

Rhoades, C., Elder, K., and Greene, E., 2010. The influence of an extensive dust event on snow chemistry in the southern Rocky Mountains. Arctic, Antarctic, and Alpine Research. 42, 1, 98-105, www.fs.fed.us/rm/boise/AWAE/scientists/profiles/Rhoades/rmrs_2010_rhoades003.pdf, doi:10.1657/S0016-7037(03)00382-X.

Riebe C.S., Kirchner, J.W., Finkel, R.C., 2003. Long-term rates of chemical weathering and physical erosion from cosmogenic nuclides and geochemical mass balance: Geochimica et Cosmochimica Acta. 67, 22, 4411–4427, doi:10.1016/S0016-7037(03)00382-X.

Salters, V.J.M., 1999. Elements: High Field Strength, in Marshall, C.P., Fairbridge, R.W. (Eds.), Encyclopedia of Geochemistry. Kluwer Academic Publishers, Dordrecht, The Netherlands, pp. 209-210.

Saxton, K.E., Rawls, W.J., Romberger, J.S., Papendick, R.I., 1986. Estimating generalized soil-water characteristics from texture. Soil Sci. Soc. Am. J. 50, 4, 1031-1036.

Schaetzl, R.J., Anderson, S., 2005. Soils: Genesis and geomorphology, New York, NY: Cambridge University Press.

Schimel, J. and Chadwick, O.A., 2013. What's in a name? Frontiers in Ecology and the Environment. 11, 8, 405-406, doi: 10.1890/13.WB.016.

Schoeneberger, P.J., Wysocki, D.A., Benham, E.C., Soil Survey Staff, 2012. Field book for describing and sampling soils, Version 3.0. Natural Resources Conservation Service. National Soil Survey Center. Lincoln, NE. ftp://ftp-fc.sc.egov.usda.gov/NSSC/Field_Book/FieldBookVer3.pdf

Stonestrom, D.A., White, A.F., Akstin, K.C., 1998. Determining rates of chemical weathering in soils—solute transport versus profile evolution. Journal of Hydrology. 209, 331–345, doi: 10.1016/S0022-1694(98)00158-9.

Soil Survey Staff, 2010. Keys to Soil Taxonomy: 11th ed. U.S. Department of Agriculture, Natural Resources Conservation Service. ftp://ftp-fc.sc.egov.usda.gov/NSSC/Soil_Taxonomy/keys/2010_Keys_to_Soil_Taxonomy.pdf, (accessed: February 2014).

Suarez, R., 2004. Troops question secretary of defense Donald Rumsfeld about armor. PBS News Hour. www.pbs.org/newshour/bb/military/july-dec04/armor_12-9.html, (accessed: February 2014).

Sugden, J.C., Hartshorn, A.S., Dixon, J.L., and Montagne, C., 2014. A slice through time: A Hyalite Canyon soil lithosequence, *in* Shaw, C.A., and Tikoff, B., eds., Exploring the Northern Rocky Mountains. Geological Society of America Field Guide. 37, 101–114, doi:10.1130/2014.0037(05).

Tegen, I., 2003. Modeling the mineral dust aerosol cycle in the climate system: Quaternary Science Reviews. 22, 1821-1834, doi:10.1016/S0277-3791(03)00163-X.

Taylor, S.R., McLennan, S.M., 1995. Geochemical evolution of continental crust. Reviews of Geophysics. 33, 2, 241-265, doi: 10.1029/95RG00262.

Taylor, S.R. and S.M. McLennan, 1985. The Continental Crust: Its composition and Evolution. Blackwell Scientific Publications. Oxford, England.

U.S. Forest Service, Montana State University, 1998. Memorandum of Understanding between the Montana State University, Bozeman and Billings Campuses and the Gallatin and Custer National Forests. http://www2.montana.edu/policy/forest_service_use/mou.html (accessed: February 2014).

Weaver, T., and Perry, D., 1979. Relationship of cover type to altitude, aspect, and substrate in the Bridger Range, Montana. Northwest Science. 52, 3, 212-219.

Weber, W.M., 1965. General geology and geomorphology of the Middle Creek area, Gallatin County, Montana [M.S. Thesis]. Bozeman, Montana. Department of Earth Sciences. Montana State University.

Veseth, R., Montagne, C., 1980. Geologic parent materials of Montana soils: Bulletin 721. Montana Agricultural Experiment Station and USDA-Soil Conservation Service, Bozeman.

Vuke, S. M, Lonn, J. D., Berg, R. B., Kellogg, K. S., 2002. Geologic map of the Bozeman south 30' x 60' quadrangle: Southwestern Montana. Open File Report

MBMG 469. Montana Bureau of Mines and Geology. Retrieved from website: http://www.mbmg.mtech.edu/pdf_100k/bozeman-text.pdf

Yaalon, D.H., Ganor, E., 1973. The influence of dust on soils during the Quaternary. Soil Science. 116, 3, 146–155, doi:10.1097/00010694-197309000-00003.

Yassoglou, N.J., Nobeli, C., Vrahamis, S.C., 1969. A study of some biosequences and lithosequences in the zone of brown forest soils in northern Greece: Morphological, physical, and chemical properties. Soil Science of Society of America Journal. 33, 291-296.

Zdanowicz, C.M., Zielinski, G.A., Germani, M.S., 1999. Mount Mazama eruption: Calendrical age verified and atmospheric impact assessed. Geology. 27, 621–624, doi:10.1130/0091-7613(1999)027<0621:MMECAV>2.3.CO;2.

APPENDICES

APPENDIX A

TERRAIN ATTRIBUTE EFFECTS ON SOIL PROCESSES

Introduction

Soils are affected by vertical throughflow and chemical weathering. While vertical hydrologic infiltration in the cool moist climate of the lithosequence (fig. 1) affects soil processes, lateral flow likely also impacts these soils. This study assumes that surface features represent and are indicative of lateral soil hydrology. As all slopes and aspects are locally similar, it is likely that vertical throughflow between soils would be comparable. Alternatively, if upslope catchment areas (UCA) vary between sites, lateral flow in each horizon and between soil horizons may vary. Bigger catchments receive and transport more precipitation than smaller ones. Pour points emerging from bigger catchments therefore transport more water and other soluble portions of soil than smaller catchments.

Methods

While much of quantitative pedology suggest that vertical throughflow and translocation drive soil formation, recent studies have focused on the importance of lateral flow to soil processes (Gillin, 2013). Areas surrounding study area soils likely exert a profound influence on soil properties and 8 and 25 meter National Elevation Dataset (NED) tiles were used to determine UCA. The single flow direction algorithm (D8) (O'Callaghan and Mark, 1984) and the triangle multiple flow direction algorithm (MD∞) (Siebert and McGlynn, 2007) were used to determine UCA. While other methods of determining UCA areas exist (Quinn et al., 1991; Wolock and McCable,

1995; Tarboton, 1997; Erskine et al., 2006), this study uses two methods to compare a range of UCA output estimates using NED tiles.

Calculated catchment areas and slopes were combined to calculate topographic wetness indices (TWI) (Beven and Kirby, 1979) for soil pits.

$$TWI = \ln(\alpha/\tan\beta) \quad \text{Equation 1}$$

where α is UCA and β is slope. Cells that have similar calculated TWI values may be more comparable than those that do not. TWI can index portions of the five soil forming factors: time and topography when considering soil development. When slopes are relatively constant in the area of interest as is the case in lithosequence soils, catchment areas calculations are the prominent driver of TWI values. Soils having larger catchments are likely found at toeslope positions in concave settings as opposed to midslope and upslope positions which will likely have smaller catchments. As a result, soils on similar slopes that have similar catchment areas will be more comparable than soils on similar slopes that have different catchment areas. These larger catchments likely transport more water and other materials laterally than smaller catchments.

The single flow direction algorithm (D8) routes all flow to the steepest of the eight cells surrounding the cell of interest. This simple method of calculating catchment areas can misrepresent surface hydrology in several ways. Surface water flow and by extension soil water flow does not move in only one of eight directions, but many directions. By routing flow to the lowest of eight cells, flow paths become artificially concentrated into fewer flow paths than may exist on the landscape. Various methods have been devised to overcome drawbacks to the D8 method. First, midpoints of cells

are connected to midpoints of two neighboring cells to make eight planar triangular facets around each cell. The relative steepness of each triangle is used to weight downward flows in the steepest direction and can be between midpoints which do not have to be straight towards the midpoint of a neighboring cell. MD∞ allows modeled flows to spread across landscapes more realistically than the D8 method and modeled hydrologic flow to move in a direction other than directly into one of cells neighboring the cell of interest.

ArcGIS was used to determine terrain attributes using the D8 method, while the System for Automated Geoscientific Applications (SAGA) was used to run the MD∞ algorithm. The output grid was immediately converted to an Arc Grid and the remainder of the processing was done in ArcGIS. USGS National Elevation Dataset tiles (1 arcsecond or 25 meter and 1/3 arcsecond or 8 meter) for portions of southwest Montana were mosaiced and used as digital elevation models (DEMs). Mosaiced NED tiles were then converted using the bilinear resampling method to the North American Datum 1983 (NAD83) UTM zone 12, so the units would change to meters. Sinks were filled in the mosaiced dataset to minimize processing errors. The mosaiced NED tiles were then used to create a flow direction raster. A handheld GPS was used in the field to determine latitude and longitude of soil pits. To determine the terrain attributes, latitude and longitude of were added as events and converted to a shape file. Using the watershed function in the Hydrology Spatial Analyst tools, the soil pit shape file was the pour point and the flow direction raster determined the size of catchment areas for both NED tiles. Slope (β) in % rise was calculated using Spatial Analysis Tools was combined with the

various calculated catchment areas to determine the Topographic Wetness Indices (TWI, eq. 1) for the various NED tiles.

The System for Automated Geoscience Applications (SAGA) was used only to run the MD∞ algorithm, while the remainder of the data processing was done in ArcGIS. The sink filled mosaiced raster 8 m NED tiles mentioned above was clipped to the ridges around soils to minimize SAGA processing times, but not overlook any potential catchment zones for these five soils. ArcGIS Conversion Tools were then used to convert from raster to an ASCII text file for use in SAGA. The Import/Export Grids package and Import ESRI Arc/Info Grid tool was used to get the ASCII text file into SAGA. The Terrain Analysis – Hydrology package and specifically the Catchment Area (Parallel) tool was used to create catchment areas using the MD∞ method. Elevation was set to the converted and imported ASCII grid, catchment area was set to create, and the method was set to Multiple Triangular Flow Direction. SAGA output a new ASCII grid which was exported using the Import/Export Grids package and export ESRI Arc/Info Grid tool also as an ASCII grid. The output was then imported back into ArcGIS using Conversion Tools to convert an ASCII grid into a raster. The soil pit shapefile was used to identify the sizes of MD∞ catchment areas from the 8 m sink filled mosaiced DEM. To determine sizes of catchment areas at 25 m resolution with the 8 m processed DEM, catchment areas for the eight cells surrounding each soil pit cell were averaged. Therefore, a grid of nine 8 m catchments was identified around each soil pit and the size of each catchment was recorded. The mean catchment areas for these nine 8 m cells were used to represent the catchment size for a 25 m resolution DEM using the MD∞ method.

A benefit of using this method to coarsen the SAGA output is that a coefficient of variance (CV) for catchment areas can be calculated

Pour point shapefiles or rasters cannot be input into the MD∞ method in SAGA. Whereas ArcGIS outputs using the D8 method highlight the cells that compose an UCA, SAGA output using the MD∞ method outputs catchment sizes for every cell in the input ASCII grid. SAGA users should limit the size of elevation data inputs to reduce processing times and for users to factor output processing times to account for the fact that a tear drop shaped watershed will not be identified in the output.

Results

Slopes (table 1) calculated by ArcGIS for both the 8 m and 25 m NED tiles are consistent with slopes observed in the field. The gentlest slopes are found at the soil on shale at which ArcGIS calculated slopes of 14.8% at both resolutions. The steepest slopes in the lithosequence are found at the soil on sandstone at which ArcGIS calculate slopes of 18.9% for the 8 m NED and 18.6% for the 25 m NED. Soils on gneiss and limestone reported more similar slopes to sandstone than shale, while soils on basaltic andesite reported more similar slopes to soils on shale for both 8 m and 25 m resolutions.

Using only TWIs (table 1) from both D8 and MD∞ methods suggests that UCAs (figs. 2 and 3) have similar influences on soils on gneiss, sandstone, and limestone at both resolutions when only slope and UCA are considered. Alternatively, a slightly larger catchment influences soil on shale and by far the largest and most variable catchment area is on basaltic andesite at both resolutions. Less variability exists between calculated catchment sizes using MD∞ than D8 consistent with the drawbacks of D8 mentioned

above. Regardless of resolution or method, the trends in calculated catchment sizes remain consistent. Soils on gneiss, sandstone, and limestone have the smallest catchment and are comparable with one another as reflected in the TWI results. While TWIs for soil on shale receive more colluvial and hydrological inputs than soils on gneiss, sandstone, and limestone, soil on basaltic andesite has the largest UCA and therefore upslope influence. The D8 method of calculating catchment sizes in locations with small catchments may not be as misleading as in larger catchments. Variability is highest by far when calculating catchment size on basaltic andesite using the D8 method. Catchment size for soil on basaltic andesite varies when calculated using 8 m resolution is 20 fold greater than when calculated using a 25 m resolution.

Discussion

While there is variability between catchment sizes and TWIs depending on which methods are used, both methods suggest that similar colluvial influences are imposed on soils on gneiss, sandstone, and limestone. Larger colluvial influences are imposed on soil on shale and even larger colluvial influences are imposed on soil on basaltic andesite. These influences likely have large effects on the role of weathering and retention of dust and loess and weathering of underlying bedrock to soil. The range of TWIs suggest that water and other soluble materials move more quickly through soil on shale and certainly basaltic andesite. While terrain attributes suggest this is so, there might be specific soil characteristics that either enhance or restrict movement through lithosequence soils with respect to colluvium. Two of three finer lithosequence soils have greater colluvial

influence and field characteristics may reflect that. Both soils on shale and basaltic andesite are clay rich, but do not have a high enough increase in clay between horizons to be argillic subsurface horizons. Therefore, forces aside from pedogenesis account for the clay content and higher TWIs observed at these soils may not allow these soils enough time to have increased clay concentrations at depth that can be accounted for by pedogenesis alone. The increased clay content is likely due to both underlying rock and lateral soil water and solute transport.

Smaller and more homogenous TWIs observed for soils on gneiss, sandstone, and limestone suggests more limited and similar colluvial influences in these soils. Even though these soils do have similar colluvial influences as suggested above, they behave differently. Soil on gneiss has a distinctive cambic horizon and weathered saprolite that maintains banding characteristic of gneiss. While the coarse soils on gneiss would enhance infiltration and throughflow, the appearance of this saprolite suggests it is protected from atmospheric inputs. Perhaps conditions exist that promote lateral movement of soil water away from soil on gneiss and prevent further weathering and degradation of banded gneiss saprolite. While soil on sandstone is similarly coarse, horizons are difficult to distinguish and are based on root and coarse fragment content. Soils on limestone are fine textured and HREE analysis suggests loess deposition is the dominant parent material in this soil.

Although mixing model results and mass fluxes between shale are dominated by rock and limestone dominated by loess, lateral movement of material likely accounts for the increasing influence of dust with depth in both of these soils. The clayey textures in

the shale are largely rock derived from seep, creep, and swale in the moist environment of the lithosequence. It is also likely that because the A horizon on shale receives the bulk of the moisture that it move quicker than deeper horizons. Perhaps the higher influence of loess on the Bt horizon of shale is in part because it moves less and is therefore more poorly mixed than the A horizon. A similar process maybe at work in the soil on limestone, but instead of clay preventing more water from deeper horizons as on shale, colluvial limestone cobbles and boulders likely dampen the influence of PF4-like loess in the soil on limestone. The A2 horizon on limestone is buffered from the influence of colluvial limestone by the A1 horizon. This may explain why rock influence in the A1 horizon is six percent, while rock influence on the A2 horizon drops to 2%.

While both resolutions suggest similar catchment areas and TWIs, it is tough not to consider the range of colluvial influences that would be calculated with higher resolution DEMs. Work in New Hampshire's forested watershed compares outputs of terrain attributes like catchment areas and TWI suggest that three and five meter resolution modeled lateral flow through soils better than one, eight, and 25 meter NED tiles (Gillin, 2013). It is difficult to think that an eight meter cell and certainly a 25 meter cell would capture the extent of heterogeneity occurring in one meter by one meter by one meter soil pit.

References

Beven, K. J., Kirby, M. J., 1979. A physically based, variable contributing area model of basin hydrology. Hydrological Sciences Bulletin, 24, 1, 43-69.

Gillin, C.P., 2013. Digital terrain analysis to predict soil spatial patterns at the Hubbard Brook Experimental Forest: [MS Thesis], Department of Forest Resources and Environmental Conservation, Virginia Polytechnic Institute and State University.

Erskine, R. H., Green, T. R., Ramirez, J. A., MacDonald, L. H., 2006. Comparison of grid-based algorithms for computing upslope contributing area. Water Resources Research. 42, W09416, doi:10.1029/2005WR004648.

Quinn, P., Beven, K., Chevallier, P., Planchon, O., 1991. The prediction of hillslope flowpaths for distributed hydrological modeling using digital terrain models. Hydrological Processes. 5, 59-79.

O'Callaghan, J.F, Mark, D.M., 1984. The extraction of drainage networks from digital elevation data. Computer Vision, Graphics, and Image Processing. 28, 323-344.

McFadden, L.D, Weldon, R.J., 1987. Rates and processes of soil development on Quaternary terraces in Cajon Pass, California. Geological Society of America Bulletin. 98, 280-293.

Seibert, J., McGlynn, B. L., 2007. A new triangular multiple flow direction algorithm for computing upslope areas from gridded digital elevation models. Water Resources Research, 43, W04501, doi:10.1029/2006WR005128.

Tarboton, D.G., 1997. A new method for the determination of flow directions and upslope areas in grid digital elevation models. Water Resources Research. 33, 2, 309-319, doi: 0043-1397/97/96WR-03137509.00

Wolock, D.M., McCable, G.J. Jr., 1995. Comparison of single and multiple flow directions algorithms for computing topographic parameters in TOPMODEL. Water Resources Research. 31, 5, 1315-1324.

List of Tables and Figures

Figure 1. Map and study locations in **(a)** southwest Montana for the **(b)** sites and local slopes in the study area.

Figure 2. Catchment areas calculated using D8 for LL soils using 8 m resolution.

Figure 3. Catchment areas calculated using D8 for LL soils using a 25 m resolution.

Table 1. Catchment sizes and slopes as calculated by ArcGIS using D8 and SAGA using MD∞.

Figure 4. Topographic Wetness Indexes (TWI) of LL sites using D8 and MD∞ at 8 and 25 m resolutions.

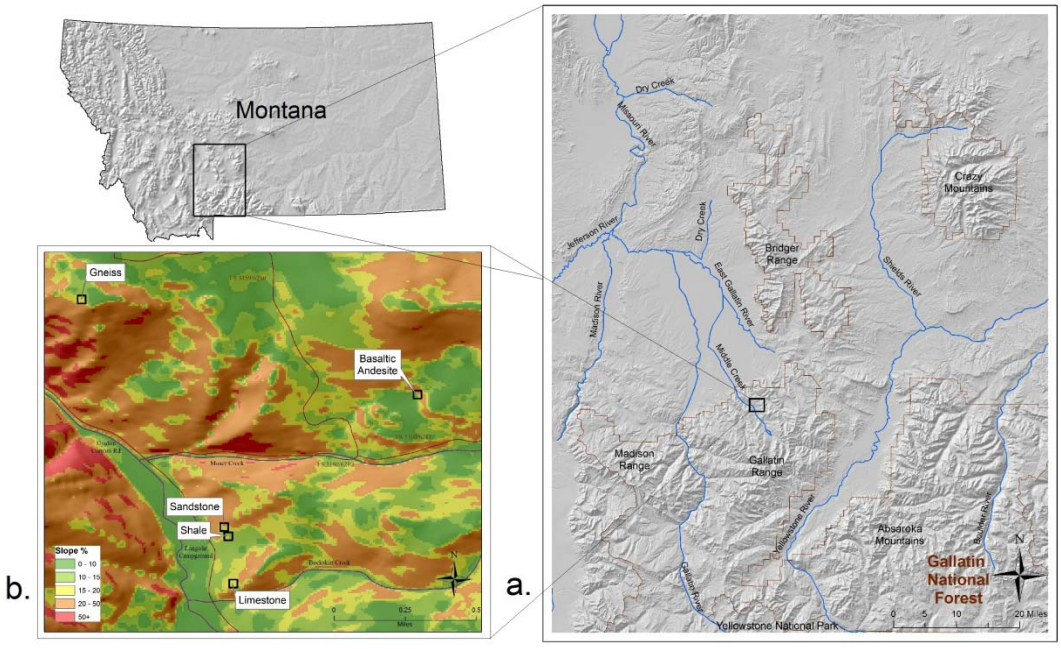

Figure 1. Map and study locations in **(a)** southwest Montana for the **(b)** sites and local slopes in the study area.

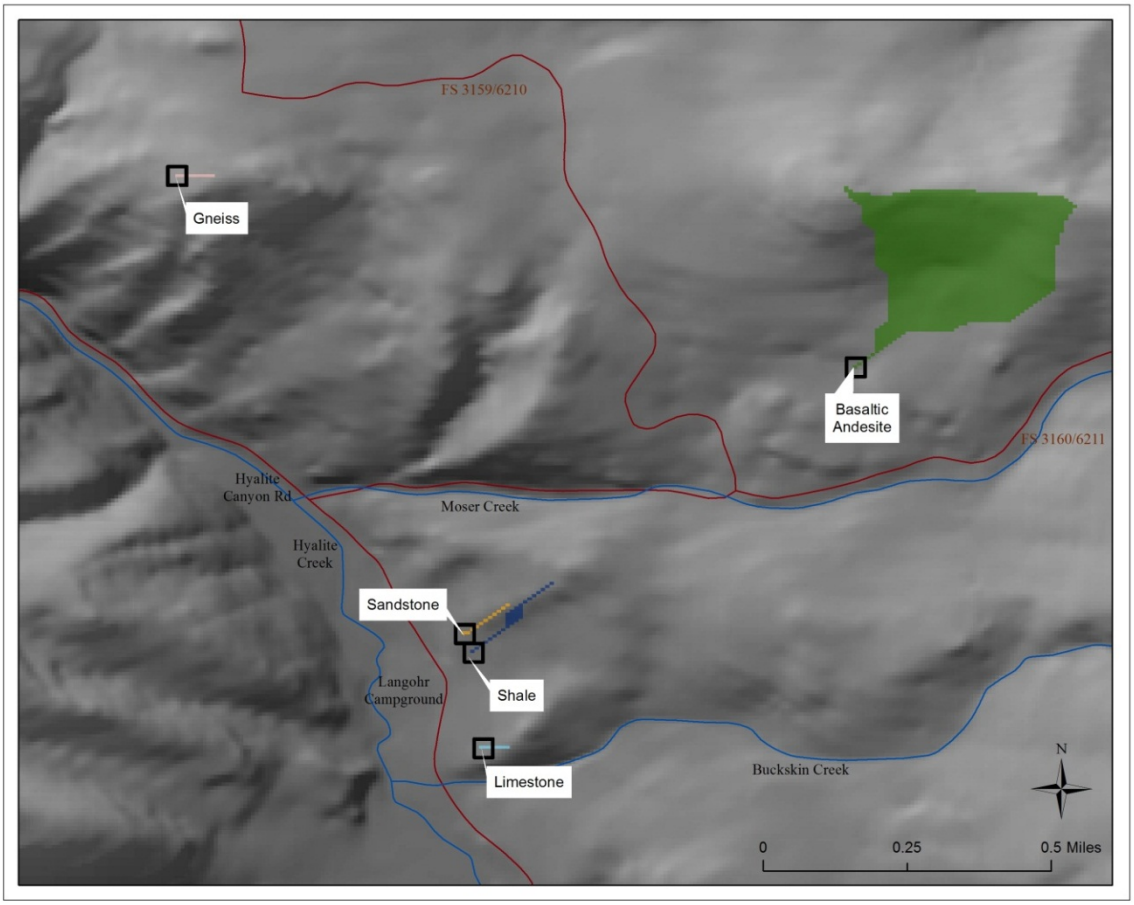

Figure 2. Catchment areas calculated using D8 for lithosequence soils using 8 m resolution.

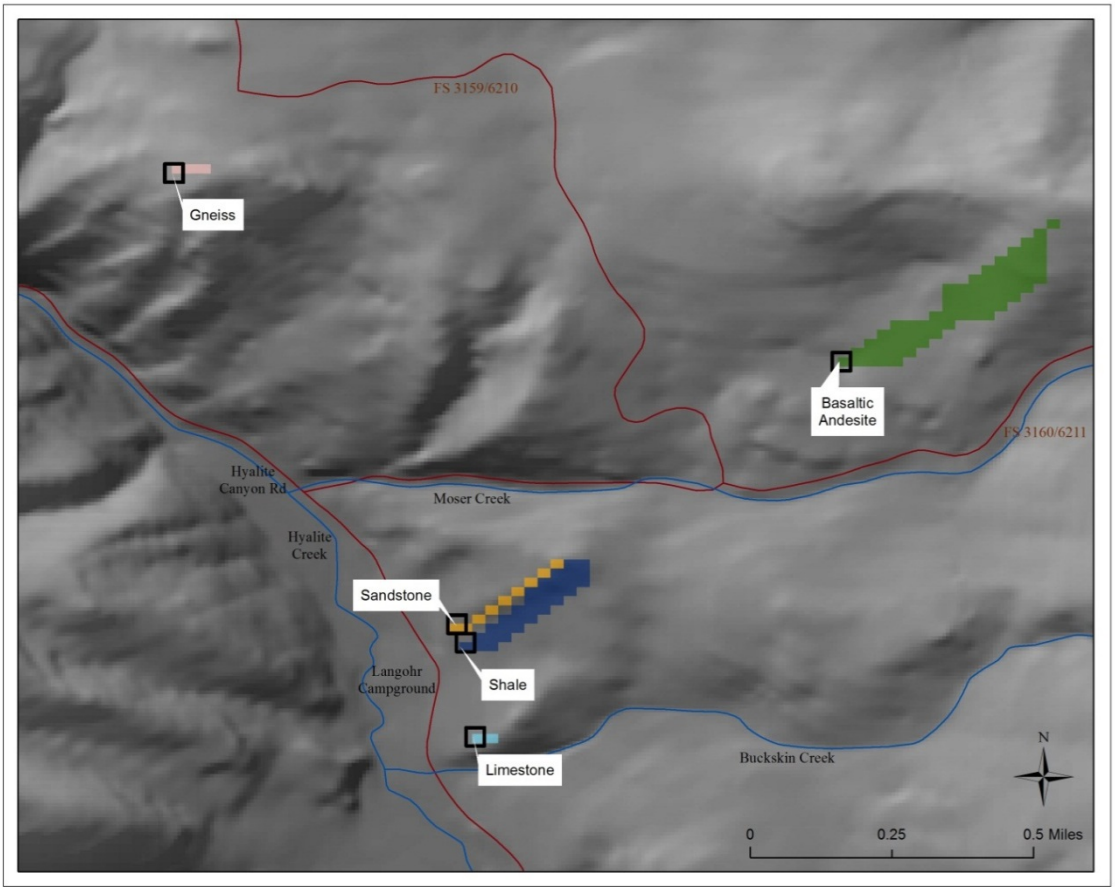

Figure 3. Catchment areas calculated using D8 for lithosequence soils using 25 m resolution

	DEM Resolution		MD∞	D8
Site	meters	% slope	Catchment Size (m^2)	
Gneiss	8	17.7	460	900
Sandstone	8	18.9	562	1100
Shale	8	14.8	3931	3500
Limestone	8	18.4	374	700
Basaltic Andesite	8	15.5	24636	179500
Gneiss	25	17.4	492	300
Sandstone	25	18.6	566	900
Shale	25	14.8	3895	3100
Limestone	25	18.0	375	200
Basaltic Andesite	25	15.5	27481	7000

Table 1. Catchment sizes and slopes as calculated by ArcGIS using D8 and SAGA using MD∞.

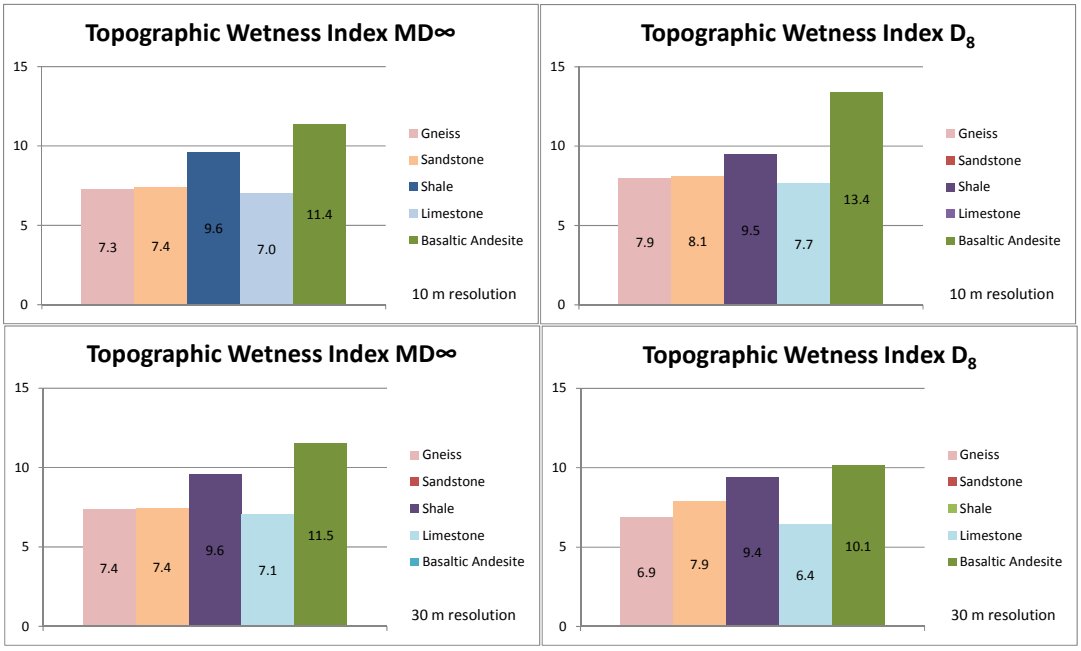

Figure 4. Topographic Wetness Indexes (TWI) of lithosequence sites using D8 and MD∞ at 8 and 25 m resolutions.

APPENDIX B

LITHOSEQUENCE DATA

Raw data and calculations for these soils and their parent materials are housed electronically at the Montana State University Library. Use to the following link to access the data and calculations: http://doi.org/10.15788/M2CC7P.